iScience

CellPress
OPEN ACCESS

Article

A Glucose-Triptolide Conjugate Selectively Targets Cancer Cells under Hypoxia

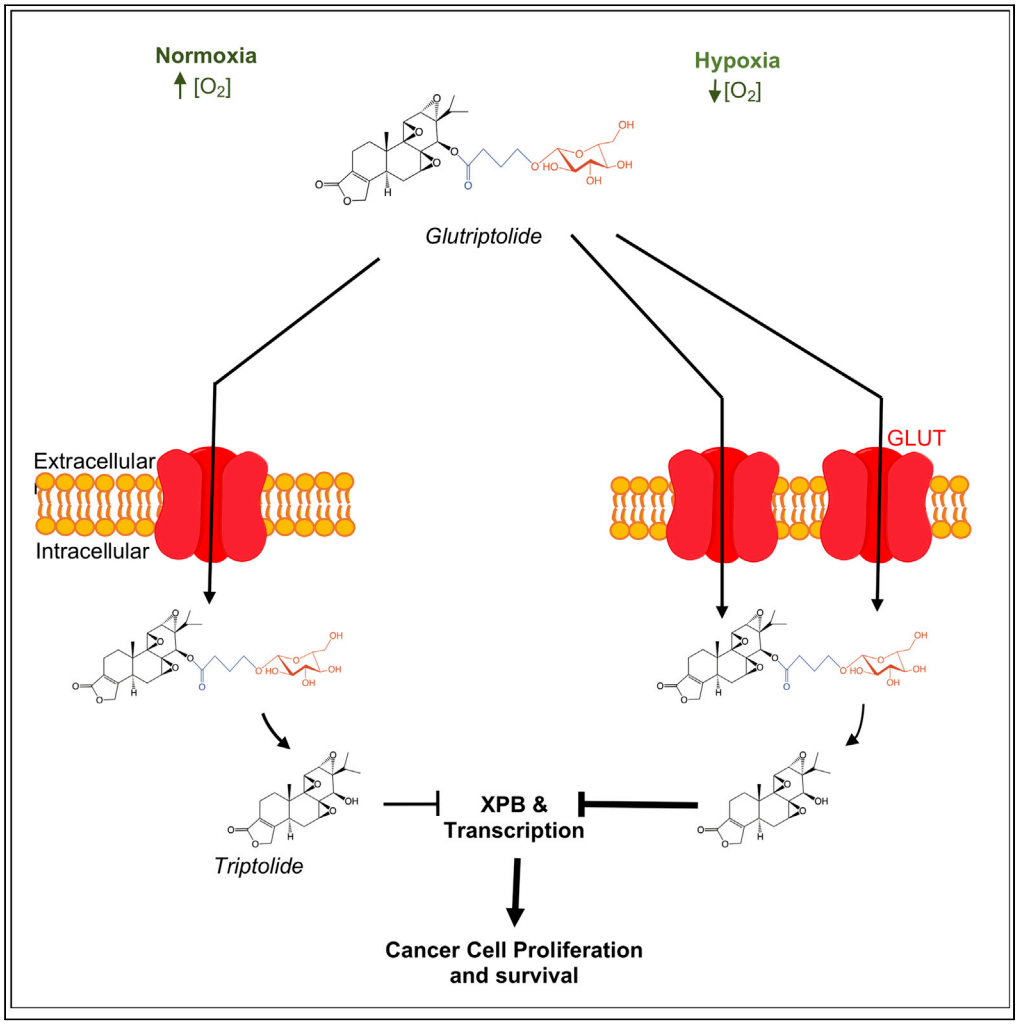

Emmanuel Datan, Il Minn, Peng Xu, ..., Biao Yu, Martin G. Pomper, Jun O. Liu

byu@mail.sioc.ac.cn (B.Y.)
mpomper@jhmi.edu (M.G.P.)
joliu@jhu.edu (J.O.L.)

HIGHLIGHTS

A second-generation glucose-triptolide conjugate (glutriptolide-2) was developed

Glutriptolide-2 exhibits selective toxicity to cancer cells over normal cells

Glutriptolide-2 possesses sustained antitumor activity *in vivo*

Glutriptolide-2 shows greater potency against cancer cells under hypoxia

Datan et al., iScience *23*, 101536
September 25, 2020 © 2020
https://doi.org/10.1016/j.isci.2020.101536

iScience

CellPress
OPEN ACCESS

Article

A Glucose-Triptolide Conjugate Selectively Targets Cancer Cells under Hypoxia

Emmanuel Datan,[1,2,6] Il Minn,[3,6] Peng Xu,[4,6] Qing-Li He,[1,2] Hye-Hyun Ahn,[3] Biao Yu,[4,*] Martin G. Pomper,[3,5,*] and Jun O. Liu[1,2,5,7,*]

SUMMARY

A major hurdle in the treatment of cancer is chemoresistance induced under hypoxia that is characteristic of tumor microenvironment. Triptolide, a potent inhibitor of eukaryotic transcription, possesses potent antitumor activity. However, its clinical potential has been limited by toxicity and water solubility. To address those limitations of triptolide, we designed and synthesized glucose-triptolide conjugates (glutriptolides) and demonstrated their antitumor activity *in vitro* and *in vivo*. Herein, we identified a lead, glutriptolide-2 with an altered linker structure. Glutriptolide-2 possessed improved stability in human serum, greater selectivity toward cancer over normal cells, and increased potency against cancer cells. Glutriptolide-2 exhibits sustained antitumor activity, prolonging survival in a prostate cancer metastasis animal model. Importantly, we found that glutriptolide-2 was more potent against cancer cells under hypoxia than normoxia. Together, this work provides an attractive glutriptolide drug lead and suggests a viable strategy to overcome chemoresistance through conjugation of cytotoxic agents to glucose.

INTRODUCTION

Despite its fundamental role in cell proliferation and survival, there exist far fewer inhibitors of eukaryotic transcription in comparison to those of translation (Bensaude, 2011; Bhat et al., 2015; McClary et al., 2017). Triptolide ((1*S*,2*S*,4*S*,5*S*,7*R*,8*R*,9*S*,11*S*,13*S*)-8-hydroxy-1-methyl-7-propan-2-yl-3,6,10,16 tetraoxaheptacyclo[11.7.0.0^{2,4}.0^{2,9}.0^{5,7}.0^{9,11}.0^{14,18}] icos-14(18)-en-17-one), an active ingredient from the traditional Chinese medicinal plant Thunder God Vine (also known as Lei Gong Teng), has emerged as one of the few specific inhibitors of eukaryotic transcription mediated by RNA polymerase II (RNAPII) (Titov et al., 2011; Wang et al., 2011). Known for its potent immunosuppressive and antiinflammatory activity, extracts of Thunder God Vine with enriched triptolide have been used as a powerful immunosuppressant for treating a wide variety of autoimmune disorders for centuries (Lipsky and Tao, 1997; Zhao, 1765). Triptolide also exhibits potent antiproliferative activity in almost all cancer cell lines tested to date. The molecular mechanism underlying the antiproliferative activity of triptolide has been investigated for decades. Although a number of putative triptolide-binding proteins have been reported, most cannot account for its antiproliferative and pro-apoptotic activity (Corson et al., 2011; Leuenroth et al., 2007; Lu et al., 2014; Soundararajan et al., 2009; Westerheide et al., 2006). The identification and validation of the XPB subunit of the general transcription factor TFIIH as the physiological target of triptolide offered a plausible molecular explanation for the broad anticancer activity of triptolide (He et al., 2015; Smurnyy et al., 2014; Titov et al., 2011).

Triptolide forms a covalent adduct with Cys342 in the active site of XPB, leading to the inhibition of the DNA-dependent ATPase activity of XPB, effectively blocking transcriptional initiation by RNAPII (He et al., 2015). We have shown that mutation of Cys342 to a threonine residue in a single remaining allele of the XPB gene produces a viable, albeit slow-growing, HEK293T cells that became nearly completely resistant to triptolide. In addition to the Cys342 residue, a number of other residues in both XPB and its regulatory subunit p52 seem to play important roles in the interaction between TFIIH and triptolide, as their mutations also caused resistance, albeit to different degrees, to triptolide among the mutant-expressing cell lines (Smurnyy et al., 2014). The effect of triptolide on transcription did not seem to be caused solely by the inhibition of the ATPase activity of TFIIH, as the binding of triptolide to XPB subsequently causes degradation of the catalytic subunit of RNAPII, exacerbating the inhibitory effect of triptolide on

[1]Department of Pharmacology and Molecular Sciences, Johns Hopkins University School of Medicine, Baltimore, MD 21205, USA

[2]SJ Yan and HJ Mao Laboratory of Chemical Biology, Johns Hopkins University School of Medicine, Baltimore, MD 21205, USA

[3]Russell H. Morgan Department of Radiology and Radiological Science, Johns Hopkins University School of Medicine, Baltimore, MD 21205, USA

[4]State Key Laboratory of Bio-organic and Natural Products Chemistry, Center for Excellence in Molecular Synthesis, Shanghai Institute of Organic Chemistry, Chinese Academy of Sciences, and University of Chinese Academy of Sciences, 345 Lingling Road, Shanghai 200032, China

[5]Sidney Kimmel Comprehensive Cancer Center, Johns Hopkins University School of Medicine, Baltimore, MD 21205, USA

[6]These authors contributed equally

[7]Lead Contact

*Correspondence: byu@mail.sioc.ac.cn (B.Y.), mpomper@jhmi.edu (M.G.P.), joliu@jhu.edu (J.O.L.)

https://doi.org/10.1016/j.isci.2020.101536

RNAPII-mediated transcription (Titov et al., 2011; Wang et al., 2011). Recent work has implicated the CDK7 kinase as part of the pathway leading to the ubiquitylation and proteasome-mediated degradation of RNAPII induced by triptolide (Manzo et al., 2012). The precise mechanism by which triptolide triggers the degradation of the RPB1 subunit of RNAPII, however, still remains to be completely elucidated. Thus, triptolide inhibits eukaryotic transcription by a unique two-step mechanism, inhibition of XPB to prevent RNAPII-mediated transcription initiation followed by degradation of RNAPII itself.

Extensive efforts have been made to develop triptolide and its analogs as immunosuppressive and anticancer drugs in the past few decades. One of the major hurdles is the general toxicity of triptolide, most likely attributed to its inhibition of transcription. Another is its limited water solubility. To date, two derivatives of triptolide remain in clinical development. One analog, (5R)-5-hydroxytriptolide, is undergoing clinical trial as an immunosuppressant (Wang et al., 2012; Zhou et al., 2005). The other, Minnelide, a phosphorylated form of triptolide with increased solubility, is undergoing human trials for treating pancreatic and other types of cancer (Chugh et al., 2012). Given the mechanism-based toxicity of triptolide, it is difficult to separate the antitumor activity and intrinsic toxicity of triptolide with existing triptolide analogs, calling for a radically different approach to addressing the problem. Recently, we designed a different class of triptolide analogs by conjugating it to glucose in hopes to target glucose-addicted tumor cells over normal cells. Moreover, the high water solubility of glucose would significantly increase the solubility of the resultant glucose-triptolide conjugates (refer to hereafter as glutriptolides). One of the lead compounds from our first-generation glutriptolide (glutriptolide-1) indeed exhibited higher solubility and tumor cell selectivity over triptolide and was shown to possess sustained antitumor activity *in vivo* (He et al., 2016). Unfortunately, an obligate degradation intermediate, triptolide-succinate (also known as F60008), has undergone early human clinical study and was found to be lethal to two patients (Kitzen et al., 2009). In addition, glutriptolide-1 suffers from instability in human serum, ruling it out as a viable drug candidate.

To identify glutriptolide analogs with improved pharmacological properties and reduced toxicity, we embarked on the design and synthesis of a series of second-generation glucose-triptolide conjugates by altering the linker structure and accompanying linkage between the linkers and glucose. Screening of these second-generation glutriptolide analogs identified a lead, glutriptolide-2, with a glycosidic linkage between the linker and glucose that upon degradation, would release an alcohol-containing intermediate. Glutriptolide-2 was found to be 4-fold more potent against cancer cells *in vitro* and exhibited greater selectivity against cancer cells over normal cells than glutriptolide-1. Glutriptolide-2 was also found to have much greater stability in human serum. Unlike triptolide, glutriptolide-2 had little effect on the ATPase activity of TFIIH *in vitro*. Similar to triptolide, however, glutriptolide-2 inhibited the proliferation of multiple cancer cell lines, induced apoptosis, and caused degradation of the catalytic subunit of RNAPII in an XPB-dependent manner. Using glutriptolide-2 as a probe, we also investigated its effects on cancer cells under hypoxic conditions and found that glutriptolide-2 is more effective against cancer cells under hypoxic than normoxic conditions. In light of the key role of hypoxia in chemoresistance against almost all known anticancer drugs, our finding with glutriptolide-2 raised the exciting possibility of overcoming hypoxia-induced drug resistance through conjugation of drugs to glucose.

RESULTS

Design and Synthesis of Glutriptolide-2 as the Most Potent Inhibitor of Cancer Cell Proliferation among Glucose-Triptolide Conjugates

Glutriptolides can be divided into three structural components: glucose, triptolide, and a linker (Figure 1A). The first-generation glutriptolide-1 (G-1) contained a 4-carbon succinate linker, giving rise to an activation intermediate previously shown to be too toxic to be used in humans (Kitzen et al., 2009). We thus selected a series of alternative linkers to connect glucose and triptolide (Table S1). In brief, these linkers attached at the C2 position of glucose include γ-hydroxybutyric acid (Compound **G2-1**), addition of two methyl groups to the succinate backbone (compounds **G2-2** and **G2-3**), incorporation of a phenyl group to the succinate backbone (compounds **G2-4**, **G2-5**), and elongation of the succinate linker by one carbon (compounds **G2-6**, **G2-7**). In addition, we also synthesized two derivatives that contained a C6-substituted glucose with succinate linkers (compounds **G2-8**, **G2-9**). We then determined the potency of the newly synthesized glutriptolides in a HEK293T cell proliferation assay (Table S1). As expected, glutriptolides have lower potency than triptolide itself. Among the second-generation glutriptolide, **G2-1** is significantly more potent than glutriptolide-1 with an IC_{50} (71 nM) that is about 13-fold higher than that for triptolide (5.6 nM). The rest of the second-generation glutriptolide analogs were less potent than glutriptolide-1 except for **G2-8**. But unlike **G2-1**, **G2-8** would release the same toxic

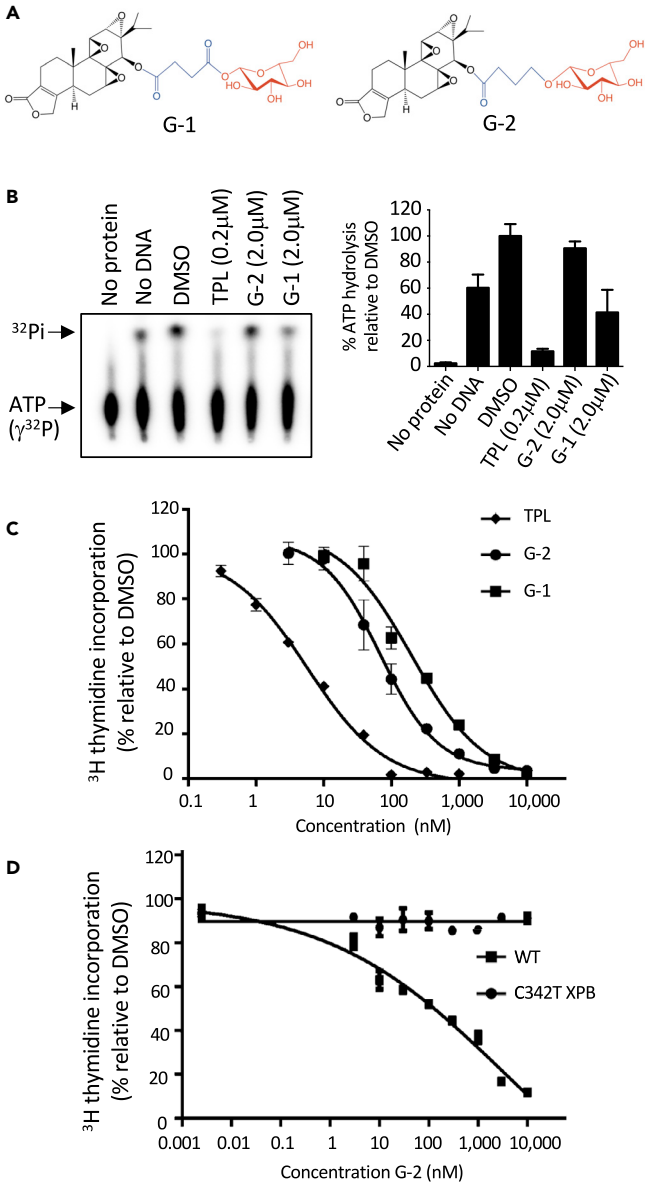

Figure 1. Glutriptolide-2 Is a Prodrug that Requires XPB Binding for Its Antiproliferative Effect

(A) Chemical structures of glutriptolides 1 (G-1) and 2 (G-2). Structural motifs in glutriptolides are highlighted (black = triptolide, blue = linker, and red = glucose).

(B) G-2 does not inhibit the ATPase activity of TFIIH *in vitro*, whereas triptolide (TPL) effectively suppresses activity at a 10-fold lower concentration. Data are represented as mean ± SE of released inorganic phosphate (^{32}Pi) relative to DMSO (n = 3).

(C) Treatment with G-2 (circle), G-1 (square), or TPL (diamond) inhibits cell proliferation after 24 h.

(D) The knock-in cell line for XPB expressing only the C342T XPB mutant is resistant to G-2 (circle), whereas inhibition of proliferation is observed in the isogenic cell line expressing WT (square) XPB. Proliferation was measured by ^{3}H thymidine incorporation and plotted using GraphPad prism. Data are represented as mean ± SEM relative to DMSO (n = 3).

triptolide-succinate intermediate upon activation as glutriptolide-1. Thus, the ensuing studies were focused on the characterization of **G2-1**, named hereafter as glutriptolide-2 (G-2).

G-2 Is a Prodrug that Inhibits Cell Proliferation in an XPB-Dependent Manner

A premise of our original design of glutriptolides is that these conjugates will serve as prodrugs with little inhibitory effect on XPB until they enter cancer cells where the linkers are cleaved by intracellular hydrolytic

enzymes to release active triptolide. We thus determined the effect of G-2 on the DNA-dependent ATPase activity of purified TFIIH using γ-[^{32}P]-ATP as a substrate. Upon hydrolysis, the released ^{32}Pi can be separated from the substrate using thin-layer chromatography and visualized with autoradiography. Although the ATPase activity of TFIIH is nearly completely inhibited by 200 nM triptolide, only a small fraction of the activity was affected by 2 μM G-2 (Figure 1B). Although G-2 has negligible effect on the ATPase activity of recombinant TFIIH, it inhibited HEK293T cell proliferation in a dose-dependent manner, being more potent than G-1 (Figure 1C and Table S1). These observations suggest that G-2 is an inactive pro-drug and can be activated inside cells. To determine if the antiproliferative effect of G-2 is mediated through inhibition of XPB, we took advantage of an engineered mutant cell line T7115 that encodes a single allele of C342T XPB mutant, which was previously shown to be resistant to triptolide (Figure S1) (He et al., 2015, 2016). Although the wild-type (WT) 293T cells were inhibited by G-2 in a dose-dependent manner, the isogenic T7115 mutant line is resistant to G-2, suggesting that G-2 works through inhibition of XPB, necessitating the intracellular hydrolytic release of triptolide from G-2 (Figure 1D).

G-2 has Greater Stability in Human Serum and Higher Selectivity for Cancer Cells over Normal Cells Than G-1

For glutriptolides to achieve selectivity toward glucose transporter (GLUT)-overexpressing cancer cells over their normal counterparts, it is imperative that they have sufficiently long half-lives in serum to reduce the amount of free triptolide released in blood prior to their entry into tumor cells. We determined the stability of G-1 and G-2 by incubating them with human serum and detecting the release of free triptolide. Although G-1 underwent degradation to produce the triptolide-succinate intermediate by 4 h with appreciable amount of free triptolide generated by 48 h (Figures 2A and 2B), G-2 remained largely intact after incubation in human serum for up to 72 h (Figure 2A). These results suggest that G-2 is considerably more stable than G-1 in human serum.

To compare the selectivity of G-2 and G-1 for cancer cells, we determined their IC_{50} values for inhibition of cell viability using a panel of normal primary cells, including human umbilical vascular endothelial cell (HUVEC), mammary epithelial cell (MEC), prostate epithelial cell (PEC), renal proximal tubule (RPT), airway epithelial cell (AEC), fibroblasts, and astrocytes. The IC_{50} values of G-2 ranged from 4 μM to 10.9 μM for the primary cells, which is significantly higher than those for cancer cell lines that ranged from 0.26 μM to 6.5 μM (with the exception of a liver cell line SNU-387 and lung cell line NCI- H1299) (Figure 2C, Table S2). This represents a significant improvement over G-1 that had lower IC_{50} values for each primary cell type and comparable IC_{50} values for most cancer cell lines (Figure S2 and Table S2). We also note that cancer cell lines seem to segregate in their sensitivity to G-2 and G-1 according to tissue or organ origin. With the limited number of cancer cell lines tested, prostate and breast cancer cells appear to be more sensitive than liver and lung cancer cells (Figure 2C, Table S2).

G-2 Causes Degradation of the Catalytic RPB1 Subunit of RNAPII through Interaction with XPB

We and others have previously shown that triptolide induced the degradation of the catalytic RPB1 subunit of RNAPII (Manzo et al., 2012; Titov et al., 2011; Wang et al., 2011), which is one of the hallmark cellular effects of triptolide. Using immunostaining, we observed that G-2 also caused the degradation of RPB1 in HeLa cells (Figure 3A). Aside from triptolide, a known steroidal drug spironolactone (SP) has been reported to bind XPB (Elinoff et al., 2018). Unlike triptolide, however, SP induces proteasome-mediated degradation of XPB without overt cellular toxicity. At 10 μM, SP caused degradation of the majority of XPB (Figure S3A) but had no effect on the stability of RPB1 (Figure 3A). To determine whether depletion of XPB by SP antagonizes the degradation of RPB1 by triptolide released from glutriptolide, we treated cells with a combination of 1 μM G-2 and 10 μM SP. Co-treatment with SP rescued RPB1 from degradation induced by G-2. Similar results were obtained using western blot analysis to detect endogenous levels of RPB1 protein (Figure 3B). To further confirm that RPB1 degradation induced by G-2 required binding of released triptolide to XPB, we determined the level of RPB1 upon treatment of both WT and C342T mutant cell lines. Although degradation of RPB1 was observed in the presence of G-2 in WT cells (Figure 3B), RPB1 level remained stable even when the concentration of G-2 reached 3 μM in the C342T XPB mutant cell line (Figure 3C). This result corroborates with observations made with SP and triptolide (Figure S3B), suggesting that the degradation of RPB1 induced by G-2 requires the covalent binding of released triptolide from G-2 to XPB.

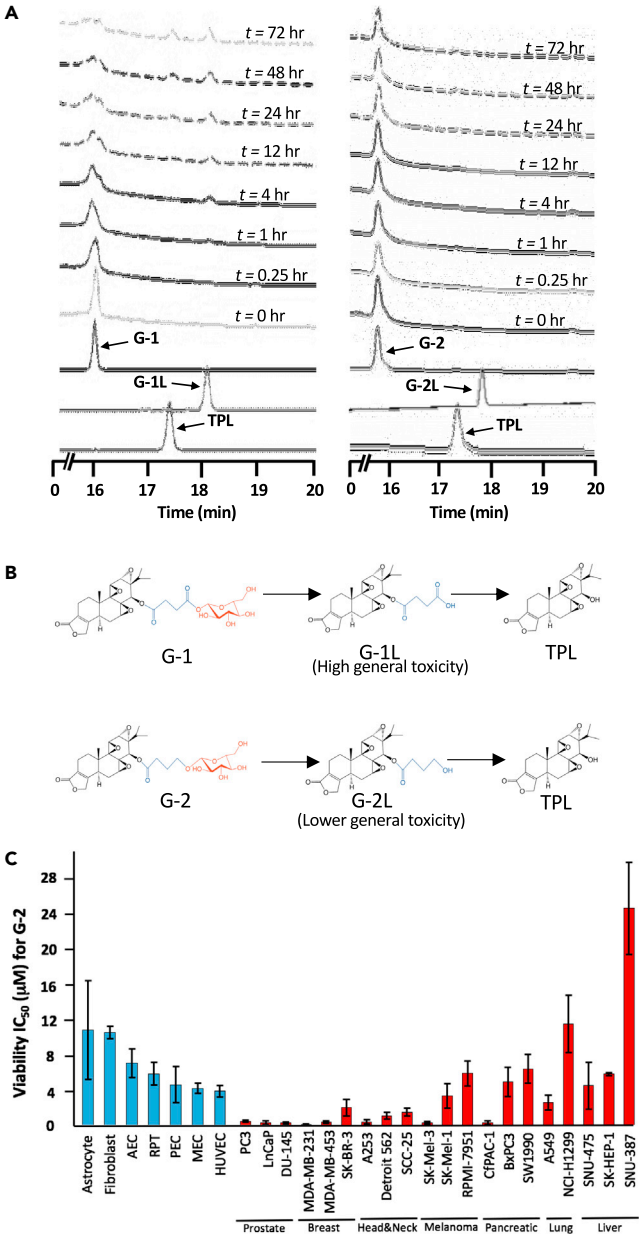

Figure 2. Glutriptolide-2 Possesses Increased Stability in Human Serum and Lower General Toxicity toward Nonmalignant, Primary Cells Relative to G-1

(A) Hydrolysis of G-1 and G-2 at different incubation times in human serum as monitored by tandem HPLC-MS. Chromatograms were taken at A_{218}.

(B) Chemical structures of G-1 and G-2 with hydrolysis intermediates G-1L and G-2L that subsequently releases triptolide (TPL). Structural motifs in glutriptolides are highlighted (black = triptolide, blue = linker, and red = glucose).

(C) Primary cell viability as measured by XTT assay exhibits reduced sensitivity to G-2 in comparison to multiple cancer cell lines. Liver, lung, melanoma, and pancreatic cancer cell lines respond poorly to G-2 treatment. HUVEC = Human Umbilical Vascular Endothelial Cell, MEC = Mammary Epithelial Cell, PEC = Prostate Epithelial Cell, RPT = Renal Proximal Tubule, AEC = Airway Epithelial Cell. Data are represented as mean ± SEM viability relative to DMSO (n = 3–7).

G-2 Induces Apoptosis of Cancer Cells via Activation of the Mitochondria-Mediated Apoptosis Pathway

Triptolide is known to induce apoptosis in a number of cancer cell lines (Zhou et al., 2012). We investigated the cellular effects of G-2 by examining the cellular morphology of HeLa cells upon exposure to G-2. G-2

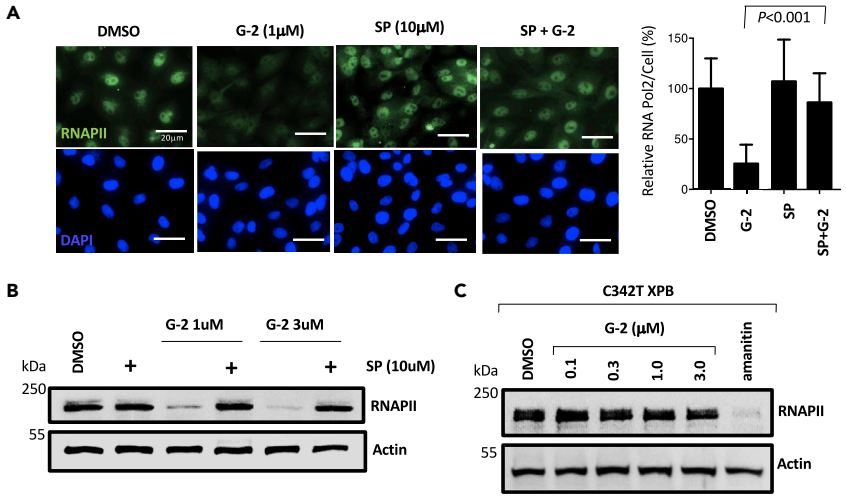

Figure 3. Glutriptolide-2-Induced RNA Polymerase 2 Degradation is XPB Dependent

(A) Treatment with 1 μM G-2 for 24 h depletes endogenous RNA polymerase II (RNAPII), whereas 10 μM spironolactone (SP) or DMSO by themselves do not affect protein levels in fixed HeLa cells processed for immunocytochemical staining of RPB1 (catalytic subunit of RNAPII) and DAPI (nuclear marker). Pre-treatment of cells with 10 μM spironolactone significantly ($P < 0.001$) rescues endogenous RNAPII from G-2-induced degradation. Representative images of RPB1 and DAPI staining are shown with quantification of intracellular RPB1 and student's t test analysis. Data are represented as mean ± SE RPB1 levels relative to DMSO ($n = 3$).

(B) Whole cell lysates of cells treated with G-2, SP, or in combination were subjected to western blot analysis of endogenous RNAPII using antibodies specific for RPB1 showing that G-2 induced RNAPII degradation at 1 or 3 μM is antagonized by 10 μM SP.

(C) Whole cell lysates from isogenic knock-in cells expressing only C342T XPB show that degradation of the catalytic subunit of RNAPII by G-2 as measured by immunoblotting for RPB1 is inhibited in the absence of WT XPB. In contrast, the RPB1-interacting inhibitor α-amanitin induced the degradation of Rpb1 at 1μM in the C342T XPB isogenic cell line. Actin was used as a loading control. Scale bar, 20 μm.

caused membrane blebbing and nuclear fragmentation indicative of apoptosis (Figure 4A). The percentage of cells with nuclear fragmentation increased from 6% to 23% in the presence of 1 μM G-2 and 53% upon treatment with 3 μM G-2. G-2 induced the release of cytochrome *c* from the mitochondria into the cytosol, a key step in the activation of the intrinsic apoptotic pathway (Figure 4B). As expected, G-2 activated caspase-3 dose dependently, which was accompanied by cleavage of PARP1 (Figure 4C). Similar to RPB1 degradation, the cleavage of PARP1 requires XPB, as co-treatment with higher concentrations of SP prevented PARP1 cleavage by caspase-3 (Figure 4D). Together, these results suggest that G-2 activated the mitochondria-mediated apoptotic pathway through induction of cytochrome *c* release and ensuing activation of caspase-3 in HeLa cells.

G-2 Showed Sustained Inhibition of Tumor Growth and Prolonged Survival *In Vivo*

We have previously shown that G-1 exhibited sustained antitumor activity *in vivo* in an experimental metastatic prostate cancer mouse model (He et al., 2016). Using the same animal model, we assessed the antitumor efficacy of G-2 side by side with G-1. Thus, PC3 prostate cancer cells expressing firefly luciferase as a reporter were injected into animals through the tail vein. Three weeks after tumor cell injection, G-2 and G-1 were administered by intraperitoneal injection once daily at various doses for a total of 30 days. The growth of tumor cells was monitored weekly through bioluminescence imaging. A rapid growth of tumor cells and metastasis to other organs occurred in untreated animals, killing all untreated animals by week 4 (Figure 5A). For animals dosed with 1 mg/kg G-1, tumor cells were cleared by week 2 of treatment and did not return until two weeks after treatment was stopped (Figure 5A). In contrast, animals receiving the same dose of G-2 had undetectable levels of cancer cells two weeks after cessation of treatment, suggesting that G-2 is more effective than G-1 *in vivo* (Figure 5A). Although G-2 and G-1 were administered for only 30 days, they both significantly prolonged the survival of animals well beyond the four-week treatment window (Figure 5B). Moreover, the prolonged survival upon treatment with G-2 was dose dependent with the longest survival achieved by the highest dose of G-2 (26 days for untreated group versus 86 days for 1 mg/kg G-2 treatment group). Furthermore, chi-square analysis shows that the survival curve for 1 mg/kg G-1 is not

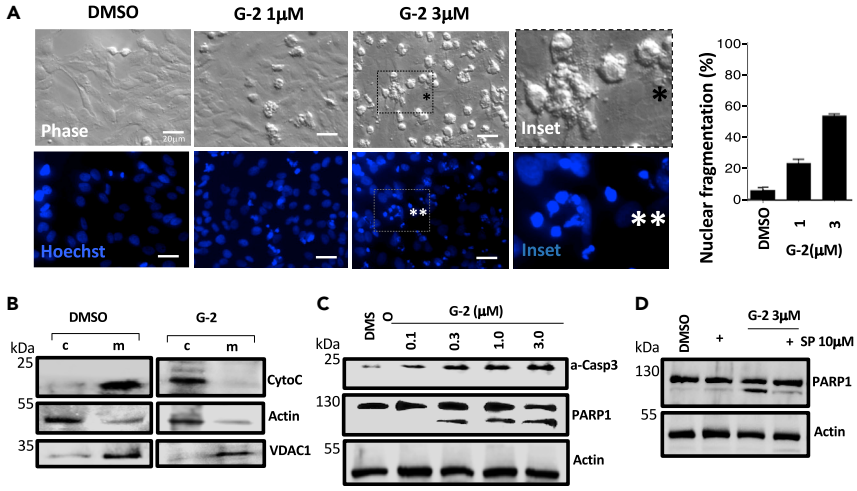

Figure 4. Glutriptolide-2 Induces Apoptosis Signaling

(A) Bright phase micrographs show minimal cytopathology with DMSO exposure in contrast to G-2 treatments especially with 3 μM G-2 where numerous cells round up and bleb (inset with black asterisk). Nuclear fragmentation, as detected by cytochemical analysis using Hoechst 33258 stain, in round up HeLa cells is dramatically increased by G-2 treatment (inset with two white asterisks) but not in DMSO. Data are represented as percentage of nuclear fragmented cells relative to total cells ±SE (n = 3).

(B) Cytochrome *c* release during G-2 treatment was assessed by centrifugal separation of mitochondria followed by western blot analysis using cytochrome-*c*-specific antibody. Exposure of HeLa cells to 3 μM G-2 triggers the release of cytochrome *c* from the mitochondria (m) to the cytosol (c). Actin- and VDAC1-specific antibodies were used to ensure the efficiency of cytoplasm and mitochondria fractionation, respectively.

(C) Western blot analysis of whole cell lysates for active caspase 3 (a-Casp3) and PARP1 during G-2 treatment shows a dose-dependent increase in caspase 3 activation. Pronounced PARP1 cleavage by active caspase 3 is also observed with increasing concentrations of G-2.

(D) Degradation of XPB in cells by 10 μM spironolactone dampens G-2-induced apoptosis signaling as indicated by reduced PARP1 cleavage in whole cell lysates subjected to western blot analysis. Actin was used as loading control. Scale bar, 20 μm.

significantly different from 0.5 mg/kg G-2 (cannot reject null hypothesis at p = 0.05). In contrast, the survival curve for G-2 at 1 mg/kg is significantly different from G-1 at the same dose (reject null hypothesis at p = 0.001). G-2 given at 0.5 mg/kg led to the same overall survival as G-1 at 1 mg/kg, consistent with the higher potency of G-2 in tumor cell lines than G-1 *in vitro*.

G-2 Is More Effective against Cancer Cells under Hypoxic Than Normoxic Conditions

The tumor microenvironment is hypoxic due to the lack of sufficient blood vessel density in rapidly growing tumors. As such, tumor cells upregulate the expression of HIF-1, which in turn drives the expression of a number of pro-survival and proangiogenic factors including multidrug resistance (*MDR*) pumps and *GLUTs* (Semenza, 2003, 2010). The upregulation of MDR and GLUTs under hypoxia renders tumor cells resistant to chemotherapeutic drugs (Tredan et al., 2007). Interestingly, the upregulation of glucose transporters under hypoxia should make cancer cells more susceptible to G-2 due to the presence of the glucose moiety. To test this possibility, we determined the effect of hypoxia on the sensitivity of cancer cells to G-2 using the prostate cancer cell line PC3 because increased HIF-1α has been shown in metastatic prostate biopsies (Semenza, 2010). Thus, PC3 cells were cultured under either hypoxic (1% O_2) or normoxic (20% O_2) conditions. As expected, HIF-1α is absent under normoxic conditions but is dramatically induced under hypoxia (Figure 6A). Western blot analysis of endogenous HIF-1α revealed a similar increase in HIF-1α with a corresponding increase in GLUT1 levels (Figure 6B). Uptake of the chromogenic glucose analogue 2-NBDG also increased under hypoxia. Importantly, PC3 cells became more sensitive to G-2 under hypoxic conditions with a reduced IC_{50} of 81 nM from an IC_{50} of 427 nM under normoxic conditions (Figure 6C), whereas the IC_{50} for triptolide was modestly reduced from 4.5 nM to 1.5 nM upon switching from normoxia to hypoxia. The same trend of enhanced susceptibility to G-2 under hypoxia was also observed with HeLa and MDA MB231 (Figure S4). In contrast to G-2, the potency of doxorubicin was decreased under hypoxia (Figure 6C). Degradation of RNAPII, an indicator of inhibition of XPB by triptolide (Figure 3), was observed as early as 6 h after treatment with G-2 under hypoxic but not in normoxic conditions

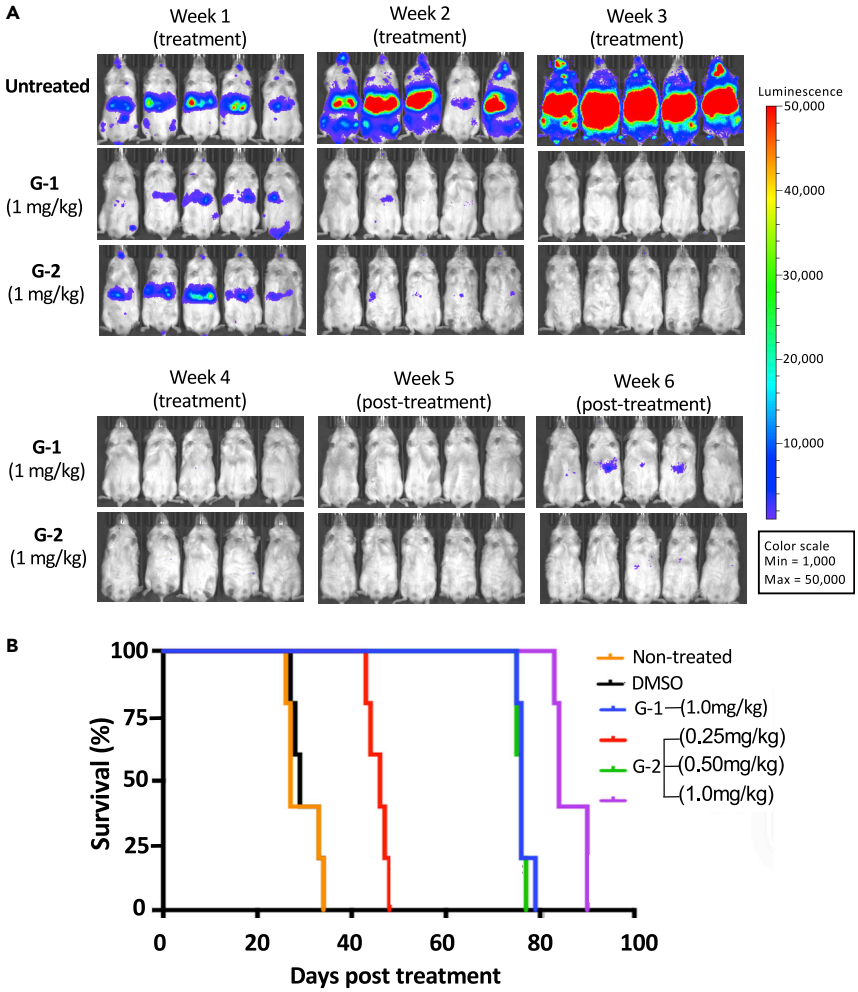

Figure 5. Glutriptolide-2 Improves Survival in an *In-Vivo* Prostate Cancer Model

(A) G-2 and G-1 have similar maximum tolerable dose (MTD) in a metastatic prostate cancer model. After confirmation of tumor growth in NOD/SCID/IL2r^{null} mice by bioluminescence imaging, daily administration of 1 mg/kg G-1 or G-2 for 30 days was tolerated by animals and able to suppress tumor growth throughout the treatment. Anti-tumor effect by G-1 or G-2 persists 2 weeks posttreatment.

(B) Kaplan-Meier curves showing survival time (days after initiation of treatments [n = 5]) for controls, G-1, or G-2 treatments. Median survival times (days) are as follows: nontreated = 27, DMSO = 29, G-1 (1mg/kg) = 76, G-2 (0.25mg/kg) = 46, G-2 (0.5mg/kg) = 76, G-2 (1mg/kg) = 84.

(Figure 6D) where G-2 induced degradation of RPB1 also occurs in an XPB-dependent manner (Figure 3). To verify whether this difference in sensitivity was due to the upregulation of GLUT1 levels and function under hypoxic conditions (Figure 6B), we utilized the GLUT1 inhibitor WZB117 (Ojelabi et al., 2016). The addition of the GLUT inhibitor WZB117 abolished the rapid degradation of endogenous RNAPII in PC3 cells by G-2 under hypoxic (1% O_2) conditions (Figure 6E), indicating that GLUT1 upregulation during hypoxia contributes to the rapid degradation of endogenous RNAPII by G-2 under hypoxic conditions. To further assess the role of GLUT1 upregulation in hypoxia-induced sensitization to G-2, we examined the effects of G-2 on the proliferation of both WT DLD-1 and its isogenic GLUT1 knockout cell line under normoxic (20% oxygen) and hypoxic (1% oxygen) conditions. The WT DLD-1 cells are more sensitive to G-2 (IC_{50}: 1.3 μM) than the GLUT1 knockout cell line under hypoxic conditions (IC_{50}: 2.5 μM), indicating GLUT1 dependence of hypoxia-induced sensitization to G-2 (Figure 6F). In contrast, no difference in sensitivity was observed between DLD-1 WT and GLUT1 KO under normoxia. Together, these results reveal that in contrast to most existing anticancer agents (Tredan et al., 2007), G-2 is more effective against tumor cells under hypoxia, making it a unique anticancer agent with potentially enhanced anti-tumor activity *in vivo*.

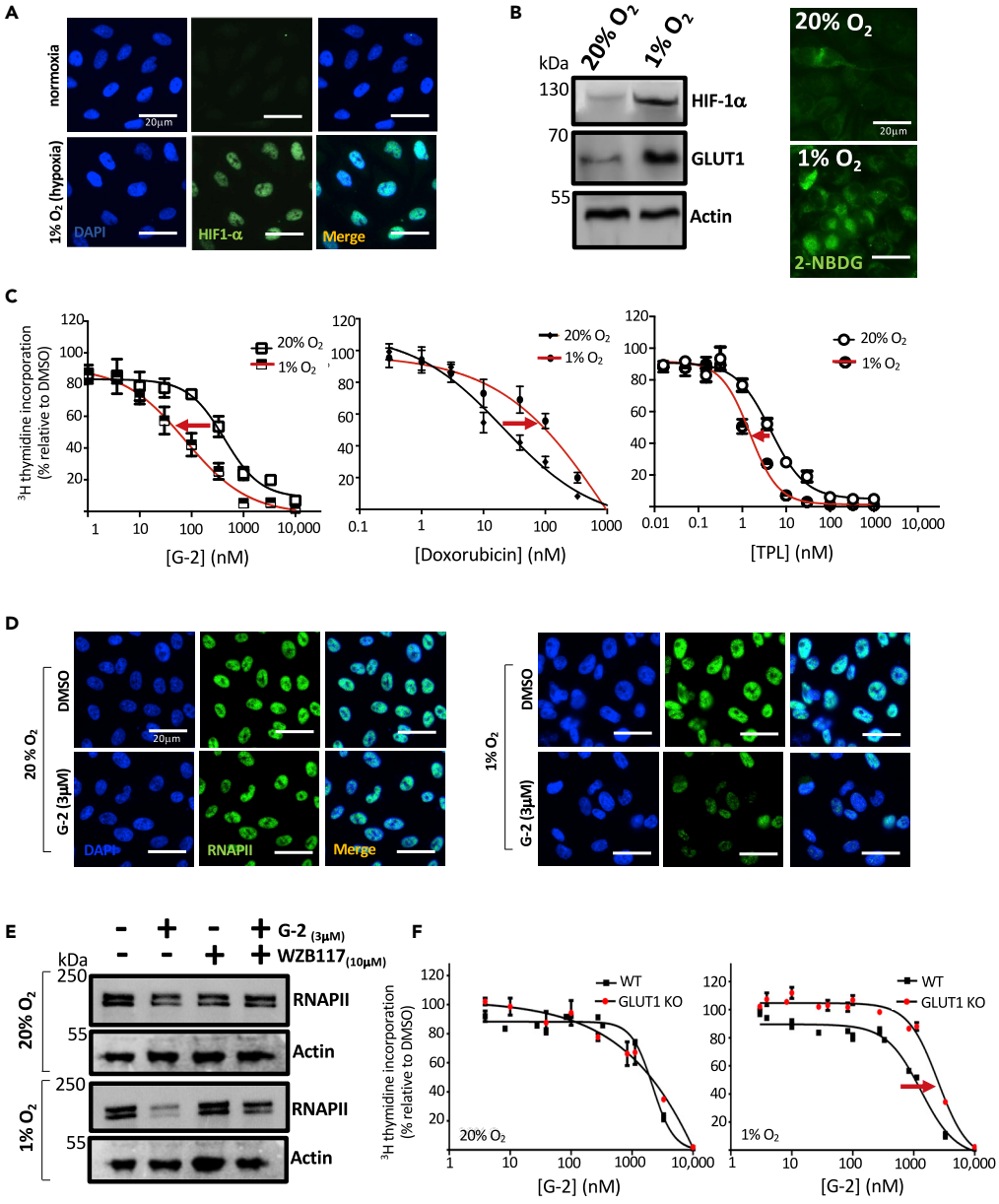

Figure 6. Hypoxia Enhances Antiproliferative Effect of Glutriptolide-2

(A) Immunocytochemical analysis of fixed cells using antibodies specific to HIF-1α show that exposure to hypoxia (1% O_2) for 24 h stabilizes endogenous HIF-1α compared with normoxia (20% O_2) in PC3 cells.

(B) Western blot analysis of whole cell lysates for endogenous HIF-1α shows an increase during hypoxia compared with normoxia, which also corresponds with an increase in glucose transporter 1 (GLUT1).

(C) Hypoxia enhances the antiproliferative effect of G-2 at 48 h posttreatment as measured by ^{3}H thymidine incorporation, whereas co-treatment with doxorubicin and hypoxia reduces drug potency. Triptolide (*TPL*) shows a modest antiproliferative effect. Data are represented as mean ± SE relative to DMSO (n = 3).

(D) Immunocytochemistry using antibody specific to RPB1 shows that exposure of cells to hypoxia triggers an early onset of RNAPII subunit RPB1 degradation by 3 μM glutriptolide-2 after 6 h.

(E) Whole cell lysates subjected to western blot using anti-RPB1-specific antibody shows that 10 μM glucose transporter 1 inhibitor WZB117 antagonizes the early onset of RNAPII degradation triggered by 3 μM G-2 and hypoxia.

(F) DLD-1 WT cells exposed to hypoxia exhibited enhanced sensitivity to G-2 in comparison to DLD-1 GLUT1 knockout (GLUT1 KO) cells. No difference in sensitivity is observed between DLD-1 WT and GLUT1 KO under normoxia. Data are represented as mean ± SEM relative to DMSO (n = 3). Scale bar, 20 μm.

DISCUSSION

Most cytotoxic anticancer drugs, including those that are currently used in the clinic such as taxol, doxorubicin, and cyclophosphamide exert their antiproliferative and proapoptotic effects on cancer cells by blocking essential cellular protein targets that are shared with normal cells. As such, it is not surprising that those chemotherapeutic agents have severe adverse effects on patients. Transcription mediated by RNAPII is essential for mammalian cell proliferation and growth. As such, it is not surprising that cancer cells are susceptible to triptolide that blocks RNAPII-mediated mRNA synthesis through covalent modification of XPB/TFIIH accompanied by induced degradation of RPB1 catalytic subunit of RNAPII (Titov et al., 2011) in an XPB-dependent manner (Figure S3B). The toxicity of triptolide can also be attributed to the same mechanism given the essential role of RNAPII-mediated transcription in normal cells, making it difficult to reduce the toxicity of triptolide without compromising its antitumor efficacy given the shared molecular mechanism. By conjugating triptolide to glucose, selectivity toward cancer cells was achieved by taking advantage of the higher levels of glucose transporters expressed in fast-growing tumor cells than most normal tissues. In the present study, we have identified a second-generation glutriptolide analog, G-2, that met our expectations with significantly enhanced selectivity for tumor cells over normal cells, improved serum stability, and sustained antitumor activity in a PC-3 tumor model. Importantly, in the course of characterizing G-2, we found that G-2 gained antitumor potency under hypoxia in contrast to conventional cytotoxic drugs *in vitro*, pointing to an emerging strategy of overcoming drug resistance during cancer treatment.

The best lead of the second-generation glutriptolide called G-2 is superior to the first-generation compound G-1 in a number of ways. First, degradation of G-1 by plasma esterases produces a highly toxic intermediate that was previously proven lethal to two of twenty subjects in a phase 1 clinical trial (Kitzen et al., 2009). Although the mechanistic basis of the toxicity for the G-1 intermediate is still unknown, our data from a limited number of primary human cells indicate a significantly lower toxicity for G-2 in comparison with G-1 in noncancerous cells (Figure S2). The reported toxicity for the G-1 intermediate occurred in two patients receiving the highest dose of therapy, suggesting dose-limiting toxicity (Kitzen et al., 2009). Maximum serum levels of F60008 and triptolide from the lethal case dosed with 18 mg/m^2 were 1,361 ng/mL (~2.96 μM) and 58.5 ng/mL (~0.16 μM), respectively (Kitzen et al., 2009). Our cell-based viability assays with primary human cells show IC_{50} values for G-1 ranging from 1.37 to 5.6 μM (Figure S2 and Table S2), which includes the above-reported plasma concentration of F60008 in the lethal case with 18 mg/m^2 F60008. We have also shown previously using a smaller panel of primary human cells that the IC_{50} of triptolide ranges from 0.0042 to 0.0235 μM (He et al., 2016), which is 7- to 38-fold lower than the maximum serum concentration of triptolide from the lethal case. In summary, the toxicities observed with G-1 intermediate F60008 are in part dose dependent as no lethality was observed in 18 of the 20 patients administered with <12 mg/m^2 F60008 (Kitzen et al., 2009). By replacing the ester linkage to glucose with a glycosidic bond, the potential intermediate will be an alcohol that is expected to have less toxicity. More importantly, given the much greater stability of G-2 in human serum than G-1, the amount of this alcohol degradation intermediate is expected to be significantly reduced, further reducing the potential toxicity of G-2 (Figure 2A). Second, G-2 exhibited greater stability in human serum than G-1 (Figure 2A). This is likely attributable to the glycosidic linkage between the linker and glucose moieties that requires a different type of hydrolytic enzyme(s) than the corresponding ester bond in G-1. The increase in serum stability makes G-2 a potentially better lead for drug development as it is a prodrug, and premature degradation in serum would release free triptolide that can exert toxicity to normal tissues. Third, G-2 showed lower cytotoxicity to normal cells than to a subset of cancer cells (Figure 2C). It is interesting to note that different types of cancer lines exhibited distinct sensitivity. Among the limited cancer cell lines tested, it appears that prostate, breast, and head and neck cancers are particularly sensitive to G-2. In contrast, melanoma, pancreatic, lung, and liver cancer lines appear to be less sensitive to G-2 with an average IC_{50} values comparable or even higher than normal cells. Extensive profiling of a large number of cancer cell lines and collections of cultured patient-derived tumor cells will be needed to comprehensively determine whether the selective toxicity of G-2 to certain types of cancer such as those of the prostate holds true.

Aside from its unique anticancer activity *in vitro*, G-2 also exhibited sustained antitumor activity in a PC3 xenograft model *in vivo* (Figure 5). Cancer cells failed to re-emerge two weeks after treatment with G-2 ceased but not with G-1. The slower reappearance of cancer cells after treatment with G-2 than G-1 is also consistent with longer survival in G-2-treated animals. G-2 at 0.5 mg/kg was as effective as G-1 at 1 mg/kg in prolonging the survival of xenograft model animals *in vivo*. The greater serum stability, the lower

cytotoxicity toward normal cells compared with a subset of cancer cells, and the increased efficacy toward cancer cells under hypoxia along with sustained antitumor activity of G-2 *in vivo* render this glutriptolide analogue an interesting example of a promising lead candidate for further development as a type of anticancer drug targeting transcription.

The microenvironment of solid tumors is known to be hypoxic, and hypoxia has been shown to confer resistance in tumor cells against cytotoxic anticancer drugs (Semenza, 2003; Tredan et al., 2007), which is a major hurdle for cancer therapy. As hypoxia is known to upregulate GLUT expression on the cancer cell surface and given that GLUTs confer the tumor cell selectivity of glutriptolides, we investigated the effect of hypoxia on the potency of G-2. The increase in potency of G-2 for inhibition of cancer cell proliferation during hypoxia contrasts the decrease in potency of the broadly used, FDA-approved, anticancer drug doxorubicin (Figures 6C and S4). This feature of G-2 as an anticancer drug candidate offers an additional advantage of being more effective toward cancer cells under hypoxia where other conventional anticancer drugs encounter resistance. It is also interesting to note that unlike doxorubicin, triptolide itself also showed a modest enhancement, rather than reduction, in its inhibitory effect on cancer cell growth under hypoxic conditions. This may be attributed in part to its inhibition of the transcriptional activity of HIF-1 that requires TFIIH and RNAPII. Because hypoxia involves the transcription of genes to adapt the survival of cancer cells to a hypoxic condition, the ability of triptolide to inhibit mammalian transcription initiation can dampen HIF-driven transcription of hypoxia-activated genes that facilitate the proliferation of cancer cells experiencing hypoxia. Treatment of cancer cells under hypoxia with triptolide inhibits the transcription of HIF-1α target genes VEGF, BNIP3, and CAIX, including a hypoxia responsive element (HRE)-driven luciferase reporter (Zhou et al., 2010). Triptolide treatment also reverses hypoxia-induced epithelial-mesenchymal transition (Liu et al., 2014) explaining the observed three-fold enhancement of triptolide's anti-proliferative effect *in vitro* (Figure 6C). The increased expression of GLUTs in cancer cells during hypoxia further amplifies the impact of transcription inhibition by G-2 on the proliferation of hypoxic cancer cells as seen with the five-fold increase in G-2 IC_{50} during hypoxia (Figure 6C). The conjugation of triptolide to glucose in G-2 enhances the effect size of triptolide during hypoxia from 0.71 during triptolide treatment alone to 64.89 in G-2-treated hypoxic PC3 cells. The GLUT1 dependence of enhanced G-2-induced anti-proliferation in hypoxic cancer cells is demonstrated in the reduced sensitivity of hypoxic DLD-1 GLUT1 knock out cells compared with parental DLD-1 cells (Figure 6F). Although the enhanced sensitivity to glucose-conjugated triptolide G-2 under hypoxia was also observed in HeLa and triple-negative breast cancer cell line MDA MB231 (Figure S4), this effect is not observed in all the cell lines tested, as the liver cancer cell line HepG2 remains resistant to G-2 under hypoxia. Despite the apparent tissue-specific sensitivity of cancer cells to G-2, our results suggest that conjugation of potent, nonspecific antiproliferative agents to glucose offers a promising strategy for targeting cancer cells in hypoxic conditions such as those in solid tumors. This finding offers an alternative albeit viable strategy to combat hypoxia-induced drug resistance in solid tumors through conjugation of cytotoxic drugs to glucose.

To summarize, triptolide is a key ingredient from a traditional Chinese medicinal plant that has been used for centuries. It possesses potent antitumor activity through irreversible inhibition of the XPB subunit of the general transcription factor TFIIH, effectively blocking transcription initiation. Its potential development as an anticancer drug has been limited by its toxicity and insolubility in water. In an attempt to address these issues, we have designed and synthesized glucose conjugates of triptolide exhibiting lower toxicity and sustained antitumor activity *in vivo*. However, the previous lead glutriptolide releases a potentially toxic degradation intermediate, rendering it unsuitable as a drug candidate. By using molecular linkers that connect triptolide to glucose, we identified a glutriptolide with enhanced stability in serum and reduced toxicity to normal cells. Importantly, glutriptolide G-2 is more potent against cancer cells under hypoxic conditions likely due to the upregulation of glucose transporters, in contrast to most cytotoxic anticancer drugs to which cancer cells gain resistance under hypoxia. G-2 showed sustained antitumor activity *in vivo* and significantly prolonged survival of treated animals. These findings suggest that conjugation of cytotoxic drugs to glucose may be a viable strategy to overcome drug resistance in general and that glutriptolide-2 is a promising candidate for further development as a targeted, anticancer pro-drug.

Limitations of the Study

Although conjugation of the cytotoxic natural product triptolide to glucose led to an increase in potency against cancer cells under hypoxia, the finding has been confined to *in vitro* studies. The observations

remain to be verified *in vivo*. Further investigation of the underlying mechanism involved in enhanced sensitivity of hypoxic tumor cells to glucose-conjugated cytotoxic agents *in vivo* will help establish glucose conjugation as a viable strategy to enhance cancer cell targeting and overcome drug resistance under hypoxia.

Resource Availability

Lead Contact

Further information and requests for resources and reagents should be directed to and will be fulfilled by the Lead Contact, Jun O. Liu (joliu@jhu.edu).

Materials Availability

All unique/stable reagents generated in this study are available from the Lead Contact with a completed Materials Transfer Agreement.

Data and Code Availability

No large-scale datasets were generated in this study. Raw data are available from the lead contact upon request.

METHODS

All methods can be found in the accompanying Transparent Methods supplemental file.

SUPPLEMENTAL INFORMATION

Supplemental Information can be found online at https://doi.org/10.1016/j.isci.2020.101536.

ACKNOWLEDGMENTS

Financial support: This work was supported by the Flight Attendant Medical Research Institute, a generous gift from Mr. Shengjun Yan and Ms. Hongju Mao (J. O. L.); the Johns Hopkins Institute for Clinical and Translational Research (ICTR), which is funded in part by Grant Number UL1 TR 001079 and NCI (P30CA006973); and an NIH-funded Pharmacology Training Program at Johns Hopkins School of Medicine (T32 GM008763) (E.D.). We thank Dr. Ronald Schnaar, Mr. Steve Fernandez, and Ms. August Li for training and access to imaging equipment. We also thank Drs. Sarah A. Head, Jennifer Schmitt, Shaima Salman, Yongmie Xie, Wukun Liu, Hanjing Peng, and Zufeng Guo for technical advice and assistance. We are also grateful to Drs. Gregg Semenza and Shaima Salman for helpful suggestions.

AUTHORS CONTRIBUTIONS

J.O.L. coordinated and supervised the study. J.O.L., M.G.P., and B.Y. initiated the work. E.D. performed the *in vitro* XPB/TFIIH ATPase activity assay, cell proliferation assay, metabolic labeling, western blot analyses, immunocytochemical and cytochemical assays, and hypoxia experiments. I.M. performed the *in vivo* animal studies while I.M. and H.A. performed the *in vitro* viability experiments. P.X. has synthesized, purified, and characterized the glutriptolide analogues. Q.L.H. performed the serum stability assays and generated the knock-in C342T XPB cell line. J.O.L., E.D., I.M., Q.L.H., and M.G.P. analyzed the data. E.D. and J.O.L. wrote the manuscript with input from all coauthors.

DECLARATION OF INTERESTS

A patent covering glutriptolides has been licensed from Johns Hopkins to Rapafusyn Pharmaceuticals, of which J.O.L. is a cofounder and an equity owner. The potential conflict of interest is being managed by Johns Hopkins University. No potential conflicts of interest were disclosed by the other authors.

Received: September 30, 2019
Revised: March 1, 2020
Accepted: September 2, 2020
Published: September 25, 2020

REFERENCES

Bensaude, O. (2011). Inhibiting eukaryotic transcription: which compound to choose? How to evaluate its activity? Transcription *2*, 103–108.

Bhat, M., Robichaud, N., Hulea, L., Sonenberg, N., Pelletier, J., and Topisirovic, I. (2015). Targeting the translation machinery in cancer. Nat. Rev. Drug Discov. *14*, 261–278.

Chugh, R., Sangwan, V., Patil, S.P., Dudeja, V., Dawra, R.K., Banerjee, S., Schumacher, R.J., Blazar, B.R., Georg, G.I., Vickers, S.M., et al. (2012). A preclinical evaluation of Minnelide as a therapeutic agent against pancreatic cancer. Sci. Transl. Med. *4*, 156ra139.

Corson, T.W., Cavga, H., Aberle, N., and Crews, C.M. (2011). Triptolide directly inhibits dCTP pyrophosphatase. Chembiochem *12*, 1767–1773.

Elinoff, J.M., Chen, L.Y., Dougherty, E.J., Awad, K.S., Wang, S., Biancotto, A., Siddiqui, A.H., Weir, N.A., Cai, R., Sun, J., et al. (2018). Spironolactone-induced degradation of the TFIIH core complex XPB subunit suppresses NF-kappaB and AP-1 signalling. Cardiovasc. Res. *114*, 65–76.

He, Q.L., Minn, I., Wang, Q., Xu, P., Head, S.A., Datan, E., Yu, B., Pomper, M.G., and Liu, J.O. (2016). Targeted delivery and sustained antitumor activity of triptolide through glucose conjugation. Angew. Chem. Int. Ed. *55*, 12035–12039.

He, Q.L., Titov, D.V., Li, J., Tan, M., Ye, Z., Zhao, Y., Romo, D., and Liu, J.O. (2015). Covalent modification of a cysteine residue in the XPB subunit of the general transcription factor TFIIH through single epoxide cleavage of the transcription inhibitor triptolide. Angew. Chem. Int. Ed. *54*, 1859–1863.

Kitzen, J.J., de Jonge, M.J., Lamers, C.H., Eskens, F.A., van der Biessen, D., van Doorn, L., Ter Steeg, J., Brandely, M., Puozzo, C., and Verweij, J. (2009). Phase I dose-escalation study of F60008, a novel apoptosis inducer, in Patients with Advanced Solid Tumours. Eur. J. Cancer *45*, 1764–1772.

Leuenroth, S.J., Okuhara, D., Shotwell, J.D., Markowitz, G.S., Yu, Z., Somlo, S., and Crews, C.M. (2007). Triptolide is a traditional Chinese medicine-derived inhibitor of polycystic kidney disease. Proc. Natl. Acad. Sci. U S A *104*, 4389–4394.

Lipsky, P.E., and Tao, X.L. (1997). A potential new treatment for rheumatoid arthritis: thunder god vine. Semin. Arthritis Rheum. *26*, 713–723.

Liu, L., Salnikov, A.V., Bauer, N., Aleksandrowicz, E., Labsch, S., Nwaeburu, C., Mattern, J., Gladkich, J., Schemmer, P., Werner, J., et al. (2014). Triptolide reverses hypoxia-induced epithelial-mesenchymal transition and stem-like features in pancreatic cancer by NF-κB downregulation. Int. J. Cancer *134*, 2489–2503.

Lu, Y., Zhang, Y., Li, L., Feng, X., Ding, S., Zheng, W., Li, J., and Shen, P. (2014). TAB1: a target of triptolide in macrophages. Chem. Biol. *21*, 246–256.

Manzo, S.G., Zhou, Z.L., Wang, Y.Q., Marinello, J., He, J.X., Li, Y.C., Ding, J., Capranico, G., and Miao, Z.H. (2012). Natural product triptolide mediates cancer cell death by triggering CDK7-dependent degradation of RNA polymerase II. Cancer Res. *72*, 5363–5373.

McClary, B., Zinshteyn, B., Meyer, M., Jouanneau, M., Pellegrino, S., Yusupova, G., Schuller, A., Reyes, J.C.P., Lu, J., Guo, Z., et al. (2017). Inhibition of eukaryotic translation by the antitumor natural product Agelastatin A. Cell Chem. Biol. *24*, 605–613.e605.

Ojelabi, O.A., Lloyd, K.P., Simon, A.H., De Zutter, J.K., and Carruthers, A. (2016). WZB117 (2-Fluoro-6-(m-hydroxybenzoyloxy) phenyl m-hydroxybenzoate) inhibits GLUT1-mediated sugar transport by binding reversibly at the exofacial sugar binding site. J. Biol. Chem. *291*, 26762–26772.

Semenza, G.L. (2003). Targeting HIF-1 for cancer therapy. Nat. Rev. Cancer *3*, 721–732.

Semenza, G.L. (2010). HIF-1: upstream and downstream of cancer metabolism. Curr. Opin. Genet. Dev. *20*, 51–56.

Smurnyy, Y., Cai, M., Wu, H., McWhinnie, E., Tallarico, J.A., Yang, Y., and Feng, Y. (2014). DNA sequencing and CRISPR-Cas9 gene editing for target validation in mammalian cells. Nat. Chem. Biol. *10*, 623–625.

Soundararajan, R., Sayat, R., Robertson, G.S., and Marignani, P.A. (2009). Triptolide: an inhibitor of a disintegrin and metalloproteinase 10 (ADAM10) in cancer cells. Cancer Biol. Ther. *8*, 2054–2062.

Titov, D.V., Gilman, B., He, Q.L., Bhat, S., Low, W.K., Dang, Y., Smeaton, M., Demain, A.L., Miller, P.S., Kugel, J.F., et al. (2011). XPB, a subunit of TFIIH, is a target of the natural product triptolide. Nat. Chem. Biol. *7*, 182–188.

Tredan, O., Galmarini, C.M., Patel, K., and Tannock, I.F. (2007). Drug resistance and the solid tumor microenvironment. J. Natl. Cancer Inst. *99*, 1441–1454.

Wang, L., Xu, Y., Fu, L., Li, Y., and Lou, L. (2012). (5R)-5-hydroxytriptolide (LLDT-8), a novel immunosuppressant in clinical trials, exhibits potent antitumor activity via transcription inhibition. Cancer Lett. *324*, 75–82.

Wang, Y., Lu, J.J., He, L., and Yu, Q. (2011). Triptolide (TPL) inhibits global transcription by inducing proteasome-dependent degradation of RNA polymerase II (Pol II). PLoS One *6*, e23993.

Westerheide, S.D., Kawahara, T.L., Orton, K., and Morimoto, R.I. (2006). Triptolide, an inhibitor of the human heat shock response that enhances stress-induced cell death. J. Biol. Chem. *281*, 9616–9622.

Zhao, X.-M. (1765). Supplement to Materia Medica (China Zhang's Jie Xing Tang Pulishing House).

Zhou, R., Zhang, F., He, P.L., Zhou, W.L., Wu, Q.L., Xu, J.Y., Zhou, Y., Tang, W., Li, X.Y., Yang, Y.F., et al. (2005). (5R)-5-hydroxytriptolide (LLDT-8), a novel triptolide analog mediates immunosuppressive effects in vitro and in vivo. Int. Immunopharmacol. *5*, 1895–1903.

Zhou, Z., Luo, Z., Yu, B., Jiang, Y., Chen, Y., Feng, J., Dai, M., Tong, L., Li, Z., Li, Y., et al. (2010). Increased accumulation of hypoxia-inducible factor-1α with reduced transcriptional activity mediates the antitumor effect of triptolide. Mol. Cancer *9*, 268.

Zhou, Z.L., Yang, Y.X., Ding, J., Li, Y.C., and Miao, Z.H. (2012). Triptolide: structural modifications, structure-activity relationships, bioactivities, clinical development and mechanisms. Nat. Prod. Rep. *29*, 457–475.

iScience, Volume *23*

Supplemental Information

A Glucose-Triptolide Conjugate Selectively Targets Cancer Cells under Hypoxia

Emmanuel Datan, Il Minn, Peng Xu, Qing-Li He, Hye-Hyun Ahn, Biao Yu, Martin G. Pomper, and Jun O. Liu

Supplemental Information

Supplemental data

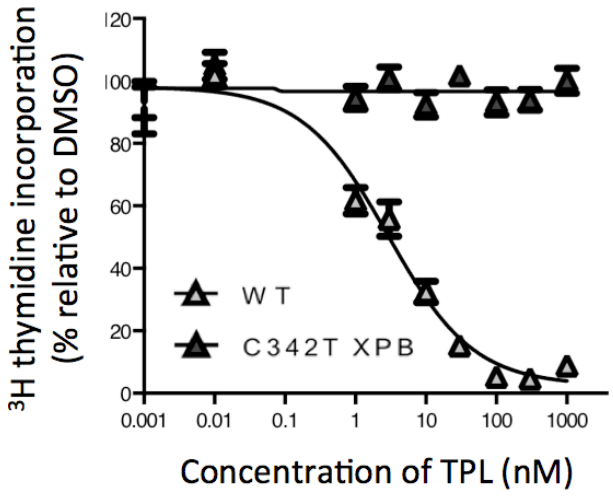

Figure S1 (related to Figure 1). XPB C342T mutation leads to resistance to triptolide. Expression of mutant XPB C342T in the knock-in cell line T7115 (dark gray triangle) leads to triptolide resistance but not in the isogenic cell line expressing wild type XPB (gray triangle). Proliferation was measured by ^{3}H thymidine incorporation and plotted using GraphPad prism. Data represents mean ± SEM relative to DMSO (*n* = 3).

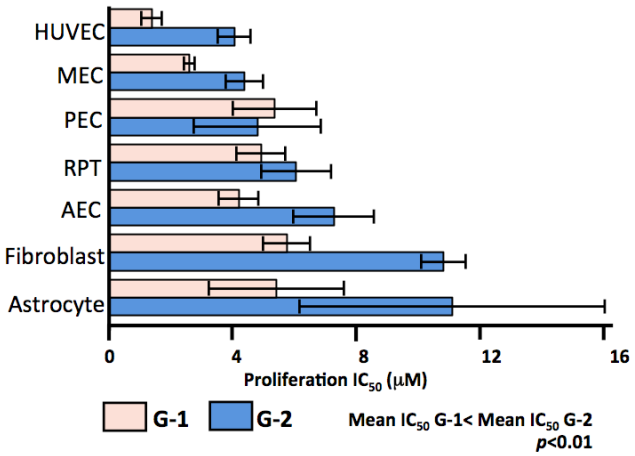

Figure S2 (related to Figure 2). G-2 is less toxic than G-1 in primary cells. Primary cells show increased sensitivity to G-1 in comparison to G-2 as measured by XTT viability assay. Mean IC_{50} for G-1 is significantly lower than mean IC_{50} for G-2, $p < 0.01$. HUVEC = Human Umbilical Vascular Endothelial Cell, MEC = Mammary Epithelial Cell, PEC = Prostate Epithelial Cell, RPT = Renal Proximal Tubule, AEC = Airway Epithelial Cell. Data represents mean ± SEM viability relative to DMSO (n = 3-7).

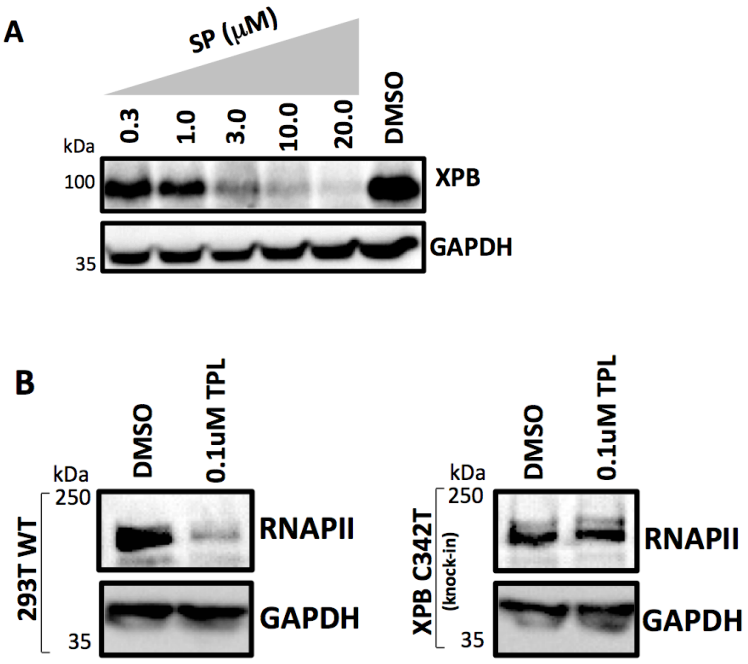

Figure S3 (related to Figure 3). Spironolactone degrades XPB while triptolide requires wild type XPB for the degradation of Rpb1. (**A**) Whole cell lysates of cells treated with increasing concentrations of spironolactone (SP) were subjected to western blot analysis using antibodies specific for XPB shows that spironolactone induces the degradation of endogenous XPB in cells in a dose dependent manner. (**B**) Isogenic cells with wild type (293T WT) or triptolide resistant mutant (XPB C342T) XPB were treated with 0.1 mM triptolide then lysed for western blot analysis using anti-Rpb1 specific antibodies. Treatment with triptolide leads to the degradation of the Rpb1 subunit of RNAPII degradation in WT XPB cells in contrast to triptolide exposed cells with XPB C342T mutation where Rpb1 levels resemble DMSO control. GAPDH was used a loading control.

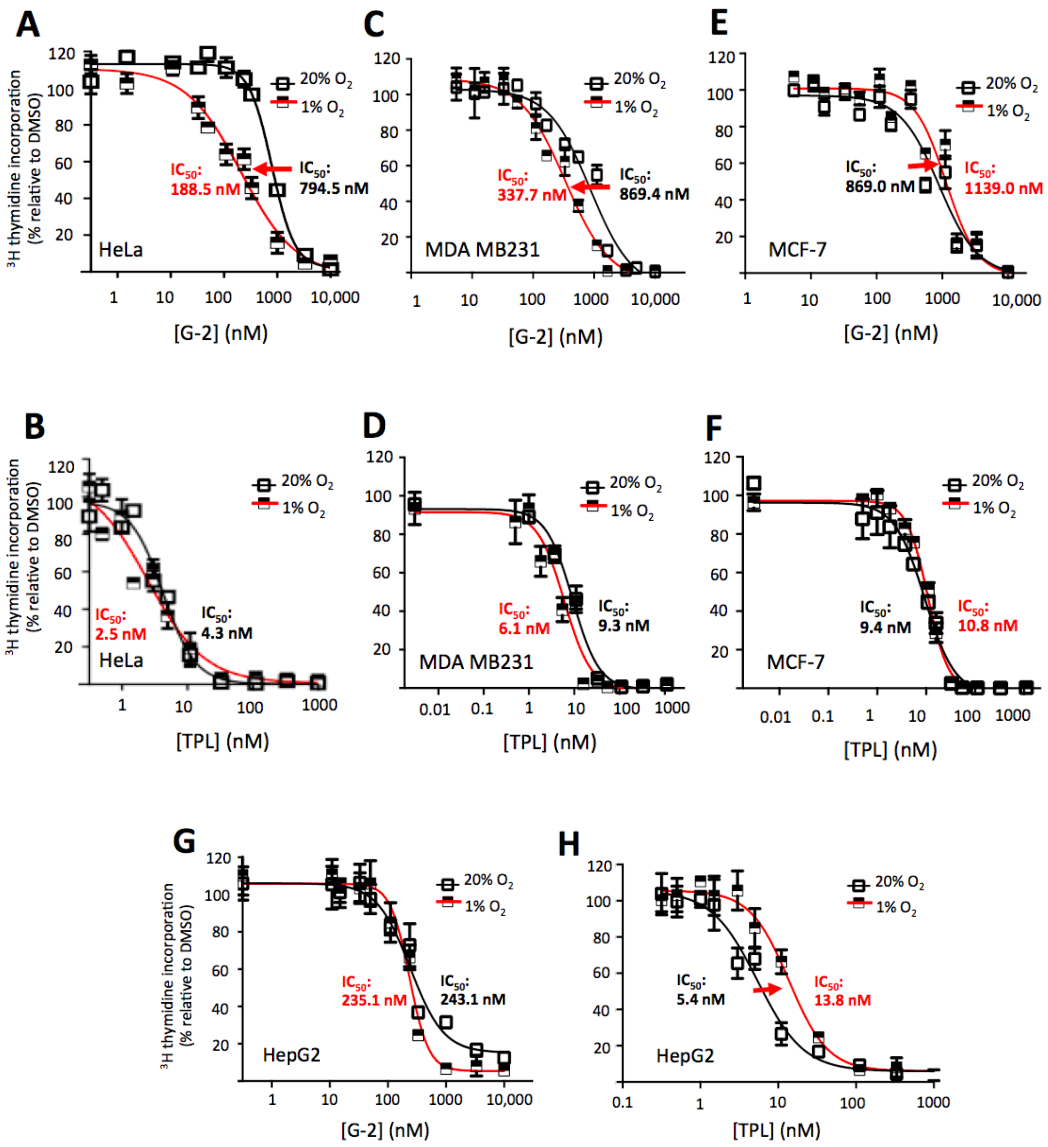

Figure S4 (related to Figure 5). Hypoxia affects sensitivity of cancer cells to glutriptolide-2. Exposure of HeLa (**A**) and MDA MB231 cells (**B**) to a hypoxic environment enhances the anti-proliferative effect of glutriptolide-2 (G-2) at 48 h post treatment as measured by ^{3}H thymidine incorporation in contrast to MCF-7 (**E**) or HepG2 (**G**) where modest enhancement or resistance is observed during hypoxia. Triptolide (*TPL*) shows modest anti-proliferative effect in all cells tested except HepG2 that showed resistance upon hypoxia. Proliferation was measured by ^{3}H thymidine incorporation and plotted using GraphPad prism. Data represents mean ± SEM relative to DMSO (n = 3).

Table S1 (related to Figure 1). Chemical structures of glucose-conjugated triptolides and their antiproliferative activities against HEK 293T cells.

Entry	Structure	IC50 ±SEM(nM)	Entry	Structure	IC50 ±SEM(nM)
TPL	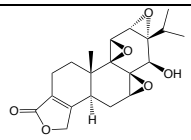	5.6 (±0.415)	G2-5	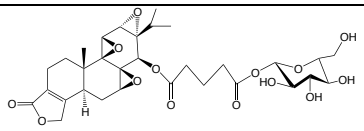	1134 (±0.1.15)
G1	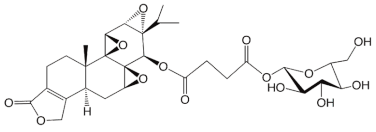	279 (±0.611)	G2-6	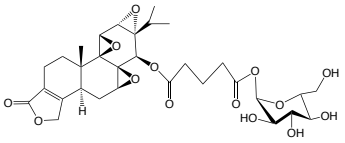	735 (±0.1.11)
G2-1	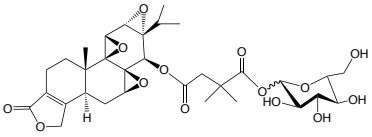	3305 (±0.980)	G2-7	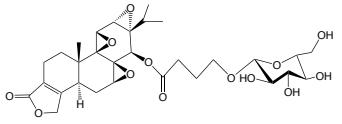	71 (±0.1.07)
G2-2	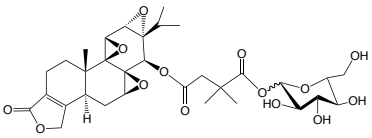	999 (±0.2.17)	G2-8	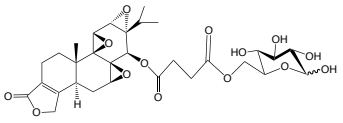	244 (±0.810)
G2-3	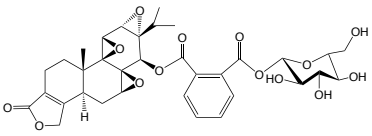	5888 (±0.1.19)	G2-9	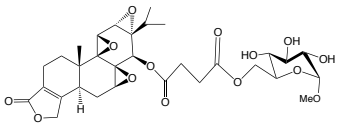	395 (±0.523)
G2-4	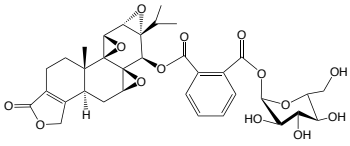	6667 (±0.2.03)			

Note: Data represents mean ± SEM relative to DMSO (*n* = 3).

Table S2 (related to Figure 2). Bioactivities of G-1 and G-2 in cancer and primary cells.

Cancer cell line		G2 IC_{50} (μM)	G9 IC_{50} (μM)
Prostate Cancer	PC3	0.50±0.10	0.61±0.18
	LNCaP	0.56±0.09	0.45±0.33
	DU-145	0.40±0.13	0.44±0.19
Breast Cancer	MDA-MB-231	0.28±0.01	0.26±0.10
	MDA-MB-453	0.53±0.20	0.53±0.28
	SK-BR-3	1.30±1.84	2.16±1.59
Head and Neck Cancer	A253	0.71±0.47	0.54±0.40
	Detroit 562	1.42±0.83	1.24±0.61
	SCC-25	1.26±0.99	1.63±0.78
Melanoma	SK-Mel-3	0.42±0.34	0.44±0.25
	SK-Mel-1	1.29±0.47	3.44±2.36
	RPMI-7951	2.67±1.34	5.95±2.45
Pancreatic Cancer	CfPAC-1	0.51±0.35	0.47±0.32
	BxPC3	4.15±0.18	5.00±2.83
	SW1990	1.52±0.33	6.48±2.79
Lung Cancer	A549	1.70±0.79	2.72±1.41
	NCI-H1299	6.40±2.43	11.49±5.51
	NCI-H1437	N/A	N/A
Liver Cancer	SNU-475	3.85±3.26	4.60±4.55
	SK-HEP-1	3.38±0.71	5.90±0.28
	SNU-387	15.51±9.28	24.43±8.90

Primary cells		G2 IC_{50} (μM)	G9 IC_{50} (μM)
Normal Cells	Astrocyte	5.31±4.29	10.88±9.66
	Fibroblast	5.64±1.28	10.61±1.22
	Airway Epithelial cell	4.12±1.39	7.13±2.84
	Renal Proximal Tubule	4.83±1.54	5.94±2.21
	Prostate Epithelial cell	5.27±2.29	4.72±3.48
	Mammary Epithelial cell	2.56±0.29	4.31±1.03
	HUVEC	1.37±0.73	3.98±1.15

Cell type	Average IC_{50} (μM)	
	G2	G9
Cancer cell lines (n = 21)	2.42±2.00	3.94±3.26
- Sensitive lines (n = 8)	0.49±0.07	0.47±0.06
- Less sensitive lines (n = 13)	3.70±2.33	6.25±3.68
Non-malignant cells	4.16±0.93	6.80±1.67

Sample comparison T-test[a]	P value[b]
Cancer cells G2 vs G9 (ALL)	0.373
- Sensitive lines	0.513
- Less sensitive lines	0.007
Primary cells G2 vs G9	0.009

Note: Sensitive cell lines (black) have IC50 < 1 μM while less sensitive cancer cell lines (red) have IC50 > 1 μM. Mean IC50 values and their standard deviation from three independent experiments are shown. N/A indicates not applicable due to absence of sigmoidal response in dose curve. Data represents mean ± SEM relative to DMSO (*n* = 3).

[a] Student T-test done with unequal variance.

[b] P values of IC50s for G-1 versus G-2.

Supplemental Schemes

Scheme S1. Reagents and conditions for synthesis of glutriptolide G1, Related to Figure 1.

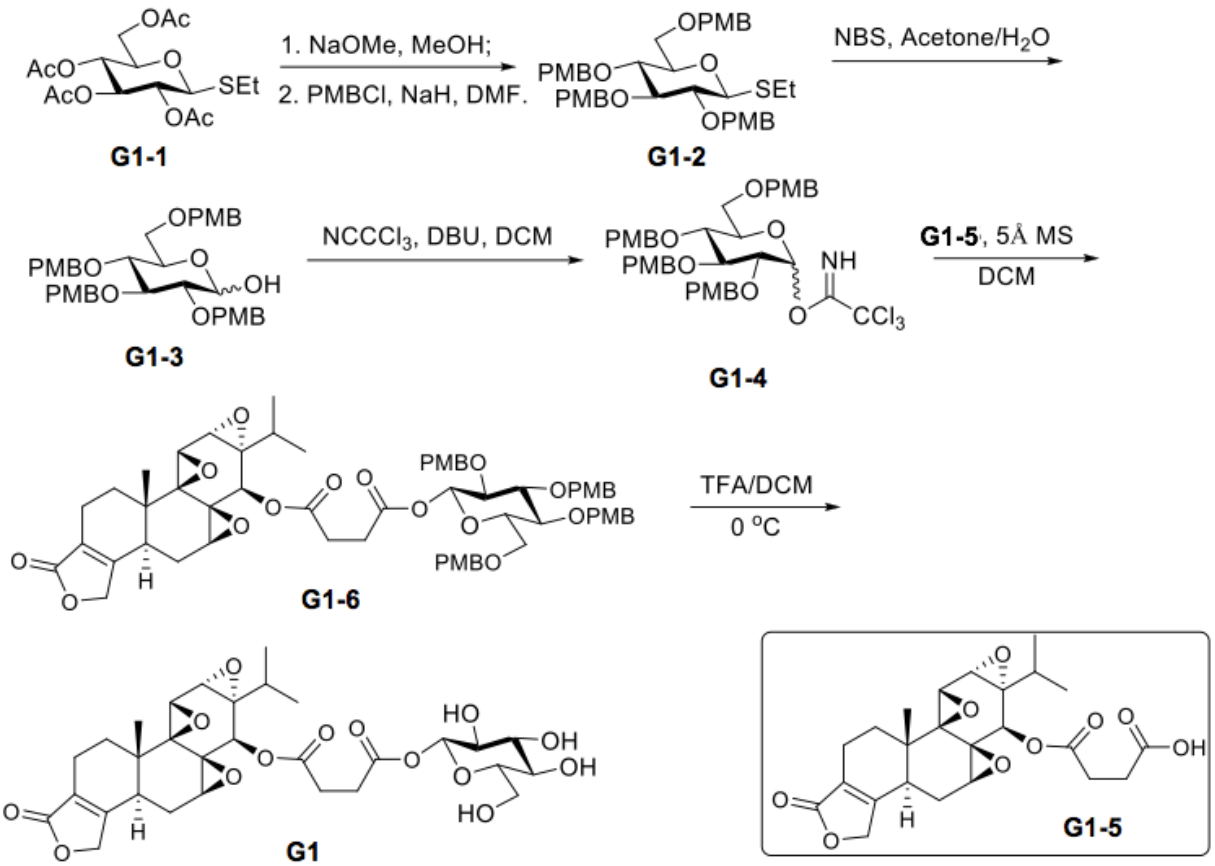

Procedures for synthesis of glutriptolide G1, Related to Figure 1.

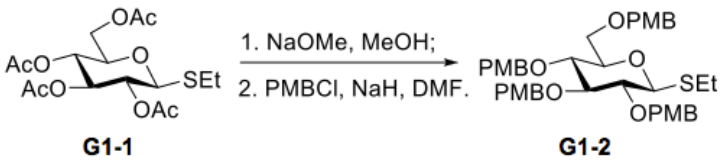

To a solution of Compound **G1-1**[1] (2.1 g, 5.3 mmol) in methanol (20 mL), was added NaOMe (29 mg, 0.5 mmol). Stirring was continued until complete conversion of the starting material

(monitored by TLC, about 2 hours). The mixture was neutralized with acidic resin, filtered and concentrated. Then the mixture was coevaporated with toluene three times and dried *in vacuo*.

The mixture was dissolved in dry DMF (27 mL), and cooled to 0 °C. NaH (1.28 g, 60% suspension, 32.1 mmol) was added slowly over 5 min. After 10 min, PMBCl (5.8 mL, 42.8 mmol) was added and the reaction stirred for another 10 min, at which time the temperature was raised to room temperature for 4 h. The reaction was re-cooled to 0 °C and water was added to quench the reaction. The organic layer was diluted with ethyl acetate, and washed twice with water, once with brine, dried over Na_2SO_4. Then, the mixture was filtered and concentrated. Column chromatography (Petroleum ether/Ethyl acetate = 4/1) afforded the product **G1-2** as a white solid (3.4 g, 4.8 mmol, 91% for two steps); ESI-MS *m/z* calcd for $C_{40}H_{48}O_9Na$ $[M+Na]^+$ 727.2911, found 727.2919.

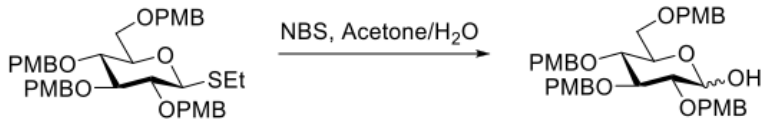

G1-2 **G1-3**

The thioglycoside **G1-2** (3.0 g, 4.25 mmol) was dissolved in acetone (50 mL) and water (5 mL), and cooled to 0 °C. N-bromosuccinimide (1.9 g, 10.7 mmol) was added which produced a bright orange color. Stirring was continued at 0 °C until TLC indicated disappearance of the starting material (about 1 h). The reaction was concentrated, then dissolved in ethyl acetate and washed with water and brine. The organic layers were dried over Na_2SO_4. Then, the mixture was filtered and concentrated. Column chromatography (Petroleum ether/Ethyl acetate = 2/1 to 1/1) afforded the product **G1-3** as a white solid (1.95 g, 3.0 mmol, 71%). ESI-MS (*m/z*): 683.6 $[M+Na]^+$.

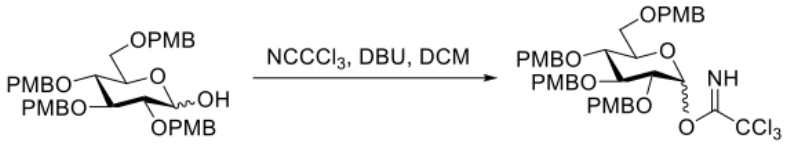

G1-3 **G1-4**

The lactol **G1-3** (380 mg, 0.58) was dissolved in CH_2Cl_2 (5 mL) and cooled to 0 °C. Trichloroacetonitrile (0.3 mL, 2.88 mmol) and DBU (cat.) were added successively. After stirring at room temperature for about 2 h, the reaction mixture was concentrated *in vacuo*. The residue was chromatographed over silica gel (Petroleum ether/EtOAc = 4:1, containing 1% Et_3N) to

yield imidate **G1-4** (400 mg, 86 %) as a colorless oil. ^{1}H NMR (400 MHz, $CDCl_3$) δ 8.57 (s, 1H), 7.42 – 6.69 (m, 16H), 6.47 (d, J = 3.4 Hz, 1H), 4.87 (d, J = 10.6 Hz, 1H), 4.79 – 4.71 (m, 2H), 4.66 (d, J = 11.3 Hz, 1H), 4.60 (d, J = 11.3 Hz, 1H), 4.56 (d, J = 11.7 Hz, 1H), 4.40 (d, J = 2.9 Hz, 1H), 4.37 (d, J = 4.4 Hz, 1H), 4.03 – 3.89 (m, 2H), 3.80 (s, 3H), 3.79 (s, 3H), 3.78 (s, 3H), 3.76 (s, 3H), 3.75 – 3.66 (m, 3H), 3.60 (dd, J = 10.8, 2.1 Hz, 1H).

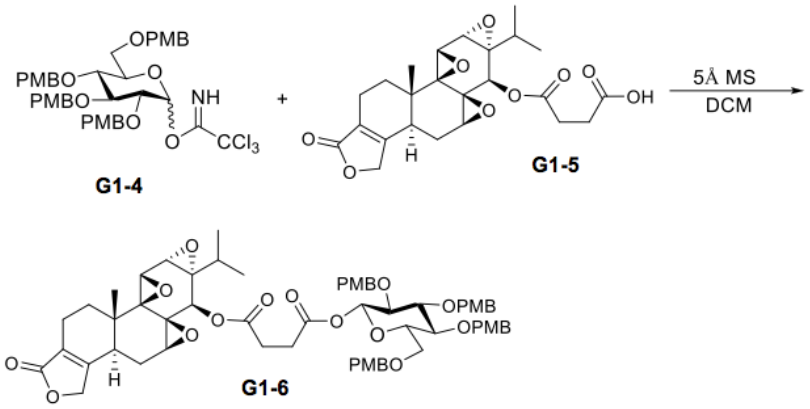

Trichloroacetimidate donor **G1-4** (2.7 g, 3.35 mmol) and acid **G1-5** (1.03g, 2.24 mmol) were dissolved in CH_2Cl_2 (100 mL) under nitrogen. Powdered freshly activated 5Å molecular sieves (200 mg) were added. Stirring was continued until TLC indicated the disappearance of the donor (about 8 h). The mixture was filtered through Celite, and the filtrated was concentrated in vacuum. The residue was purified by silica gel column chromatography (petroleum ether/EtOAc, 1:1) to give compound **G1-6** (2.43 g, 2.2 mmol, 98%) as a white solid. ^{1}H NMR (400 MHz, $CDCl_3$) δ 7.42 – 6.71 (m, 16H), 5.58 (d, J = 8.0 Hz, 1H), 5.08 (s, 1H), 4.93 – 4.50 (m, 9H), 4.46 – 4.26 (m, 2H), 3.74 – 3.26 (m, 10H), 2.72 (m, 6H), 1.04 (s, 3H), 0.95 (d, J = 7.0 Hz, 3H), 0.83 (d, J = 6.9 Hz, 3H); ^{13}C NMR (100 MHz, $CDCl_3$) δ 173.43, 171.55, 170.70, 160.18, 159.36, 159.29, 130.72, 130.37, 130.27, 130.03, 129.81, 129.67, 129.62, 129.56, 125.66, 113.90, 113.86, 94.49, 84.57, 80.68, 75.60, 75.44, 74.70, 73.17, 71.44, 70.11, 67.65, 63.61, 63.41, 61.28, 59.72, 55.45, 55.37, 55.32, 55.08, 40.44, 35.74, 29.90, 29.22, 28.95, 28.00, 23.50, 17.58, 17.13, 16.79, 13.85; ESI-MS m/z calcd for $C_{62}H_{70}O_{18}Na$ $[M+Na]^+$ 1125.4454, found 1125.4471.

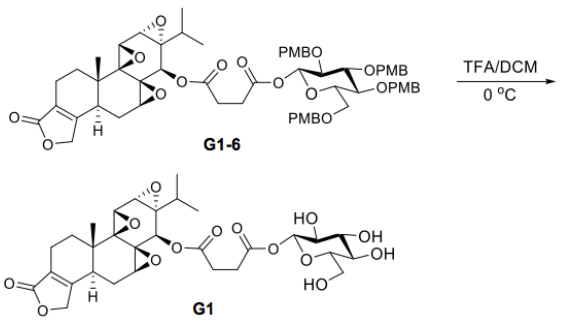

Compound **G1-6** (2.0 g, 1.81 mmol) was dissolved in DCM (36.0 mL), and cooled to 0 °C. Then TFA (3.6 mL) was added. After stirring at this temperature for about 10 min, the reaction mixture was concentrated *in vacuo*. The residue was chromatographed over silica gel (DCM/Methanol = 10:1) to yield the product **G1** (1.1 g, 1.77 mmol, 98%) as a white solid. ^{1}H NMR (500 MHz, CD_3OD) δ 5.54 – 5.43 (d, J = 8.0, 1H), 5.08 (s, 1H), 3.97 (d, J = 3.1 Hz, 1H), 3.90 – 3.77 (m, 1H), 3.68 (dd, J = 12.0, 4.4 Hz, 1H), 3.64 (d, J = 2.7 Hz, 1H), 3.48 (d, J = 5.7 Hz, 1H), 3.46 – 3.35 (m, 4H), 2.85 – 2.67 (m, 4H), 2.39 – 2.18 (m, 2H), 2.07 (m, 1H), 1.91 (m, 2H), 1.50 (dd, J = 12.4, 4.9 Hz, 1H), 1.34 (td, J = 12.1, 5.8 Hz, 1H), 1.03 (s, 3H), 0.93 (d, J = 7.0 Hz, 3H), 0.84 (d, J = 6.9 Hz, 3H);); ^{13}C NMR (125 MHz, CD_3CN) δ 174.53, 172.51, 172.04, 162.45, 125.25, 94.96, 76.48, 73.09, 72.68, 71.29, 64.56, 63.91, 62.65, 62.33, 60.67, 56.37, 55.70, 41.05, 36.46, 30.50, 29.67, 29.48, 28.78, 23.75, 17.88, 17.72, 17.11, 14.29; ESI-MS *m/z* calcd for $C_{30}H_{38}O_{14}Na$ $[M+Na]^+$ 645.2154, found 645.2166.

Scheme S2. Synthetic route of Glutriptolide G2-2 and G2-3, Related to Figure 1.

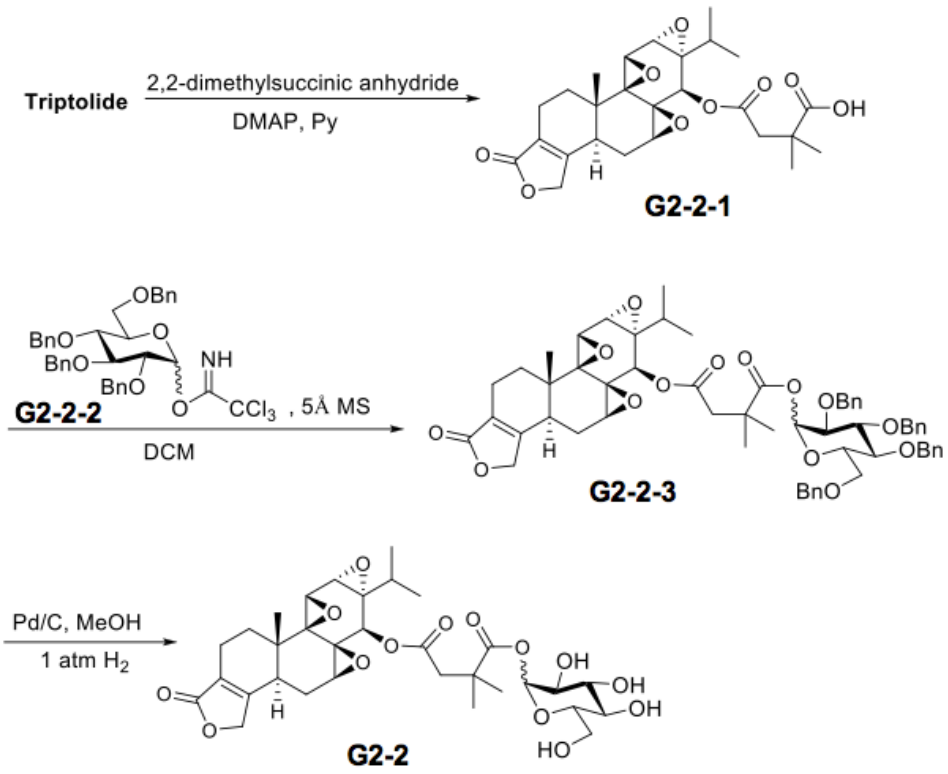

Synthetic procedures for Glutriptolide G2-2 and G2-3, Related to Figure 1.

To a solution of Triptolide (200 mg, 0.56 mmol) in pyridine (4 mL) were added 2,2-dimethylsuccinic anhydride (285 mg, 2.22 mmol) and DMAP (14 mg, 0.11 mmol). After stirring overnight, the mixture was diluted with ethyl acetate, then washed with saturated copper sulfate, water and brine, respectively. The organic layers were dried over Na_2SO_4 and filtered. The filtrate was concentrated using a rotary evaporator to give a residue. The residue was purified by silica gel column chromatography (CH_2Cl_2/CH_3OH, 15:1) to give compound **G2-2-1** (215 mg, 0.44 mmol, 80%) as a white solid; ^{1}H NMR (400 MHz, $CDCl_3$) δ 5.07 (s, 1H), 4.68 (s, 2H), 3.81 (d, J = 3.1 Hz, 1H), 3.53 (d, J = 2.7 Hz, 1H), 3.45 (d, J = 5.6 Hz, 1H), 2.71 (dd, J = 23.2, 7.1 Hz, 4H), 2.32 (d, J = 16.4 Hz, 1H), 2.15 (ddd, J = 25.7, 15.9, 10.0 Hz, 2H), 2.00 – 1.81 (m, 2H), 1.37 (s, 3H), 1.35 (s, 3H), 1.23 (dt, J = 11.6, 7.9 Hz, 3H), 1.05 (s, 3H), 0.94 (d, J = 6.9 Hz, 3H), 0.82 (d, J = 6.9 Hz, 3H); ESI-MS (*m/z*): 511.3 $[M+Na]^+$.

Trichloroacetimidate donor **G2-2-2** (100 mg, 0.15 mmol) and acid **G2-2-1** (49 mg, 0.1 mmol) were dissolved in CH_2Cl_2 (2 mL) under nitrogen. Powdered freshly activated 5Å molecular sieves (200 mg) were added. Stirring was continued until TLC indicated the disappearance of the donor (about 8 h). The mixture was filtered through Celite, and the filtrated was concentrated in vacuum. The residue was purified by silica gel column chromatography

(petroleum ether/EtOAc, 2:1 to 1:1) to give the product **G2-2-3** (48 mg, 0.047 mmol, α/β = 1.1: 1.0, 47%) as a white solid.

Palladium on charcoal (10%, 10 mg) was added to a solution of compound **G2-2-3** (22 mg, 0.022 mmol) in CH_3OH. The mixture was placed under an atmosphere of hydrogen for about 4 h. The mixture was filtered and concentrated. The residue was purified by silica gel column chromatography (CH_2Cl_2/CH_3OH, 15:1) to give the product **G2-2** (10 mg, 0.015 mmol, α/β = 1.0: 1.0, 71%) as a white solid; ^{1}H NMR (400 MHz, CD_3OD) δ 6.11 (d, J = 3.7 Hz, 0.5H), 5.45 (d, J = 7.7 Hz, 0.5H), 5.07 (d, J = 4.3 Hz, 1H), 4.80 (dd, J = 19.6, 10.1 Hz, 2H), 3.96 (d, J = 3.0 Hz, 1H), 3.84 (d, J = 11.2 Hz, 1H), 3.80 – 3.59 (m, 4H), 3.56 (dd, J = 9.8, 3.7 Hz, 1H), 3.51 – 3.33 (m, 4H), 2.76 (p, J = 15.9 Hz, 3H), 2.33 – 2.16 (m, 2H), 2.02 (d, J = 47.8 Hz, 1H), 1.90 (ddt, J = 11.6, 9.3, 7.6 Hz, 2H), 1.50 (dd, J = 12.5, 4.6 Hz, 1H), 1.35 (d, J = 5.8 Hz, 6H), 1.03 (s, 3H), 0.94 (dd, J = 7.0, 2.0 Hz, 3H), 0.84 (d, J = 6.9 Hz, 3H) ; ESI-MS *m/z* calcd for $C_{32}H_{42}O_{14}Na$ $[M+Na]^+$ 673.2467, found 673.2466.

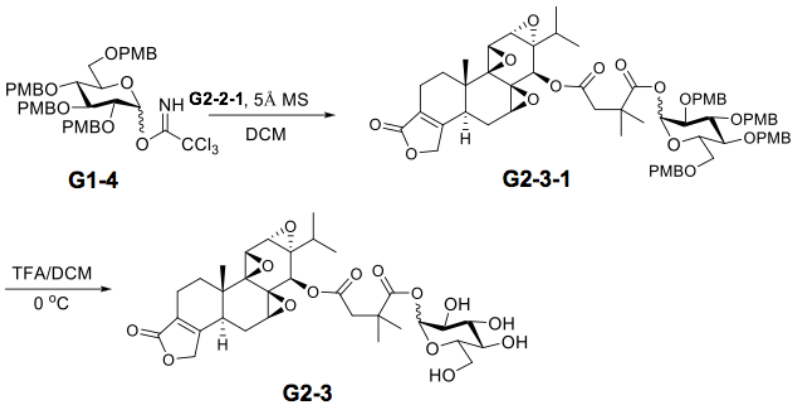

Trichloroacetimidate donor **G1-4** (371 mg, 0.46 mmol) and acid **G2-2-1** (150 mg, 0.31 mmol) were dissolved in CH_2Cl_2 (6 mL) under nitrogen. Powdered freshly activated 5Å molecular sieves (600 mg) were added. Stirring was continued until TLC indicated the disappearance of the donor (about 8 h). The mixture was filtered through Celite, and the filtrated was concentrated in vacuum. The residue was purified by silica gel column chromatography (petroleum ether/EtOAc, 2:1 to 1:1) to give the product **G2-3-1** (180 mg, 0.16 mmol, α/β = 6.6: 1.0, 52%) as a white solid. ^{1}H NMR (400 MHz, $CDCl_3$) δ 7.24 (dd, J = 5.7, 2.8 Hz, 6H), 7.03 (d, J = 8.6 Hz, 3H), 6.89 – 6.70 (m, 10H), 6.37 (d, J = 3.5 Hz, 1H), 5.02 (d, J = 0.9 Hz, 1H), 4.86 (d, J = 10.6 Hz, 1H), 4.73 (dd, J = 10.3, 7.6 Hz, 2H), 4.66 – 4.43 (m, 6H), 4.39 (dd, J = 11.1, 4.5 Hz, 2H), 3.83 – 3.72 (m, 18H), 3.71 – 3.62 (m, 4H), 3.62 – 3.52 (m, 2H), 3.51 – 3.39 (m, 1H), 3.30 (d, J = 5.5 Hz, 1H), 1.35 (d, J = 5.1 Hz, 7H), 1.00 (s, 3H), 0.92 (d, J = 6.9 Hz, 4H), 0.79 (d, J = 6.9 Hz, 4H); ESI-MS *m/z* calcd for $C_{64}H_{74}O_{18}Na$ $[M+Na]^+$ 1153.4767, found 1153.4781.

Compound **G2-3-1**(148 mg, 0.13 mmol) was dissolved in DCM (5 mL), and cooled to 0 °C. Then TFA (0.5 mL) was added. After stirring at this temperature for about 10 min, the reaction

mixture was concentrated *in vacuo*. The residue was chromatographed over silica gel (DCM/Methanol = 10:1) to yield the product **G2-3** (77 mg, 0.12 mmol, α/β = 5.2: 1.0, 91%) as a white solid. ^{1}H NMR (500 MHz, CD_3OD) δ 6.08 (d, *J* = 3.6 Hz, 1H), 5.42 (d, *J* = 7.9 Hz, 0H), 5.02 (d, *J* = 4.6 Hz, 1H), 4.86 – 4.68 (m, 2H), 4.01 – 3.85 (m, 1H), 3.79 – 3.51 (m, 5H), 3.43 (dd, *J* = 12.2, 7.4 Hz, 2H), 2.89 – 2.64 (m, 3H), 2.21 (tt, *J* = 16.9, 4.6 Hz, 2H), 2.03 (t, *J* = 13.4 Hz, 1H), 1.93 – 1.76 (m, 2H), 1.45 (dd, *J* = 12.7, 5.3 Hz, 1H), 1.32 (d, *J* = 5.4 Hz, 7H), 0.99 (s, 3H), 0.89 (d, *J* = 6.9 Hz, 3H), 0.79 (d, *J* = 6.8 Hz, 3H); ^{13}C NMR (126 MHz, CD_3OD) δ 177.13, 176.06, 172.35, 163.93, 125.43, 93.92, 75.92, 74.90, 72.96, 72.51, 71.99, 70.80, 64.83, 64.10, 62.82, 62.05, 61.04, 56.68, 56.14, 49.85, 44.78, 42.35, 41.38, 36.75, 30.71, 29.31, 25.63, 25.26, 24.12, 17.91, 17.85, 17.14, 14.16; ESI-MS (*m/z*): 673.6 $[M+Na]^+$; ESI-MS *m/z* calcd for $C_{32}H_{42}O_{14}Na$ $[M+Na]^+$ 673.2467, found 673.2466.

Scheme S3. Synthetic route of Glutriptolide G2-4 and G2-5, Related to Figure 1.

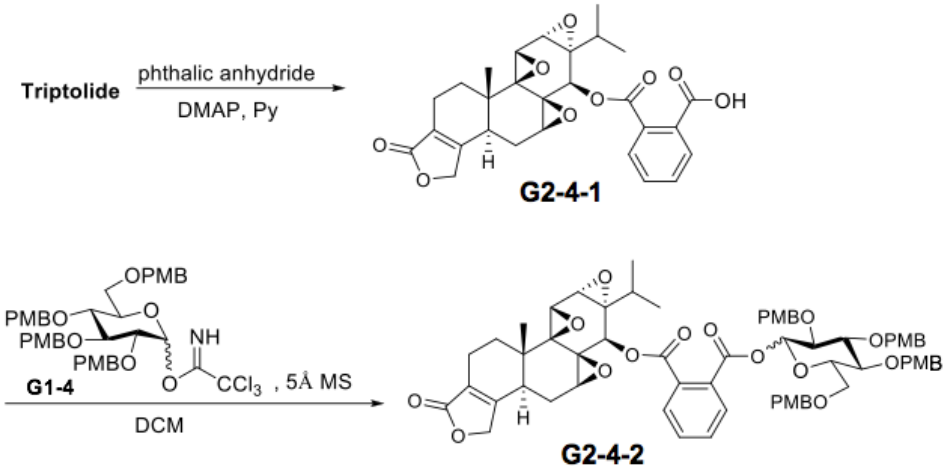

Synthetic procedures for Glutriptolide G2-4 and G2-5, Related to Figure 1.

To a solution of Triptolide (200 mg, 0.56 mmol) in pyridine (4 mL) were added phthalic anhydride (285 mg, 2.22 mmol) and DMAP (14 mg, 0.11 mmol). After stirring overnight, the mixture was diluted with ethyl acetate, then washed with saturated copper sulfate, water and brine, respectively. The organic layers were dried over Na_2SO_4 and filtered. The filtrate was concentrated using a rotary evaporator to give a residue. The residue was purified by silica gel column chromatography (CH_2Cl_2/CH_3OH, 15:1) to give compound **G2-4-1** (260 mg, 0.51 mmol, 91%) as a white solid; ^{1}H NMR (400 MHz, CD_3Cl) δ 5.07 (s, 1H), 4.68 (s, 2H), 3.81 (d, J = 3.1 Hz, 1H), 3.53 (d, J = 2.7 Hz, 1H), 3.45 (d, J = 5.6 Hz, 1H), 2.71 (dd, J = 23.2, 7.1 Hz, 4H), 2.32 (d, J = 16.4 Hz, 1H), 2.15 (ddd, J = 25.7, 15.9, 10.0 Hz, 2H), 2.00 – 1.81 (m, 2H), 1.37 (s, 3H), 1.35 (s, 3H), 1.23 (dt, J = 11.6, 7.9 Hz, 3H), 1.05 (s, 3H), 0.94 (d, J = 6.9 Hz, 3H), 0.82 (d, J = 6.9 Hz, 3H); ESI-MS (*m/z*): 511.3 $[M+Na]^+$.

Trichloroacetimidate donor **G1-4** (618 mg, 0.77 mmol) and acid **G2-4-1** (260 mg, 0.51 mmol) were dissolved in CH_2Cl_2 (10 mL) under nitrogen. Powdered freshly activated 5Å molecular sieves (900 mg) were added. Stirring was continued until TLC indicated the disappearance of the donor (about 8 h). The mixture was filtered through Celite, and the filtrated was concentrated in vacuum. The residue was purified by silica gel column chromatography (petroleum ether/EtOAc, 2:1 to 1:1) to give the products **G2-4-2α** (75 mg, 0.065 mmol, 13%) and **G2-4-2β** (225 mg, 0.195 mmol, 39%) as a white solid.

G2-4-2α: ^{1}H NMR (400 MHz, $CDCl_3$) δ 7.92 (dd, J = 7.5, 1.4 Hz, 1H), 7.69 (dd, J = 7.6, 1.4 Hz, 1H), 7.62 – 7.50 (m, 2H), 7.35 – 7.23 (m, 6H), 7.06 – 7.00 (m, 2H), 6.91 – 6.77 (m, 8H), 6.53 (d, J = 3.5 Hz, 1H), 5.28 (s, 1H), 4.86 (d, J = 10.6 Hz, 1H), 4.78 – 4.54 (m, 9H), 4.40 (dd, J = 11.0, 8.4 Hz, 2H), 3.97 – 3.86 (m, 2H), 3.83 – 3.67 (m, 21H), 3.61 (dd, J = 10.8, 2.0 Hz, 1H), 3.54 (d, J = 3.1 Hz, 1H), 3.46 (d, J = 5.6 Hz, 1H), 2.68 (d, J = 12.9 Hz, 1H), 2.31 (d, J = 17.6 Hz,

1H), 2.19 (ddd, *J* = 24.9, 12.5, 6.3 Hz, 4H), 1.90 – 1.79 (m, 1H), 1.54 (dd, *J* = 12.1, 5.4 Hz, 1H), 1.06 (s, 3H), 1.01 (d, *J* = 6.9 Hz, 3H), 0.81 (d, *J* = 6.9 Hz, 3H); ^{13}C NMR (100 MHz, $CDCl_3$) *δ* 173.37, 166.23, 165.61, 160.19, 159.44, 159.40, 159.28, 131.78, 131.64, 131.47, 131.03, 130.42, 130.11, 130.02, 129.79, 129.74, 129.72, 129.67, 129.19, 125.63, 113.92, 113.90, 113.87, 91.22, 81.48, 78.70, 77.36, 76.60, 75.38, 75.03, 73.25, 72.72, 72.27, 70.08, 67.60, 63.70, 61.21, 60.50, 60.06, 55.60, 55.38, 55.34, 55.02, 40.47, 35.76, 29.97, 27.36, 23.53, 21.17, 17.58, 17.16, 16.76, 14.31, 13.88; ESI-MS *m/z* calcd for $C_{66}H_{70}O_{18}Na$ $[M+Na]^+$ 1173.4454, found 1173.4466.

G2-4-2β: ^{1}H NMR (400 MHz, $CDCl_3$) *δ* 7.77 (dd, *J* = 7.8, 1.2 Hz, 1H), 7.63 (dd, *J* = 7.8, 1.3 Hz, 1H), 7.52 (td, *J* = 7.6, 1.3 Hz, 1H), 7.42 (td, *J* = 7.6, 1.3 Hz, 1H), 7.21 – 7.11 (m, 5H), 7.11 – 7.04 (m, 2H), 7.03 – 6.96 (m, 2H), 6.80 – 6.63 (m, 9H), 5.77 – 5.70 (m, 1H), 5.22 (s, 1H), 4.77 – 4.45 (m, 9H), 4.37 (dd, *J* = 12.9, 11.0 Hz, 2H), 3.73 (d, *J* = 3.2 Hz, 1H), 3.71 (s, 3H), 3.69 (s, 3H), 3.67 (s, 3H), 3.65 (s, 3H), 3.63 (q, *J* = 5.4, 4.2 Hz, 5H), 3.55 – 3.48 (m, 1H), 3.46 (d, *J* = 3.0 Hz, 1H), 3.40 (d, *J* = 5.5 Hz, 1H), 2.56 (d, *J* = 12.7 Hz, 1H), 2.20 (d, *J* = 17.8 Hz, 1H), 2.15 – 1.91 (m, 3H), 1.77 (t, *J* = 14.0 Hz, 1H), 1.45 (dd, *J* = 12.4, 5.3 Hz, 1H), 1.10 (td, *J* = 12.3, 5.8 Hz, 1H), 0.97 (s, 3H), 0.93 (d, *J* = 6.9 Hz, 3H), 0.73 (d, *J* = 6.9 Hz, 3H); ^{13}C NMR (100 MHz, $CDCl_3$) δ 173.30, 166.56, 164.77, 160.22, 159.30, 159.22, 132.90, 132.04, 130.97, 130.66, 130.30, 130.26, 130.20, 130.18, 129.76, 129.73, 129.66, 129.56, 129.51, 129.45, 129.24, 125.43, 113.80, 113.77, 94.88, 84.68, 80.50, 77.01, 75.81, 75.24, 74.59, 74.51, 73.15, 72.16, 70.02, 67.75, 63.61, 63.57, 61.29, 60.02, 55.56, 55.29, 55.24, 55.21, 54.89, 40.33, 35.65, 29.85, 27.33, 23.36, 17.54, 17.06, 16.81, 13.80; ESI-MS *m/z* calcd for $C_{66}H_{70}O_{18}Na$ $[M+Na]^+$ 1173.4454, found 1173.4466.

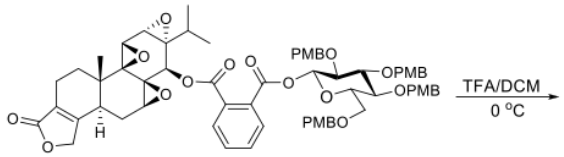

G2-4-2

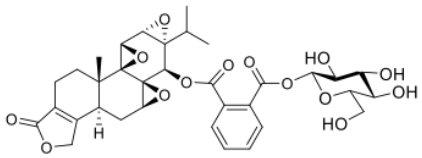

G2-4

Compound **G2-4-2β** (118 mg, 0.10 mmol) was dissolved in DCM (5 mL), and cooled to 0 °C. Then TFA (0.5 mL) was added. After stirring at this temperature for about 10 min, the reaction mixture was concentrated *in vacuo*. The residue was chromatographed over silica gel (DCM/Methanol = 10:1) to yield the product **G2-4** (55 mg, 80%) as a white solid. ^{1}H NMR (400 MHz, CD_3OD) *δ* 8.05 – 7.57 (m, 4H), 5.72 (d, *J* = 7.7 Hz, 1H), 5.29 (d, *J* = 1.0 Hz, 1H), 4.85 – 4.69 (m, 2H), 4.01 (d, *J* = 3.2 Hz, 1H), 3.88 (dd, *J* = 12.2, 2.2 Hz, 1H), 3.76 – 3.67 (m, 2H), 3.58

(d, J = 5.6 Hz, 1H), 3.54 – 3.37 (m, 4H), 2.87 – 2.71 (m, 1H), 2.36 – 1.98 (m, 4H), 1.57 – 1.43 (m, 1H), 1.33 (ddd, J = 17.0, 11.4, 4.9 Hz, 1H), 1.06 (s, 3H), 1.03 (d, J = 6.8 Hz, 3H), 0.86 (d, J = 6.9 Hz, 3H); ^{13}C NMR (100 MHz, CD_3OD) δ 184.70, 176.86, 175.66, 172.48, 142.00, 141.68, 141.49, 141.09, 139.42, 139.36, 134.12, 105.44, 87.66, 86.46, 83.20, 82.88, 80.62, 79.63, 73.61, 72.96, 71.45, 71.02, 70.16, 65.58, 64.91, 50.00, 45.41, 39.42, 37.60, 32.78, 26.61, 26.49, 25.84, 22.88; ESI-MS m/z calcd for $C_{34}H_{38}O_{14}Na$ $[M+Na]^+$ 693.2154, found 693.2143.

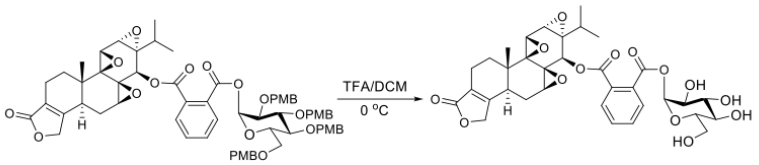

G2-4-2 **G2-5**

Compound **G2-4-2α** (50mg, 0.043 mmol) was dissolved in DCM (2 mL), and cooled to 0 °C. Then TFA (0.2 mL) was added. After stirring at this temperature for about 10 min, the reaction mixture was concentrated *in vacuo*. The residue was chromatographed over silica gel (DCM/Methanol = 10:1) to yield the product **G2-5** (24 mg, 83%) as a white solid. ^{1}H NMR (400 MHz, CD_3OD) δ 8.14 – 7.51 (m, 4H), 6.38 (d, J = 3.7 Hz, 1H), 5.27 (d, J = 0.9 Hz, 1H), 4.86 – 4.70 (m, 2H), 4.00 (d, J = 3.1 Hz, 1H), 3.93 – 3.71 (m, 3H), 3.71 – 3.67 (m, 1H), 3.66 (d, J = 3.7 Hz, 1H), 3.58 (d, J = 5.6 Hz, 1H), 3.48 (s, 1H), 2.78 (d, J = 12.3 Hz, 1H), 2.33 – 2.18 (m, 2H), 2.10 (q, J = 6.9 Hz, 1H), 1.99 – 1.87 (m, 1H), 1.56 – 1.46 (m, 1H), 1.39 – 1.27 (m, 2H), 1.04 (s, 3H), 1.00 (d, J = 6.9 Hz, 3H), 0.86 (d, J = 6.9 Hz, 3H); ^{13}C NMR (100 MHz, CD_3OD) δ 176.08, 167.95, 167.72, 163.89, 133.99, 133.20, 132.53, 132.10, 130.94, 130.25, 125.48, 94.92, 76.28, 74.86, 74.50, 72.61, 71.99, 70.83, 64.95, 64.33, 62.89, 62.11, 61.52, 56.89, 56.28, 41.41, 36.79, 30.80, 29.13, 24.15, 17.98, 17.89, 17.23, 14.23; ESI-MS m/z calcd for $C_{34}H_{38}O_{14}Na$ $[M+Na]^+$ 693.2154, found 693.2143.

Scheme S4. Synthetic route of Glutriptolide G2-6 and G2-7, Related to Figure 1.

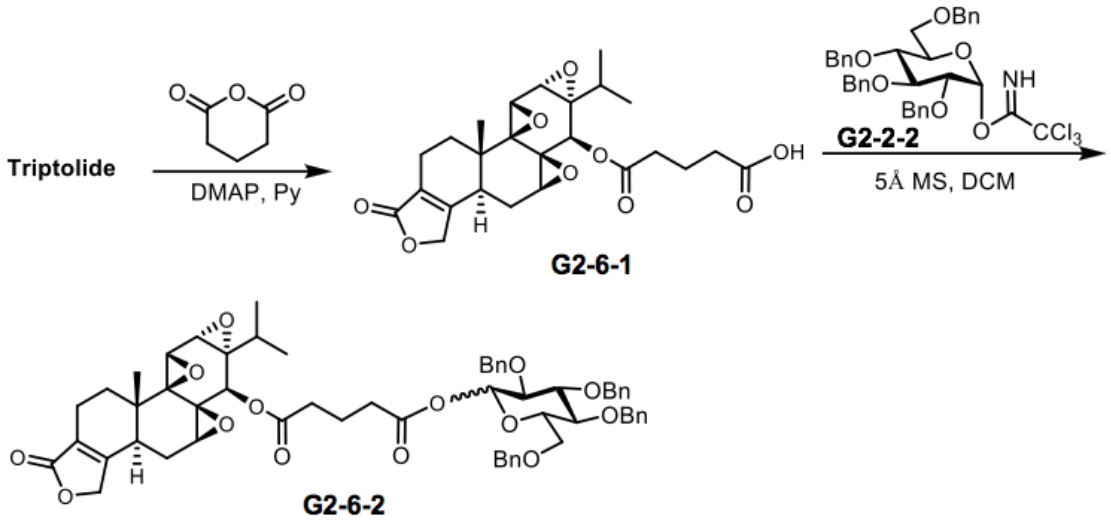

Synthetic procedures for Glutriptolide G2-6 and G2-7, Related to Figure 1.

To a solution of Triptolide (50 mg, 0.14 mmol) in pyridine (2 mL) were added glutaric anhydride (63 mg, 4 mmol) and DMAP (24 mg, 0.556 mmol). After stirring overnight, the mixture was diluted with ethyl acetate, then washed with saturated copper sulfate, water and brine, respectively. The organic layers were dried over Na_2SO_4 and filtered. The filtrate was concentrated using a rotary evaporator. The residue was purified by silica gel column chromatography (CH_2Cl_2/CH_3OH, 15:1) to give the product **G2-6-1** (48 mg, 0.10 mmol, 73%) as a white solid; ^{1}H NMR (400 MHz, $CDCl_3$) δ 5.08 (s, 1H), 4.67 (s, 2H), 3.83 (d, J = 3.1 Hz, 1H), 3.53 (d, J = 2.7 Hz, 1H), 3.47 (d, J = 5.6 Hz, 1H), 2.68 (d, J = 13.1 Hz, 1H), 2.61 – 1.81 (m, 14H), 1.04 (s, 3H), 0.95 (d, J = 7.0 Hz, 3H), 0.84 (d, J = 6.9 Hz, 3H); ESI-MS (*m/z*): 497.3 $[M+Na]^+$.

Trichloroacetimidate donor **G2-2-2** (103 mg, 0.15 mmol) and acid **G2-6-1** (48 mg, 0.1 mmol)were dissolved in CH_2Cl_2 (2 mL) under nitrogen. Powdered freshly activated 5Å molecular sieves (200 mg) were added. Stirring was continued until TLC indicated the disappearance of the donor (about 8 h). The mixture was filtered through Celite, and the filtrated was concentrated in vacuum. The residue was purified by silica gel column chromatography (petroleum ether/EtOAc, 1:1) to give the products **G2-6-2α** (12 mg, 0.012 mmol, 12%) and **G2-6-2β** (15 mg, 0.015 mmol, 15%) as a white solid.

G2-6-2α: ^{1}H NMR (400 MHz, $CDCl_3$) δ 7.43 – 7.00 (m, 21H), 6.39 (d, J = 3.4 Hz, 1H), 5.08 (s, 1H), 4.96 (d, J = 10.9 Hz, 1H), 4.82 (t, J = 10.2 Hz, 2H), 4.76 – 4.41 (m, 7H), 4.02 – 3.81 (m, 2H), 3.81 – 3.56 (m, 5H), 3.45 (dd, J = 14.9, 4.1 Hz, 2H), 2.63 (d, J = 13.1 Hz, 1H), 2.52 (dt,

J = 17.8, 7.2 Hz, 4H), 2.33 – 2.17 (m, 1H), 2.17 – 1.92 (m, 4H), 1.92 – 1.73 (m, 2H), 1.67 – 1.44 (m, 2H), 1.34 – 1.05 (m, 3H), 1.00 (s, 3H), 0.94 (d, J = 7.0 Hz, 3H), 0.81 (d, J = 6.9 Hz, 3H); ESI-MS m/z calcd for $C_{59}H_{64}O_{14}Na$ $[M+Na]^+$ 1019.4188, found 1019.4183.

G2-6-2β: ^{1}H NMR (400 MHz, $CDCl_3$) δ 7.43 – 7.04 (m, 21H), 5.61 (d, J = 8.1 Hz, 1H), 5.08 (s, 1H), 4.79 (d, J = 24.9 Hz, 5H), 4.63 (d, J = 12.1 Hz, 5H), 3.73 (s, 5H), 3.67 – 3.52 (m, 2H), 3.48 (d, J = 3.0 Hz, 1H), 3.44 (d, J = 5.5 Hz, 1H), 2.65 (d, J = 13.3 Hz, 1H), 2.59 – 2.22 (m, 5H), 2.04 (s, 7H), 1.66 – 1.47 (m, 2H), 1.33 – 1.12 (m, 3H), 1.01 (s, 3H), 0.94 (d, J = 7.0 Hz, 3H), 0.82 (d, J = 6.9 Hz, 3H); ESI-MS m/z calcd for $C_{59}H_{64}O_{14}Na$ $[M+Na]^+$ 1019.4188, found 1019.4183.

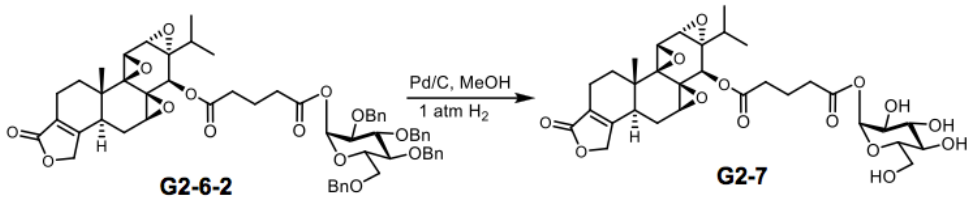

G2-6-2 G2-7

Palladium on charcoal (10%, 5 mg) was added to a solution of compound **G2-6-2α** (10 mg, 0.01 mmol) in CH_3OH. The mixture was placed under an atmosphere of hydrogen for about 4 h. The mixture was filtered and concentrated. The residue was purified by silica gel column chromatography (CH_2Cl_2/CH_3OH, 15:1) to give the product **G2-7** (5 mg, 0.008 mmol, 82%) as a white solid; ^{1}H NMR (400 MHz, CD_3OD) δ 6.04 (d, J = 3.7 Hz, 1H), 4.99 (s, 1H), 4.73 – 4.68 (m, 2H), 3.86 (d, J = 3.1 Hz, 1H), 3.70 – 3.63 (m, 1H), 3.62 – 3.51 (m, 4H), 3.45 (dd, J = 9.7, 3.8 Hz, 1H), 3.38 (d, J = 5.6 Hz, 1H), 3.33 – 3.24 (m, 2H), 2.76 – 2.29 (m, 6H), 2.22 – 2.09 (m, 2H), 2.06 – 1.72 (m, 6H), 1.46 – 1.38 (m, 1H), 0.95 (s, 3H), 0.85 (d, J = 7.0 Hz, 3H), 0.75 (d, J = 7.0 Hz, 3H); ^{13}C NMR (100 MHz, CD_3OD) δ 176.11, 173.91, 173.68, 163.89, 125.54, 93.47, 75.99, 74.81, 72.77, 72.30, 71.99, 70.98, 64.92, 64.15, 62.84, 62.27, 61.15, 56.79, 56.24, 41.45, 36.83, 34.17, 33.87, 30.79, 29.62, 24.17, 21.28, 17.95, 17.11, 14.25; ESI-MS (m/z): 659.5 $[M+Na]^+$.

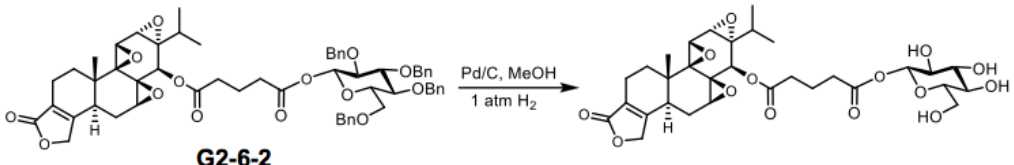

G2-6-2 G2-6

Palladium on charcoal (10%, 5 mg) was added to a solution of compound **G2-6-2β** (10 mg, 0.010 mmol) in CH_3OH. The mixture was placed under an atmosphere of hydrogen for about 4 h. The mixture was filtered and concentrated. The residue was purified by silica gel column chromatography (CH_2Cl_2/CH_3OH, 15:1) to give compound **G2-6** (5 mg, 0.008 mmol, 82%) as a white solid; ^{1}H NMR (400 MHz, CD_3OD) δ 5.49 (d, J = 8.1 Hz, 1H), 5.09 (s, 1H), 4.83 – 4.78 (m, 1H), 3.96 (d, J = 3.2 Hz, 1H), 3.83 (dd, J = 12.1, 1.7 Hz, 1H), 3.70 – 3.57 (m, 2H), 3.48 (d, J

= 5.6 Hz, 1H), 3.45 – 3.35 (m, 3H), 2.78 (d, *J* = 15.3 Hz, 1H), 2.60 – 2.42 (m, 4H), 2.27 (dt, *J* = 15.0, 5.9 Hz, 2H), 2.15 – 1.81 (m, 5H), 1.51 (dd, *J* = 12.7, 4.5 Hz, 1H), 1.39 – 1.19 (m, 3H), 1.04 (s, 2H), 0.95 (d, *J* = 7.0 Hz, 2H), 0.85 (d, *J* = 7.0 Hz, 3H); ^{13}C NMR (100 MHz, CD_3OD) δ 176.11, 173.91, 173.68, 163.89, 125.54, 93.47, 75.99, 74.81, 72.77, 72.30, 71.99, 70.98, 64.92, 64.15, 62.84, 62.27, 61.15, 56.79, 56.24, 41.45, 36.83, 34.17, 33.87, 30.79, 29.62, 24.17, 21.28, 17.95, 17.11, 14.25; ESI-MS (m/z): 659.5 $[M+Na]^+$.

Scheme S5. Synthetic route 1 for Glutriptolide G2-1, Related to Figure 1.

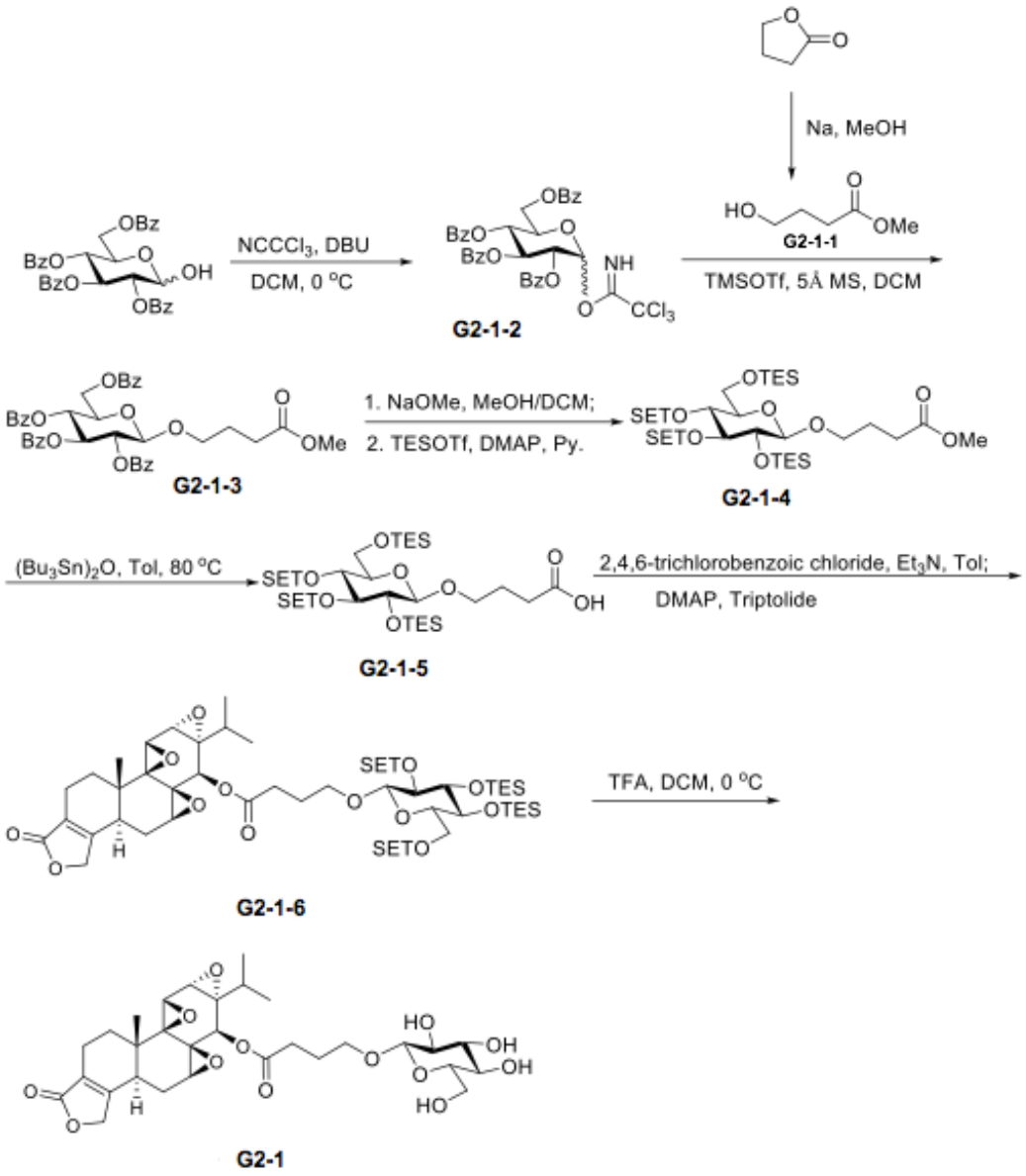

Synthetic procedures for Glutriptolide G2-1, Related to Figure 1.

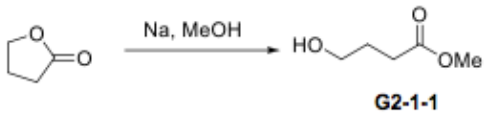

To a solution of gamma-Butyrolactone (4.3 mL, 56.5 mmol) in methanol (150 mL) at 0 °C, was added Na (1.3 g, 56.5 mmol). Stirring was continued until complete conversion of the

starting material (monitored by TLC, about 24 hours). The reaction was quenched with saturated ammonium chloride (300 mL), extracted with ethyl acetate (150 mL × 4), the organic layer was combined, washed with brine (100 mL × 4), dried over Na_2SO_4. The mixture was filtered and concentrated. Column chromatography (Petroleum ether/Ethyl acetate = 2/1) afforded the product **G2-1-1** as a colorless liquid (4.5 g, 38.1 mmol, 67%). ^{1}H NMR (500 MHz, $CDCl_3$) δ 3.68 – 3.59 (m, 5H), 2.41 (t, J = 7.2 Hz, 2H), 1.85 (ddd, J = 7.2, 6.1, 1.0 Hz, 2H). ^{13}C NMR (125 MHz, $CDCl_3$) δ 174.54, 61.94, 51.76, 30.82, 27.75

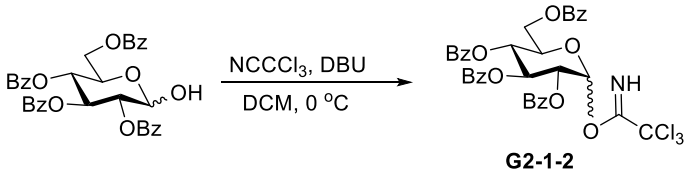

G2-1-2

The lactol (4.4 g, 7.4 mmol) was dissolved in CH_2Cl_2 (50 mL) and cooled to 0 °C. Trichloroacetonitrile (3.7 mL, 36.9 mmol) and DBU (52 µL, 0.4 mmol) were added successively. After stirring at room temperature for about 2 h, the reaction mixture was concentrated *in vacuo*. The residue was chromatographed over silica gel (Petroleum ether/EtOAc = 4:1, containing 1% Et_3N) to yield imidate **G2-1-2** (4.9 g, 6.6 mmol, 90 %) as a colorless oil.

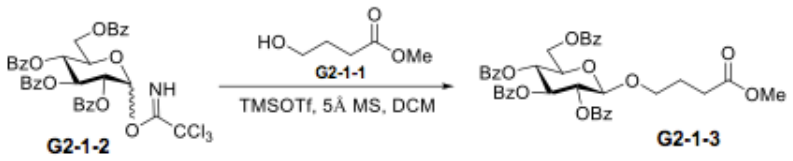

G2-1-2 **G2-1-3**

Trichloroacetimidate donor **G2-1-2** (1.8 g, 2.4 mmol) and **G2-1-1** (260 mg, 2.2 mmol) were dissolved in CH_2Cl_2 (25 mL) under nitrogen at 0 °C. Powdered freshly activated 5Å molecular sieves (2 g) were added. After 15 min, TMSOTf (40 µL, 0.22 mmol) was added and stirring was continued at 0 °C until TLC indicated the disappearance of the donor (about 8 h). The mixture was filtered through Celite, and the filtrated was concentrated in vacuum. The residue was purified by silica gel column chromatography (petroleum ether/EtOAc, 2:1) to give compound **G2-1-3** (1.23 g, 1.77 mmol, 80%) as a white foam. ^{1}H NMR (400 MHz, $CDCl_3$) δ 8.06 – 8.00 (m, 2H), 8.00 – 7.93 (m, 2H), 7.93 – 7.87 (m, 2H), 7.88 – 7.81 (m, 2H), 7.61 – 7.28 (m, 13H), 5.90 (t, J = 9.6 Hz, 1H), 5.67 (t, J = 9.7 Hz, 1H), 5.51 (dd, J = 9.8, 7.8 Hz, 1H), 4.84 (d, J = 7.9 Hz, 1H), 4.64 (dd, J = 12.1, 3.3 Hz, 1H), 4.50 (dd, J = 12.1, 5.2 Hz, 1H), 4.20 – 4.14 (m, 1H), 3.95 (dt, J = 9.8, 5.9 Hz, 1H), 3.62 (ddd, J = 9.8, 7.0, 5.6 Hz, 1H), 3.52 (s, 3H), 2.29 (t, J = 7.3 Hz, 2H), 1.95 – 1.76 (m, 2H). ^{13}C NMR (100 MHz, $CDCl_3$) δ 173.72, 166.25, 165.92, 165.28, 165.20, 133.54, 133.35, 133.32, 133.25, 130.00, 129.91, 129.87, 129.86, 129.84, 129.82, 129.63, 129.31, 128.84, 128.82, 128.50, 128.47, 128.46, 128.39, 101.30, 72.97, 72.27, 71.94, 69.80, 68.94, 63.21, 51.51, 30.04, 24.79. ESI-MS *m/z* calcd for $C_{39}H_{36}O_{12}Na$ $[M+Na]^+$ 719.2099, found 719.2102.

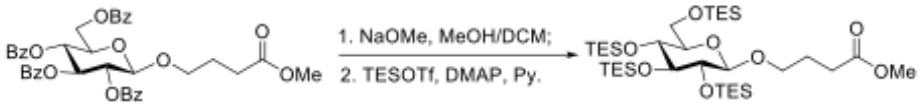

G2-1-3 **G2-1-4**

To a solution of Compound **G2-1-3** (2.9 g, 4.4 mmol) in methanol (20 mL), was added NaOMe (120 mg, 2.2 mmol). Stirring was continued until complete conversion of the starting material (monitored by TLC, about 8 hours). The mixture was neutralized with acidic resin, filtered and concentrated. Then the mixture was coevaporated with toluene three times and dried *in vacuo*.

The mixture was dissolved in dry pyridine (20 mL), and cooled to 0 °C. DMAP (108 mg, 0.9 mmol) and TESOTf (6.0 mL, 26.4 mmol) was added slowly over 5 min. Stirring was continued at 0 °C until complete conversion of the starting material (monitored by TLC, about 8 hours). The reaction was concentrated, then diluted with ethyl acetate, and washed twice with 2% HCl, once with saturated and brine, dried over Na_2SO_4. Then, the mixture was filtered and concentrated. Column chromatography (Petroleum ether/Ethyl acetate = 30/1) afforded the product **G2-1-4** as a colorless liquid (2.4 g, 3.3 mmol, 75% for two steps). ^{1}H NMR (400 MHz, $CDCl_3$) δ 4.38 (d, J = 6.9 Hz, 1H), 3.92 – 3.81 (m, 1H), 3.77 (dd, J = 10.4, 5.4 Hz, 1H), 3.72 – 3.63 (m, 5H), 3.60 (dd, J = 5.9, 4.6 Hz, 1H), 3.53 – 3.37 (m, 3H), 2.41 (d, J = 19.8 Hz, 2H), 1.94 (t, J = 7.0 Hz, 2H), 0.98 – 0.92 (m, 36H), 0.62 (dd, J = 15.4, 7.6 Hz, 24H). ^{13}C NMR (100 MHz, $CDCl_3$) δ 174.01, 102.48, 79.79, 79.27, 77.23, 71.27, 67.95, 63.28, 51.66, 30.98, 25.25, 7.17, 7.10, 6.89, 5.28, 5.20, 5.13, 4.56; ESI-MS *m/z* calcd for $C_{35}H_{76}O_8Si_4Na$ $[M+Na]^+$ 759.4509, found 759.4515.

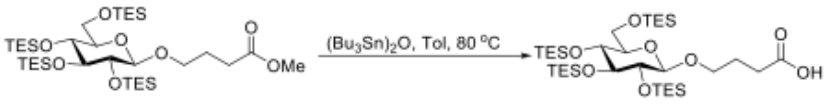

G2-1-4 **G2-1-5**

To a solution of Compound **G2-1-4** (850 mg, 1.2 mmol) in toluene (12 mL), was added bis(tributyltin) oxide (4.7 mL, 9.2 mmol). The reaction was heated to 80 °C overnight. The mixture was concentrated. Then the mixture was coevaporated with toluene three times. Column chromatography (Petroleum ether/Ethyl acetate = 20/1 to 10/1) afforded the product as a colorless liquid **G2-1-5** (450 mg, 0.62 mmol, 54%), recovered starting material (250 mg, 0.34 mmol, 29%). ^{1}H NMR (400 MHz, $CDCl_3$) δ 4.40 (d, J = 6.9 Hz, 1H), 3.86 (d, J = 9.5 Hz, 1H), 3.76 (d, J = 5.2 Hz, 1H), 3.75 – 3.64 (m, 2H), 3.60 (t, J = 5.2 Hz, 1H), 3.55 – 3.40 (m, 3H), 2.52 - 2.45 (m, 2H), 1.96 (q, J = 7.0 Hz, 2H), 0.98 - 0.92 (m, 36H), 0.74 – 0.48 (m, 24H); ESI-MS *m/z* calcd for $C_{34}H_{74}O_8Si_4Na$ $[M+Na]^+$ 745.4353, found 745.4358.

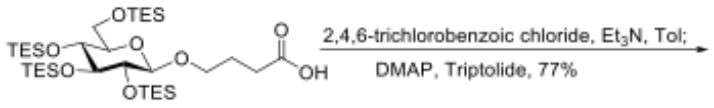

G2-1-5

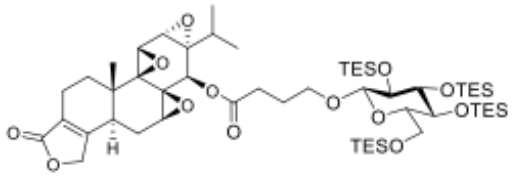

G2-1-6

To a solution of **G2-1-5** (475 mg, 0.53 mmol) in toluene (9 mL) was added NEt_3 (0.29 mL, 2.1 mmol) and 2,4,6-trichlorobenzoyl chloride (0.25 mL, 1.6 mmol) at 0 °C and was stirred at room temperature for 0.5h. After the formation of mixed anhydride (TLC), the solution was cooled to 0°C and 4-(dimethylamino)pyridine (428 mg, 3.5 mmol) and triptolide (126 mg, 0.35 mmol) was introduced dropwise in to the reaction mixture. The reaction mixture was warmed to room temperature and was stirred for additional 5h. After the completion of the reaction (TLC), it was quenched by addition of saturated $NaHCO_3$ solution (10 mL) and the aqueous layer was washed with DCM (3×10 mL). The combined organic layer was washed with brine (5 mL), dried over Na_2SO_4. The mixture was filtered and concentrated. Purification by silica gel column chromatography (PE/EtOAc, 2:1) afforded ester **G2-1-6** (339 mg, 0.32 mmol, 91%). ^{1}H NMR (400 MHz, $CDCl_3$) δ 5.02 (d, J = 1.0 Hz, 1H), 4.60 (s, 2H), 4.34 (d, J = 6.9 Hz, 1H), 3.88 – 3.77 (m, 1H), 3.76 – 3.67 (m, 2H), 3.68 – 3.58 (m, 2H), 3.54 (dd, J = 5.8, 4.5 Hz, 1H), 3.50 – 3.32 (m, 6H), 2.60 (s, 1H), 2.55 – 2.35 (m, 2H), 2.31 – 2.19 (m, 1H), 2.14 – 2.01 (m, 2H), 1.98 – 1.89 (m, 3H), 1.84 – 1.77 (m, 2H), 0.93 – 0.86 (m, 36H), 0.64 – 0.47 (m, 24H); ESI-MS *m/z* calcd for $C_{54}H_{96}O_{13}Si_4Na$ $[M+Na]^+$ 1087.5820, found 1087.5801.

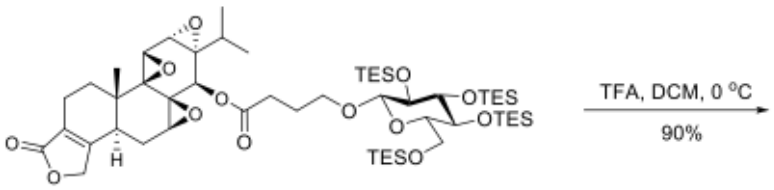

G2-1-6

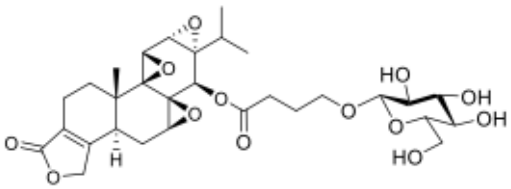

G2-1

Compound **G2-1-6** (570 mg, 0.54 mmol) was dissolved in DCM (10 mL), and cooled to 0 ^{o}C. Then TFA (1.0 mL) was added. After stirring at this temperature for about 15 min, the reaction mixture was concentrated *in vacuo*. The residue was chromatographed over silica gel (DCM/Methanol = 15:1) to yield **G2-1** (300 mg, 0.49 mml, 91%) as a white solid. ^{1}H NMR (500 MHz, CD_3OD) δ 5.09 (d, J = 1.0 Hz, 1H), 4.83 – 4.72 (m, 2H), 4.26 (d, J = 7.8 Hz, 1H), 4.03 – 3.92 (m, 2H), 3.86 (dd, J = 11.9, 2.1 Hz, 1H), 3.72 – 3.59 (m, 3H), 3.47 (d, J = 5.7 Hz, 1H), 3.18 (dd, J = 9.1, 7.8 Hz, 1H), 2.78 (d, J = 13.1 Hz, 1H), 2.69 – 2.46 (m, 2H), 2.32 – 2.19 (m, 2H), 2.08 (t, J = 13.8 Hz, 1H), 2.03 – 1.77 (m, 4H), 1.51 (dd, J = 12.4, 5.0 Hz, 1H), 1.37-1.27 (m, 1H), 1.04 (s, 3H), 0.95 (d, J = 7.0 Hz, 3H), 0.84 (d, J = 6.9 Hz, 3H). ^{13}C NMR (100 MHz, CD_3OD) δ 176.07, 174.57, 163.87, 125.51, 104.49, 78.00, 77.90, 75.08, 72.66, 71.98, 71.61, 69.68, 64.88, 64.21, 62.76, 61.10, 56.74, 56.21, 41.44, 36.81, 31.85, 30.82, 29.48, 26.35, 24.17, 17.94, 17.91, 17.13, 14.23; ESI-MS *m/z* calcd for $C_{30}H_{40}O_{13}Na$ $[M+Na]^+$ 631.2361, found 631.2368.

Scheme S6. Synthetic route 2 for Glutriptolide G2-1, Related to Figure 1.

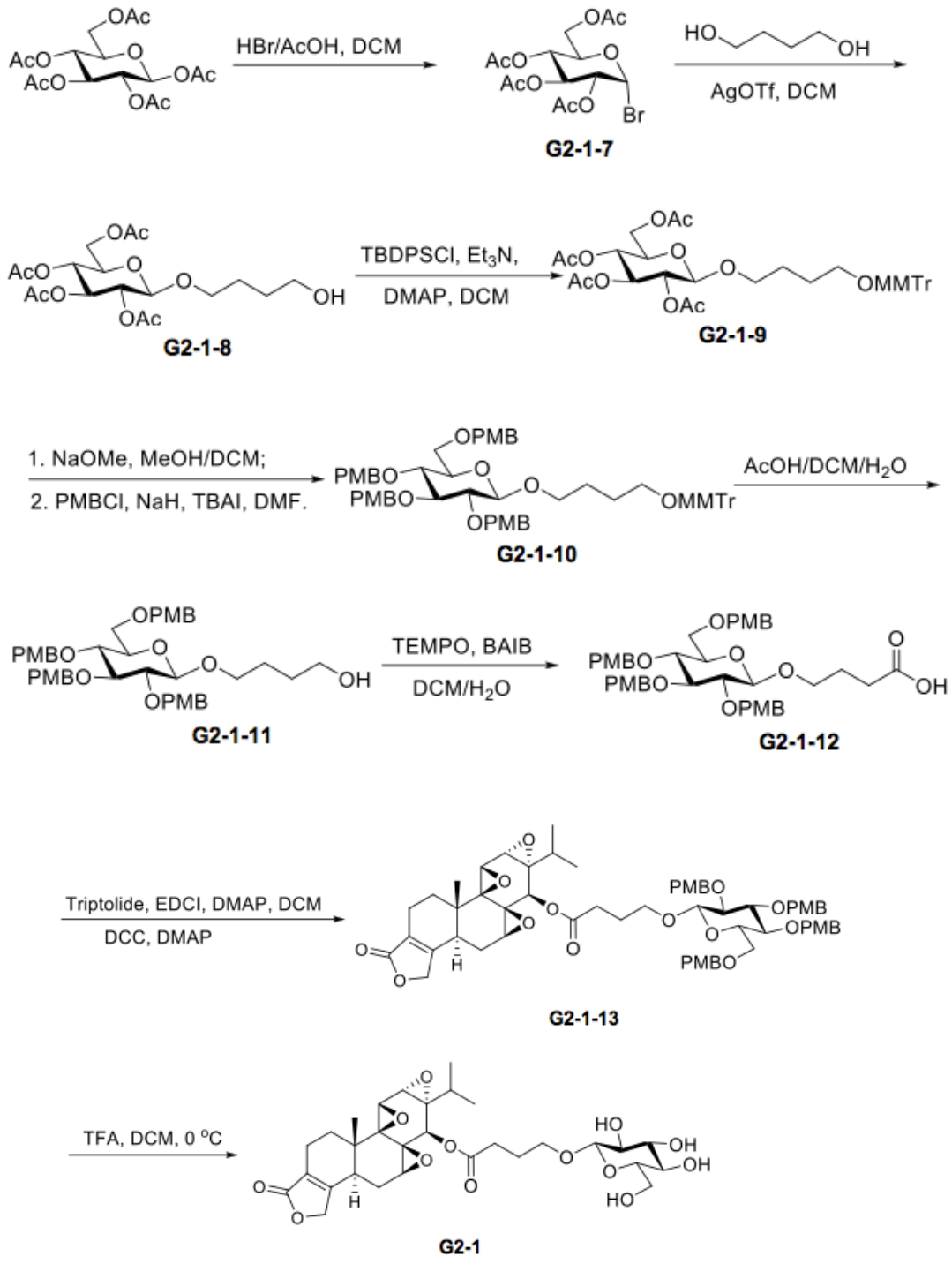

Synthetic procedure (route 2) for Glutriptolide G2-1, Related to Figure 1.

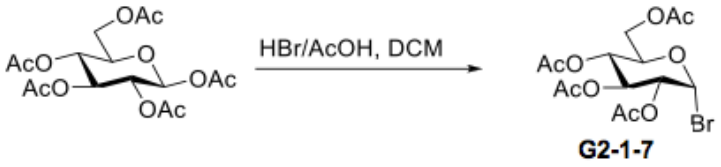

G2-1-7

To a solution of β-D-glucose pentaacetate (5.0 g, 12.8 mmol) in DCM (30 mL) at 0 °C, was added hydrobromic acid solution in acetic acid (8 mL). Stirring was continued at 0 °C until complete conversion of starting material (about 3 h). The reaction mixture was quenched with ice water (200 mL), and extracted with DCM (3×80 mL). The organic layer was combined and washed with ice water (3×80 mL), saturated $NaHCO_3$, and brine, dried over Na_2SO_4. The mixture was filtered and concentrated to provide 2,3,4,6-Tetra-O-acetyl-α-D-glucopyranosyl bromide **G2-1-7** (4.85 g, 11.8 mmol, 92%) as a white solid.

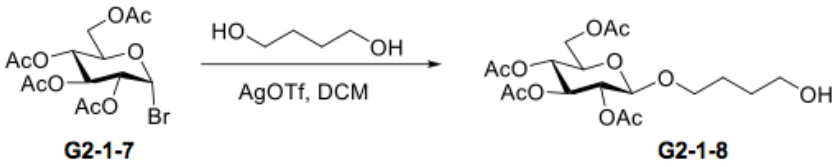

G2-1-7 **G2-1-8**

2,3,4,6-Tetra-O-acetyl-α-D-glucopyranosyl bromide **G2-1-7** (8.0 g, 2.4 mmol) and 1,4-Butylene glycol (260 mg, 2.2 mmol) were dissolved in CH_2Cl_2 (25 mL) under nitrogen. AgOTf (5.5 g, 21.5 mmol) were added. Stirring was continued until TLC indicated the disappearance of the donor (about 2 h). The mixture was quenched with saturated $NaHCO_3$, and filtered through Celite. The filtration was diluted with DCM, and washed with saturated $NaHCO_3$ and brine, dried over Na_2SO_4. The mixture was filtered and concentrated in vacuum. The residue was coevaporated with toluene twice.

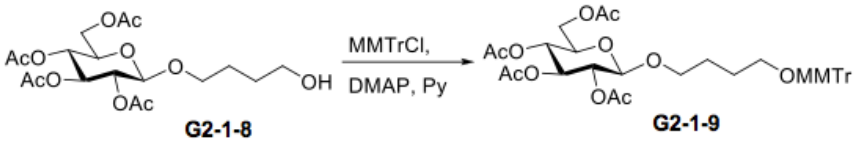

G2-1-8 **G2-1-9**

To a solution of **G2-1-8** in pyridine (40 mL) at 0 °C, DMAP (500 mg, 3.9 mmol) and MMTrCl (12.0 g, 39.0 mmol) was added. Stirring was continued at room temperature until complete consume of starting material. The mixture was concentrated, then diluted with ethyl acetate. The organic layer was was washed with saturated $CuSO_4$ (2×100 mL), and brine, dried over Na_2SO_4. The mixture was filtered and concentrated. Purification by silica gel column

chromatography (PE/EtOAc, 3:1) afforded ester **G2-1-9** (6.8 g, 9.5 mmol, 50% for two steps). ^{1}H NMR (400 MHz, $CDCl_3$) δ 7.42 – 7.31 (m, 4H), 7.29 – 7.11 (m, 8H), 6.76 (d, J = 8.9 Hz, 2H), 5.12 (t, J = 9.5 Hz, 1H), 5.01 (t, J = 9.7 Hz, 1H), 4.90 (dd, J = 9.6, 8.0 Hz, 1H), 4.36 (d, J = 7.9 Hz, 1H), 4.19 (dd, J = 12.3, 4.6 Hz, 1H), 4.10 – 3.98 (m, 1H), 3.80 (dt, J = 10.7, 5.6 Hz, 1H), 3.73 (s, 3H), 3.59 (ddd, J = 9.8, 4.6, 2.4 Hz, 1H), 3.45 – 3.32 (m, 1H), 3.03 – 2.93 (m, 2H), 2.00 (s, 3H), 1.96 (s, 3H), 1.94 (s, 6H), 1.61 – 1.56 (m, 4H). ^{13}C NMR (100 MHz, $CDCl_3$) δ 170.89, 170.49, 169.56, 158.80, 147.19, 144.93, 139.32, 130.41, 129.35, 128.51, 128.03, 127.96, 127.86, 127.32, 126.89, 113.33, 113.11, 100.95, 100.91, 81.86, 77.36, 72.92, 71.92, 71.42, 70.15, 68.51, 62.52, 62.02, 55.40, 29.48, 25.99, 20.93, 20.85, 20.80, 20.78; ESI-MS *m/z* calcd for $C_{38}H_{44}O_{12}Na$ $[M+Na]^+$ 715.2725, found 715.2722.

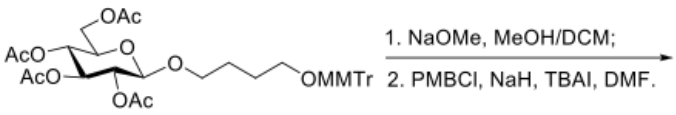

G2-1-9

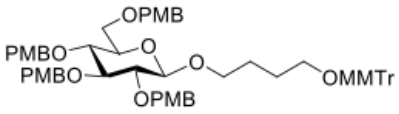

G2-1-10

To a solution of Compound **G2-1-9** (8.0 g, 11.6 mmol) in methanol (60 mL) and DCM (15 mL), was added NaOMe (312 mg, 5.8 mmol). Stirring was continued until complete conversion of the starting material (monitored by TLC, about 6 hours). The mixture was neutralized with acid resin, filtered and concentrated. Then the mixture was coevaporated with toluene three times and dried *in vacuo*.

The mixture and TBAI (854 mg, 2.3 mmol) was dissolved in dry DMF (100 mL), and cooled to 0 °C. NaH (2.8 g, 60% suspension, 69.4 mmol) was added slowly over 5 min. After 20 min, PMBCl (9.4 mL, 69.4 mmol) was added and the reaction stirred for another 10 min, at which time the temperature was raised to room temperature for 4 h. The reaction was re-cooled to 0 °C and water was added to quench the reaction. The organic layer was diluted with ethyl acetate, and washed twice with water, once with brine, dried over Na_2SO_4. Then, the mixture was filtered and concentrated. Column chromatography (Petroleum ether/Ethyl acetate = 3/1) afforded the product **G2-1-10** as a white solid (11.0 g, 10.9 mmol, 94% for two steps). ^{1}H NMR (400 MHz, $CDCl_3$) δ 7.50 – 7.43 (m, 4H), 7.37 – 7.20 (m, 14H), 7.11 – 7.04 (m, 2H), 6.94 – 6.78 (m, 10H), 4.88 (dd, J = 10.6, 4.7 Hz, 2H), 4.74 (d, J = 10.3 Hz, 2H), 4.69 – 4.61 (m, 1H), 4.57 (d, J = 11.8 Hz, 1H), 4.49 (d, J = 11.8 Hz, 1H), 4.43 (d, J = 10.4 Hz, 1H), 4.36 (d, J = 7.8 Hz, 1H), 3.99 (dd, J = 9.8, 5.1 Hz, 1H), 3.87 – 3.75 (m, 15H), 3.72 – 3.48 (m, 5H), 3.46 – 3.36 (m, 2H), 3.13 (d, J = 5.6 Hz, 2H), 1.79 (t, J = 5.4 Hz, 4H). ^{13}C NMR (100 MHz, $CDCl_3$) δ 159.34,

159.28, 159.27, 159.23, 158.48, 144.98, 136.22, 131.03, 130.75, 130.39, 130.34, 129.96, 129.74, 129.60, 128.74, 128.52, 127.82, 126.81, 114.03, 113.89, 113.87, 113.86, 113.84, 113.08, 103.74, 86.10, 84.52, 82.08, 77.76, 75.44, 74.94, 74.73, 74.61, 73.18, 70.01, 68.64, 63.28, 55.37, 55.34, 55.28, 26.97, 26.91; ESI-MS *m/z* calcd for $C_{62}H_{68}O_{12}Na$ $[M+Na]^+$ 1027.4603, found 1027.4600.

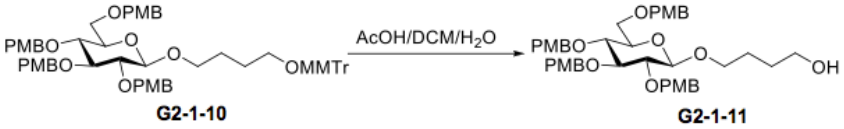

G2-1-10 **G2-1-11**

After a solution of **G2-1-10** (11.0 g, 10.9 mmol) in $AcOH/CH_2Cl_2/H_2O$ (15:4:1, 120 mL) was stirred at room temperature for 2.0 h, it was diluted with CH_2Cl_2 and poured into cold water. The organic layer was washed with water (4×80 mL), saturated aqueous $NaHCO_3$ and brine, then dried over Na_2SO_4. After concentration in vacuum, the residue was purified by silica gel column chromatography (Petroleum ether/Ethyl acetate = 1/1) to give **G2-1-11** (7.2 g, 9.8 mmol, 90%) as a white solid. ^{1}H NMR (400 MHz, $CDCl_3$) δ 7.26 – 7.13 (m, 6H), 7.07 – 6.86 (m, 2H), 6.86 – 6.55 (m, 8H), 4.77 (dd, J = 10.6, 2.6 Hz, 2H), 4.64 (dd, J = 10.5, 2.0 Hz, 2H), 4.59 (d, J = 10.6 Hz, 1H), 4.47 (d, J = 11.8 Hz, 1H), 4.40 (d, J = 11.8 Hz, 1H), 4.33 (d, J = 10.4 Hz, 1H), 4.29 (d, J = 7.8 Hz, 1H), 3.96 – 3.87 (m, 1H), 3.79 – 3.68 (m, 12H), 3.66 – 3.47 (m, 6H), 3.42 (t, J = 9.2 Hz, 1H), 3.37 – 3.27 (m, 2H), 1.64 (dt, J = 18.4, 6.1 Hz, 4H). ^{13}C NMR (100 MHz, $CDCl_3$) δ 159.32, 159.28, 159.26, 159.21, 130.95, 130.73, 130.32, 130.24, 129.83, 129.73, 129.60, 129.55, 113.86, 113.84, 113.82, 103.68, 84.53, 82.05, 77.72, 75.40, 74.88, 74.71, 74.59, 73.14, 70.02, 68.59, 62.62, 55.35, 55.32, 29.67, 26.38; ESI-MS *m/z* calcd for $C_{42}H_{52}O_{11}Na$ $[M+Na]^+$ 755.3402, found 755.3409.

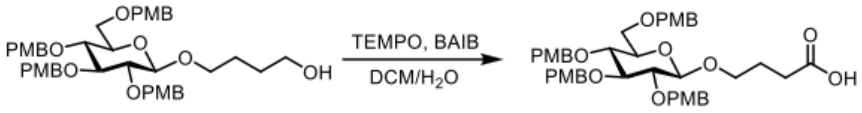

G2-1-11 **G2-1-12**

To a solution of **G2-1-11** (1.8 g, 2.4 mmol) in DCM (12 mL) and water (6 mL), TEMPO (75 mg, 0.48 mmol) and BAIB (2.3 g, 7.2 mmol) was added. Stirring was continued until complete conversion of starting material (about 3 hours). The mixture was quenched with saturated $NaHSO_3$, and extracted with DCM three times. The organic layer was combined and washed with brine, dried over Na_2SO_4. After concentration in vacuum, the residue was purified by silica gel column chromatography (Petroleum ether/Ethyl acetate = 1/4) to give **G2-1-12** (1.3 g, 1.7 mmol, 73%) as a white solid. ^{1}H NMR (400 MHz, $CDCl_3$) δ 7.30 – 7.11 (m, 6H), 6.96 (d, J = 8.2 Hz, 2H), 6.88 – 6.63 (m, 8H), 4.75 (dd, J = 10.6, 3.0 Hz, 2H), 4.61 (dd, J = 23.8, 10.7 Hz, 3H), 4.51 – 4.28 (m, 3H), 4.27 (d, J = 7.7 Hz, 1H), 3.96 – 3.81 (m, 1H), 3.72 – 3.71 (m, 12H),

3.65 – 3.23 (m, 8H), 2.43 (t, J = 7.4 Hz, 2H), 2.06 – 1.90 (m, 2H). ^{13}C NMR (100 MHz, $CDCl_3$) δ 178.66, 159.35, 159.31, 159.24, 130.96, 130.66, 130.36, 130.22, 129.93, 129.75, 129.65, 129.59, 113.92, 113.87, 103.63, 84.52, 82.04, 77.68, 75.44, 74.90, 74.73, 73.18, 68.74, 68.52, 55.38, 30.77, 25.03; ESI-MS *m/z* calcd for $C_{42}H_{50}O_{12}Na$ $[M+Na]^+$ 769.3194, found 769.3196.

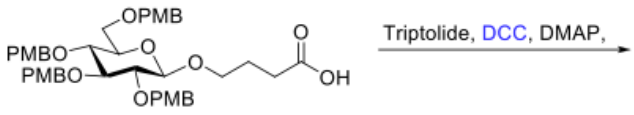

G2-1-12

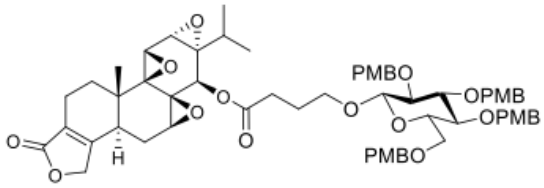

G2-1-13

A solution of compound **G2-1-12** (1.3 g, 1.7 mmol), Triptolide (523 mg, 1.45 mmol), DMAP (36 mg, 0.3 mmol), and DCC (462 mg, 2.2 mmol) in CH_2Cl_2 (30 mL) was stirred for 8 h at RT. The resulting mixture was concentrated and diluted with ethyl acetate, then filtrated. The filtrate was concentrated in vacuum. The residue was purified by silica gel column chromatography (petroleum ether/EtOAc, 1:1) to give compounds **G2-1-13** (1.3 g, 1.2 mmol, 82%) as a white solid. ^{1}H NMR (400 MHz, $CDCl_3$) δ 7.27 – 7.12 (m, 6H), 6.96 (d, J = 8.6 Hz, 2H), 6.85 – 6.66 (m, 8H), 5.06 – 4.97 (m, 1H), 4.77 (t, J = 11.0 Hz, 2H), 4.69 – 4.54 (m, 5H), 4.48 (d, J = 11.8 Hz, 1H), 4.39 (d, J = 11.9 Hz, 1H), 4.32 (d, J = 10.4 Hz, 1H), 4.28 (d, J = 7.8 Hz, 1H), 4.11 – 4.03 (m, 1H), 3.79 – 3.70 (m, 13H), 3.60 – 3.30 (m, 10H), 2.67 – 2.42 (m, 4H), 0.95 (s, 3H), 0.87 (d, J = 6.9 Hz, 3H), 0.73 (d, J = 6.9 Hz, 3H). ^{13}C NMR (100 MHz, $CDCl_3$) δ 173.38, 172.76, 160.16, 159.33, 159.27, 159.21, 130.97, 130.77, 130.36, 130.28, 130.00, 129.72, 129.61, 129.56, 125.64, 113.88, 113.85, 103.75, 84.49, 82.01, 77.66, 75.42, 74.92, 74.73, 74.64, 73.18, 70.94, 70.09, 68.78, 68.55, 63.61, 63.40, 61.25, 59.83, 55.37, 55.34, 55.09, 49.20, 40.43, 35.75, 34.04, 31.18, 29.89, 28.15, 25.72, 25.37, 25.05, 23.52, 17.66, 17.14, 16.80, 13.83. ESI-MS *m/z* calcd for $C_{62}H_{72}O_{17}Na$ $[M+Na]^+$ 1111.4662, found 1111.4649.

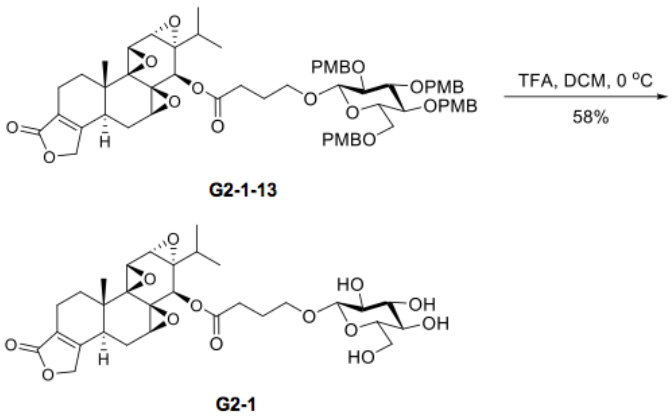

Compound **G2-1-13** (1.0 g, 1.45 mmol) was dissolved in DCM (30 mL), and cooled to 0 °C. Then TFA (3.0 mL) was added. After stirring at this temperature for about 15 min, the reaction mixture was concentrated *in vacuo*. The residue was chromatographed over silica gel (DCM/Methanol = 15:1) to yield **G2-1** (510 mg, 0.84 mmol, 58%) as a white solid. ^{1}H NMR (500 MHz, CD_3OD) δ 5.09 (d, J = 1.0 Hz, 1H), 4.83 – 4.72 (m, 2H), 4.26 (d, J = 7.8 Hz, 1H), 4.03 – 3.92 (m, 2H), 3.86 (dd, J = 11.9, 2.1 Hz, 1H), 3.72 – 3.59 (m, 3H), 3.47 (d, J = 5.7 Hz, 1H), 3.18 (dd, J = 9.1, 7.8 Hz, 1H), 2.78 (d, J = 13.1 Hz, 1H), 2.69 – 2.46 (m, 2H), 2.32 – 2.19 (m, 2H), 2.08 (t, J = 13.8 Hz, 1H), 2.03 – 1.77 (m, 4H), 1.51 (dd, J = 12.4, 5.0 Hz, 1H), 1.37-1.27 (m, 1H), 1.04 (s, 3H), 0.95 (d, J = 7.0 Hz, 3H), 0.84 (d, J = 6.9 Hz, 3H). ^{13}C NMR (100 MHz, CD_3OD) δ 176.07, 174.57, 163.87, 125.51, 104.49, 78.00, 77.90, 75.08, 72.66, 71.98, 71.61, 69.68, 64.88, 64.21, 62.76, 61.10, 56.74, 56.21, 41.44, 36.81, 31.85, 30.82, 29.48, 26.35, 24.17, 17.94, 17.91, 17.13, 14.23; ESI-MS *m/z* calcd for $C_{30}H_{40}O_{13}Na$ $[M+Na]^+$ 631.2361, found 631.2368.

Scheme S7. Synthetic route of Glutriptolide G2-8, Related to Figure 1.

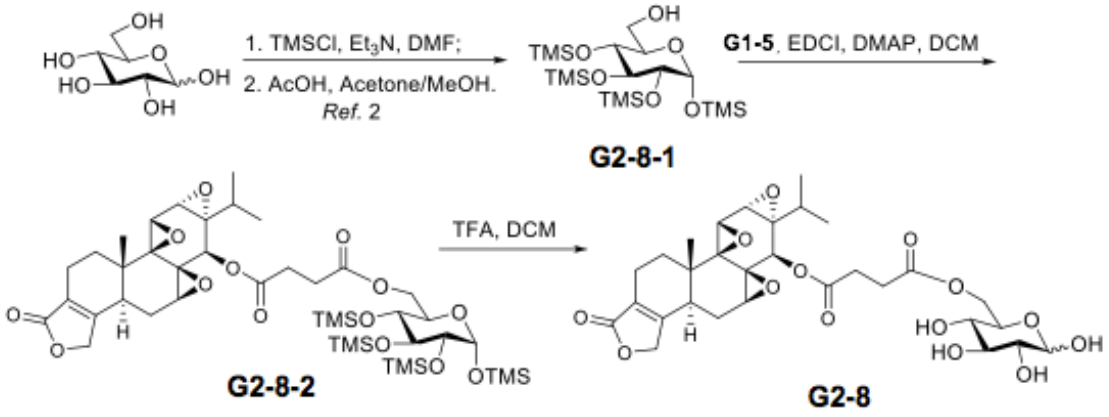

Synthetic procedures for Glutriptolide G2-8, Related to Figure 1.

A solution of Acid **G1-5** (60 mg, 0.13 mmol), compound **G2-8-1** (92 mg, 0.20 mmol), DMAP (cat.), and EDCI (50 mg, 0.26 mmol) in CH_2Cl_2 (4 mL) was stirred for 8 h at RT. The resulting mixture was diluted with CH_2Cl_2, then washed with water and brine, respectively. The organic layers were dried over Na_2SO_4 and filtered. The filtrate was concentrated *in vacuo*. The residue was purified by silica gel column chromatography (petroleum ether/EtOAc, 3:2) to give compounds **G2-8-2** (97 mg, 0.11 mmol, 82%) as white solid. ^{1}H NMR (500 MHz, $CDCl_3$) δ 5.04 (d, J = 0.9 Hz, 1H), 4.96 (d, J = 3.0 Hz, 1H), 4.63 (s, 2H), 4.32 (dd, J = 11.8, 2.3 Hz, 1H), 4.01 (dd, J = 11.8, 5.4 Hz, 1H), 3.86 (ddd, J = 9.8, 5.3, 2.2 Hz, 1H), 3.78 (d, J = 3.2 Hz, 1H), 3.74 (t, J = 8.8 Hz, 1H), 3.49 (dd, J = 3.1, 0.9 Hz, 1H), 3.41 (d, J = 5.8 Hz, 1H), 3.40 – 3.36 (m, 1H), 3.32 (dd, J = 9.1, 3.0 Hz, 1H), 2.80 – 2.60 (m, 5H), 2.31 – 2.02 (m, 4H), 1.93 – 1.81 (m, 2H), 1.52 (dd, J = 11.9, 5.8 Hz, 1H), 1.01 (s, 3H), 0.90 (d, J = 6.9 Hz, 3H), 0.79 (d, J = 6.9 Hz, 3H) , 0.11 (s, 3H) , 0.11 (s, 3H) , 0.10 (s, 3H) , 0.09 (s, 3H); ^{13}C NMR (125 MHz, $CDCl_3$) δ 173.25, 172.00, 171.70, 160.11, 125.54, 93.91, 73.93, 73.84, 72.38, 71.23, 70.02, 69.91, 64.16, 63.52, 63.35, 61.19, 59.70, 55.36, 55.02, 40.38, 35.69, 29.86, 29.14, 29.00, 27.99, 23.46, 17.53, 17.09, 16.74, 13.79, 1.27, 0.96, 0.48, 0.17; ESI-MS *m/z* calcd for $C_{42}H_{70}O_{14}NaSi$ $[M+Na]^+$ 933.3735, found 933.3740.

Compound **G2-8-2** (25 mg, 0.027 mmol) was dissolved in DCM (1.5 mL), and cooled to 0 ^{o}C. Then TFA (0.15 mL) was added. After stirring at this temperature for about 45 min, the reaction mixture was concentrated *in vacuo*. The residue was chromatographed over silica gel (DCM/Methanol = 10:1) to yield the product **G2-8** (15 mg, 0.024 mmol, 89%) as a white solid. ^{1}H NMR (500 MHz, CD_3OD) δ 5.51 (s, 0.37H), 5.11 (d, J = 3.7 Hz, 0.66H), 5.09 (d, J = 1.1 Hz, 1H), 4.86 – 4.76 (m, 2H), 4.50 (d, J = 7.8 Hz, 0.33H), 4.49 – 4.43 (m, 0.32H), 4.39 (dd, J = 11.7, 2.2 Hz, 0.63H), 4.29 – 4.17 (m, 1H), 4.03 – 3.98 (m, 0.57H), 3.98 (dd, J = 3.3, 1.2 Hz, 1H), 3.69 (t, J = 9.3 Hz, 0.62H), 3.65 (td, J = 3.5, 1.0 Hz, 1H), 3.52 (ddd, J = 9.5, 6.1, 2.1 Hz, 0.35H), 3.48

(d, J = 5.7 Hz, 1H), 3.37 (s, 1H), 3.31 – 3.26 (m, 1.45H), 3.16 (dd, J = 9.0, 7.8 Hz, 032H), 2.84 – 2.76 (m, 1H), 2.76 – 2.65 (m, 4H), 2.27 (ddt, J = 17.0, 11.0, 5.7 Hz, 2H), 2.16 – 2.04 (m, 1H), 1.99 – 1.85 (m, 2H), 1.53 (ddd, J = 12.5, 5.6, 1.5 Hz, 1H), 1.34 (ddd, J = 21.7, 10.8, 5.2 Hz, 2H), 1.26 (t, J = 7.1 Hz, 0H), 1.06 (s, 3H), 0.96 (d, J = 7.0 Hz, 3H), 0.85 (d, J = 6.9 Hz, 3H); ^{13}C NMR (100 MHz, CD_3OD) δ 176.10, 173.92, 173.85, 173.35, 173.31, 163.91, 125.50, 98.22, 93.96, 77.93, 76.16, 75.31, 74.73, 73.73, 73.06, 73.05, 72.00, 71.96, 71.71, 70.60, 65.35, 65.27, 64.87, 64.27, 62.70, 61.00, 56.74, 56.18, 41.45, 36.79, 30.82, 30.06, 29.84, 29.82, 29.11, 24.16, 17.91, 17.87, 17.08, 14.21, 14.19; ESI-MS *m/z* calcd for $C_{30}H_{38}O_{14}Na$ $[M+Na]^+$ 645.2154, found 645.2159.

Reference: [2]Fan, W.; Wu, Y.; Li, X.; Yao, N.; Yu, Y.; Hai, L. *Eur. J. Med. Chem.,* **2011**, *46*, 3651–3661; Cui, Y.; Cheng, Z.; Mao, J.; Yu, Y. *Tetrahedron Lett.*, **2013**, *54*, 3831–3833.

Scheme S8. Synthetic route of Glutriptolide G2-9, Related to Figure 1.

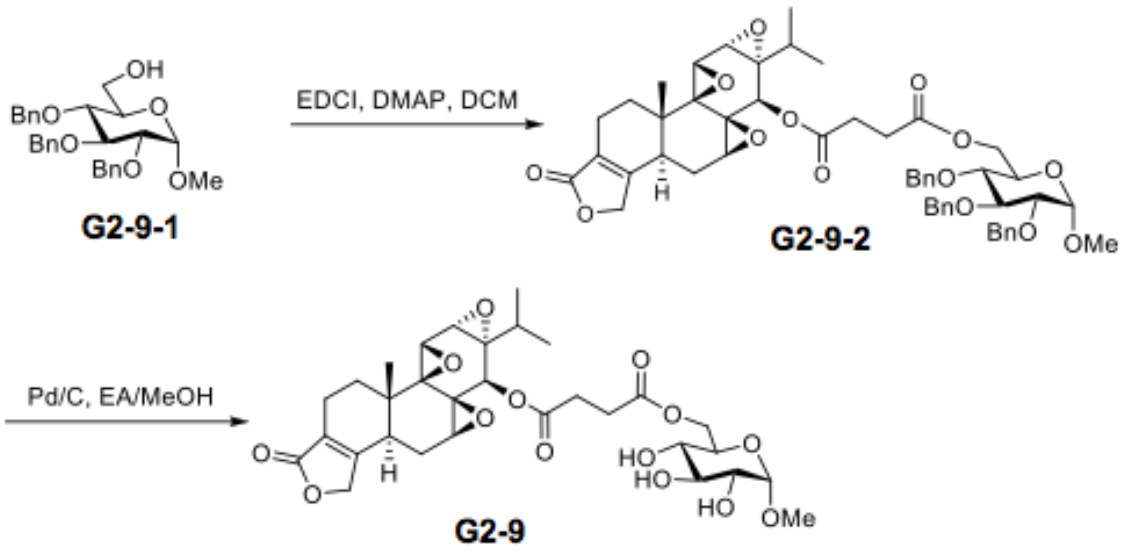

Synthetic procedures for Glutriptolide G2-9, Related to Figure 1.

A solution of Acid **G1-5** (25 mg, 0.054 mmol), compound **G2-9-1**[3] (50 mg, 0.11 mmol), DMAP (2 mg, 0.011mmol), and DCC (22 mg, 0.11 mmol) in CH_2Cl_2 (2 mL) was stirred for 8 h at RT. The resulting mixture was diluted with CH_2Cl_2, then washed with water and brine, respectively. The organic layers were dried over Na_2SO_4 and filtered. The filtrate was concentrated *in vacuo*. The residue was purified by silica gel column chromatography (petroleum ether/EtOAc, 3:2) to give the product **G2-9-2** (41 mg, 0.045 mmol, 83%) as a white solid: ^{1}H NMR (500 MHz, $CDCl_3$) δ 7.46 – 7.13 (m, 13H), 5.04 (s, 1H), 4.99 (d, J = 10.8 Hz, 1H), 4.86 (d, J = 10.8 Hz, 1H), 4.82 (d, J = 10.8 Hz, 1H), 4.78 (d, J = 12.1 Hz, 1H), 4.70 – 4.53 (m, 5H), 4.35 (dd, J = 11.9, 4.5 Hz, 1H), 4.26 (dd, J = 11.9, 2.1 Hz, 1H), 3.99 (t, J = 9.2 Hz, 1H), 3.84 – 3.75 (m, 2H), 3.54 (dd, J = 9.6, 3.6 Hz, 1H), 3.51 – 3.45 (m, 2H), 3.39 (d, J = 5.6 Hz, 1H), 3.36 (s, 3H), 2.30 (d, J = 15.1 Hz, 1H), 1.54 (dd, J = 12.5, 4.7 Hz, 1H), 1.02 (s, 3H), 0.90 (d, J = 7.0 Hz, 3H), 0.80 (d, J = 6.9 Hz, 3H); ^{13}C NMR (125 MHz, $CDCl_3$) δ 173.32, 171.95, 171.77, 160.05, 138.75, 138.16, 128.61, 128.55, 128.24, 128.18, 128.12, 128.10, 127.98, 127.80, 125.70, 98.19, 82.16, 80.03, 77.47, 75.95, 75.19, 73.52, 71.34, 70.06, 68.70, 63.62, 63.42, 63.35, 61.30, 59.76, 55.47, 55.38, 55.10, 40.46, 35.77, 29.96, 29.16, 29.03, 28.16, 23.51, 17.58, 17.18, 16.81, 13.88; ESI-MS (*m/z*): 930.4 $[M+Na]^+$.

Palladium on charcoal (10%, 10 mg) was added to a solution of compound **G2-9-2** (17 mg, 0.019 mmol) in CH_3OH. The mixture was placed under an atmosphere of hydrogen for about 14 h. The mixture was filtered and concentrated. The residue was purified by silica gel column chromatography (CH_2Cl_2/CH_3OH, 15:1) to give compound **G2-9** (7 mg, 0.011 mmol, 60%) as a

white solid: ^{1}H NMR (400 MHz, CD_3OD) δ 5.07 (s, 1H), 4.87 – 4.72 (m, 2H), 4.65 (d, J = 3.7 Hz, 1H), 4.41 (dd, J = 11.7, 2.0 Hz, 1H), 4.26 – 4.14 (m, 1H), 3.96 (d, J = 3.2 Hz, 1H), 3.80 – 3.69 (m, 1H), 3.63 (d, J = 3.0 Hz, 1H), 3.60 (d, J = 9.2 Hz, 1H), 3.46 (d, J = 5.6 Hz, 1H), 3.45 – 3.38 (m, 4H), 2.71 (t, J = 3.6 Hz, 6H), 2.37 – 1.83 (m, 5H), 1.04 (s, 3H), 0.94 (d, J = 7.0 Hz, 3H), 0.83 (d, J = 6.9 Hz, 3H); ^{13}C NMR (100 MHz, CD_3OD) δ 176.08, 173.82, 173.27, 163.89, 125.51, 101.25, 75.04, 73.45, 73.07, 71.98, 71.89, 71.02, 65.23, 64.87, 64.27, 62.69, 61.00, 56.73, 56.19, 55.63, 41.46, 36.80, 30.83, 30.09, 29.86, 29.10, 24.17, 17.92, 17.87, 17.08, 14.19; ESI-MS (*m/z*): 659.6 $[M+Na]^+$.

KEY RESOURCES TABLE

REAGENT or RESOURCE	SOURCE	IDENTIFIER
Biological samples		
Human serum	Sigma	Cat#H4522-20mL
Anti-Rpb1	Santa Cruz Biotechnology	Cat#SC-17798
Anti-XPB	Biotechne	Cat#AF6349-SP
Anti-Actin	Developmental Studies Hybridoma Bank	Cat#JLA20
Anti-GAPDH	Santa Cruz Biotechnology	Cat#SC-20357
Anti-cytochrome C	Santa Cruz Biotechnology	Cat#SC-7159
Anti-PARP1	Santa Cruz Biotechnology	Cat#SC-7150
Anti-cleaved caspase 3	Cell Signaling Technology	Cat#9661
Anti-VDAC	ProteinTech	Cat#10866-1-AP
Anti-HIF 1a	BD Sciences	Cat#610958
Anti-GLUT1	Santa Cruz Biotechnology	Cat#SC-377228
Anti-mouse IgG HRP	GE	Cat#NXA931-1mL
Anti-rabbit IgG HRP	GE	Cat#NXA934-1mL
Anti-mouse Alexa Fluor 488	Invitrogen	Cat#A28175
Chemicals, Peptides, and Recombinant Proteins		
Triptolide	Sigma	Cat#T3652
Glutriptolides	He et al., 2016	N/A
Purified TFIIH complex	Titov et al. 2011	N/A
Spironolactone	Acros Organics/Fisher Scientific	Cat#AC207460010
Doxorubicin	APExBio	Cat#A1832
1% O_2	Airgas	Cat#X03NI94C2000650
[^{3}H] Thymidine	Perkin Elmer	Cat# NET027W001MC
[γ-^{32}P] ATP	Perkin Elmer	Cat#BLU002A250UC
DAPI	ThermoFisher	Cat#D1306
Hoechst 33258	Sigma	Cat#861405

2-NBDG	ThermoFisher	Cat#N13195
Critical Commercial Assays		
TACS XTT Cell Proliferation/Viability Assay	R&D Systems	Cat#4891-025-K
Experimental Models: Animal		
Male NOD/SCID/IL2Rγnull Mouse	JHU Animal Resources Core	N/A
Experimental Models: Cell lines		
PC3/ML/fluc	Bhatnagar et al. 2014	N/A
Primary astrocytes	Lonza	Cat#CC-2565
Fibroblast	ATCC	Cat#PCS-201-012
Airway epithelial cell	ATCC	Cat#PCS-301-010
Renal proximal tubule cell	ATCC	Cat#PCS-400-010
Prostate Epithelial cell	Lonza	Cat#CC-2555
Mammary Epithelial cell	Lonza	Cat#CC-2551
PC3	ATCC	Cat#CRL-1435
LNCap	ATCC	Cat#CRL-1740
DU-145	ATCC	Cat#HTB-81
MDA-MB-231	ATCC	Cat#HTB-26
MDA-MB-453	ATCC	Cat#HTB-131
SK-BR-3	ATCC	Cat#HTB-30
A253	ATCC	Cat#HTB-41
Detroit 562	ATCC	Cat#CCL-138
SCC-25	ATCC	Cat#CRL-1625
SK-Mel-3	ATCC	Cat#HTB-69
SK-Mel-1	ATCC	Cat#HTB-67
RPMI-7951	ATCC	Cat#HTB-66
CFPAC-1	ATCC	Cat#CRL-1918
BxPC3	ATCC	Cat#CRL-1687

SW1990	ATCC	Cat#CRL-2172
A549	ATCC	Cat#CCL-185
NCI-H1299	ATCC	Cat#CRL-5803
NCI-H1437	ATCC	Cat#CRL-5872
SNU-475	ATCC	Cat#CRL-2236
SK-HEP-1	ATCC	Cat#HTB-52
SNU-387	ATCC	Cat#CRL-2237
HeLa	ATCC	Cat#CCL-2
HEK 293T WT	ATCC	Cat#CRL-3216
HEK 293T 7115 (C342T XPB)	He et al. 2016	N/A
HUVEC	Lonza	Cat#C2517A
MCF-7	ATCC	Cat#HTB-22
HepG2	ATCC	Cat#HB-8065
Recombinant DNA		
RNA Polymerase II promoter positive control DNA	Promega	Cat#E3621
Software and Algorithms		
ImageJ	NIH	http:// imagej.nih.gov/ij/index.html
GraphPad Prism	GraphPAd Software Inc	http://www.graphpad.com/scientific- software/prism/
Other		
Hypoxia chamber	Billups-Rothenberg	Cat#MIC-101
PEI cellulose plates	Sigma	Cat#Z122882-25EA
Typhoon FLA 9500 Variable Imager system	GE Healthcare Life Sciences	Cat# 28996943
Nikon Eclipse TE200 Inverted microscope	Nikon Instruments Inc./Johns Hopkins School of Medicine, Department of Pharmacology and Molecular Sciences	N/A
IVIS Spectrum Imaging System	Caliper Life Sciences	Cat#124262

Transparent Methods

Cells and culture conditions

Primary astrocytes (Lonza, Walkersville, MD; ABMÔ Basal Media with AGMTM SingleQuotsTM Supplement Pack), fibroblast (ATCC; Fibroblast Basal Medium (ATCC® PCS-201-030TM) with Fibroblast Growth Kit-Serum-free (ATCC® PCS-201- 040TM)), airway epithelial cell (ATCC; Airway Epithelial Cell Basal Medium (ATCC® PCS- 300-030TM) with Bronchial Epithelial Cell Growth Kit (ATCC® PCS-300-040TM)), renal proximal tubule (ATCC; Renal Epithelial Cell Basal Medium (ATCC® PCS-400-030TM) with Renal Epithelial Cell Growth Kit (ATCC® PCS-400-040TM)), prostate epithelial cell (Lonza; PrEGMTM BulletKitTM) and mammary epithelial cell (Lonza; MEBMTM BulletKitTM) were kept in a humidified incubator at 37 °C adjusted to 5% CO2. Prostate (PC3, LNCaP, DU-145), breast (MDA-MB-231, MDA-MB-453, SK-BR-3), head and neck (A253, Detroit 562, SCC-25), melanoma (SK-Mel-3, SK-Mel-1, RPMI-7951), pancreatic (CfPAC-1, BxPC3, SW1990), lung (A549, NCI-H1299, NCI-H1437) and liver (SNU-475, SK-HEP-1, SNU-387) cancer cell lines were obtained from ATCC and cultured in their respective media (prostate cells: RPMI-1640, MDA-MB-231: RPMI-1640, MDA-MB-453: Leibovitz's L-15, SK-BR-3: McCoy's 5a, A253: McCoy's 5a, Detroit 562: EMEM, SCC-25: DMEM, SK-Mel-3: McCoy's 5a, SK-Mel-1: EMEM, RPMI-7951: EMEM), CfPAC-1: IMDM, BxPC3: RPMI-1640, SW1990: Leibovitz's L-15), A549: F-12K, NCI-H1299: RPMI-1640, NCI-H1437: RPMI-1640, SNU-475: RPMI-1640, SK-HEP-1: EMEM, SNU-387: RPMI-1640. All media were supplemented with 10% (vol/vol) filtered fetal bovine serum (FBS, Invitrogen, Carlsbad, CA), 1% penicillin/streptomycin (Invitrogen) and maintained in a humidified incubator at 37 °C with 5% CO2 except for MDA-MB-453 and SW1990 grown at 37 °C without CO2 control. Wild type (ATCC) and C342T XPB knock-in cells (named T7115) of Human Embryonic Kidney 293T (HEK293T), HeLa (ATCC), DLD-1 parental and GLUT1 KO (provided by Dr. Bert Vogelstein at Johns Hopkins University School of Medicine) were cultured in DMEM (GIBCO) with 10% (vol/vol) filtered fetal bovine serum (FBS, Invitrogen, Carlsbad, CA), 1% penicillin/streptomycin (Invitrogen).

In vivo tumor xenograft assay

Animal experiments were performed following the protocols approved by the Johns Hopkins University Animal Care and Use Committee. The experimental murine model of human prostate cancer metastasis used in this study was generated based on a published procedure (Bhatnagar et al., 2014). Briefly, four-to-six-week-old, male NOD/SCID/IL2Rgnull (NSG, purchased from Animal Resources Core, JHU) were injected with a million PC3/ML/fluc cells via tail vein. Tumor formation was confirmed by bioluminescence imaging (BLI) using the IVIS Spectrum Imaging System (Caliper Life Sciences, Hopkinton, MA) three weeks after injection and the mice were given indicated doses of drug once daily (intraperitoneal injection) for 30 days. Tumor progression was then monitored weekly by BLI and survival monitored concurrently.

Reagents

Triptolide and WZB117 were purchased from Sigma while spironolactone was obtained from Acros Organics. Doxorubicin was from APExBio. Glutriptolides were synthesized following procedures detailed in the Supplemental Information.

Proliferation and viability assays

[3H]-thymidine incorporation. HEK293T cells (10,000 cells/well) were seeded into 96-well plates then cultured in DMEM plus 10% FBS and 1% penicillin/streptomycin at 37°C with 5% CO2 overnight. Drugs were added at indicated concentrations and incubation was continued for an additional 24 h. For hypoxia, PC3 (5,000 cells/well) were exposed to 1% O2 (Airgas) in a humidified hypoxia chamber (Billups-Rothenberg) in 37°C for 48 h prior to drug exposure for 48 h. Treated cells were then pulsed using an aliquot of 1 μCi of [^{3}H]-thymidine (Perkin Elmer) per well for an additional 6 h. Radiolabelled cells were harvested onto a printed Filtermat A glass fiber filter (Perkin Elmer) using a Tomtec Harvester 96 Mach III M. Betaplate Scint (Perkin Elmer) scintillation fluid was added to radiolabelled filters followed by scintillation counting on Microbeta2 LumiJET Microplate Counter (Perkin Elmer).

XTT assay. Five thousand cells/well were plated on flat-bottom, transparent 96-well plate in a full growth media and incubated at appropriate culture conditions. Twenty four hours after seeding, cells were treated with indicated drugs and incubated for 47 hrs. Cell viability was measured using the R&D SystemsTM TACS XTT Cell Proliferation/Viability Assay (R&D Systems, Minneapolis, MN).

ATPase activity assay

The TFIIH complex was purified and its DNA-dependent ATPase assay was performed based on a published protocol (Titov et al., 2011). Briefly, a 10-µl reaction mixture contained 20 mM Tris (pH 7.9), 4 mM $MgCl_2$, 1 µM of ATP, 0.1 μCi [γ-^{32}P]ATP (3000 Ci/mmol), 100 μg/ml BSA, 100 nM RNA Polymerase II promoter positive control DNA , 1 nM TFIIH and indicated concentrations of triptolide or its analogs. The reactions were started by either addition of TFIIH for 2 hr and stopped by addition of 2 μl of 0.5 M EDTA. An aliquot of 1 μl reaction mixture was spotted on PEI-cellulose (sigma) and the chromatogram was developed with 0.5 M LiCl and 1 M HCOOH. The percent of ATP hydrolysis was quantified using a Typhoon FLA 9500 Variable Imager (GE Healthcare).

Stability of glutriptolides in human serum

Human serum (Sigma,10% in DMEM media) was treated with 10 μM drug (triptolide or glutriptolides) at room temperature for various time points. The incubation was stopped by placing samples on dry ice followed by overnight storage in -80 °C. Frozen samples were then lyophilized and reconstituted in DMSO at room temperature for an hour. Samples were centrifuged at 12,000 RPM for 10 minutes and supernatants loaded into an HPLC-MS with the following conditions: (Varian pursuit XR5 Diphenyl 150x 4.6 mm; A phase: Millipore water with 0.1% HCOOH; B phase: Acetonitrile with 0.1% HCOOH; 0 - 6 min: 95% B; 6 - 24 min: 5% B-100% B; 24 - 28 min: 100% B; 28 - 29 min: 100% B-5% B; 29 -30 min: 5% B).

Western blot analysis

Whole cell lysates were prepared by adding lysis buffer [4% SDS, 20% glycerol, 10% 2-mercaptoethanol, 0.004% bromophenol blue, 0.125 M Tris-HCl (pH 6.8)] to the cell pellets for 30 minutes in ice followed by centrifugation at 12,000 x g for 10 minutes then boiling for 5 minutes. For isolation of cytosolic and mitochondrial fractions of cytochrome C, cell pellets were resuspended in CLAMI buffer (250 mM sucrose, 70 mM KCl, 50 mg/ml digitonin in 1X PBS, protease inhibitor cocktail (1 tablet/ 10 ml CLAMI buffer)) then incubated on ice for 5 minutes. After centrifugation at 12,000 x g for 5 minutes at 4°C, supernatant (cytoplasmic fraction) was collected and the pellet resuspended in lysis buffer as described above. Proteins were then separated by SDS-PAGE and transferred to nitrocellulose membranes (Bio-Rad). After blocking at room temperature for 1 h, membranes were incubated at 4°C overnight with the primary antibodies including anti-Rpb1 (Santa Cruz Biotechnology), anti–XPB (Biotechne), anti-Actin (Developmental Studies Hybridoma Bank), anti-GAPDH (Santa Cruz Biotechnology), anti-cytochrome C (Santa Cruz Biotechnology), anti-PARP1 (Santa Cruz Biotechnology), anti-cleaved caspase 3 (Cell Signaling Technology), anti-VDAC (ProteinTech), anti-HIF-1 (BD sciences), and anti-GLUT1 (Santa Cruz Biotechnology) antibodies followed by incubation with horseradish peroxidase–conjugated anti-mouse or anti-rabbit IgG (GE Healthcare) at room temperature for 2 hours. Antibody–protein complexes were detected using enhanced chemiluminescence (ECL) immunoblotting detection reagent (EMD Millipore).

Immunocytochemistry and cytochemistry

HeLa or PC3 cells (2 × 105) were seeded on a MatTek glass bottom culture dish (Fisher Scientific, Pittsburgh, PA, USA) and allowed to adhere for 24 h. Cells were then treated with either DMSO or drugs for 6 or 24 h then fixed with 4% paraformaldehyde, permeabilized using 1X PBS with 0.5% triton X 100 then probed for endogenous RNA Polymerase II catalytic subunit Rpb1 or HIF-1a using anti-RNAPII (Santa Cruz Biotechnology) and anti-HIF-1a (BD sciences) antibodies, respectively. Detection was then done using anti-mouse Alexa Fluor 488 (Invitrogen). For nuclear staining, fixed and permeabilized cells were incubated in DAPI (ThermoFisher) or Hoechst 33258 (Sigma) for 30 minutes prior to imaging. Glucose uptake was monitored by incubating cells in 200 μM 2-NBDG (ThermoFisher) for 6 hours prior to fixation. Fluorescence was observed under the Nikon Eclipse TE200 Inverted microscope (Nikon Instruments Inc., Melville, NY, USA). ImageJ software (NIH, Bethesda, MD, USA; http:// imagej.nih.gov/ij/index.html) was used to measure intracellular protein levels in immuno-cytochemistry samples (Li et al., 2015). Rpb1 levels were measured using the MEASURE feature of ImageJ where all the background signals were subtracted from the intergrated density of nuclear Rpb1.

Statistical analysis

Data fitting for dose curves was performed using GraphPad Prism for Mac, GraphPad

Software (www.graphpad.com). Statistical values were reported in the Figures (Figures 3A and S2) and Tables (Table 2). Results are presented as mean with SEM unless otherwise specified and statistical significance was determined using two-tailed Student's *t-test* (unequal variance). Survival curves were estimated using Kaplan-Meier method and chi-square testing was used to determine significant differences among groups (Sullivan, 2017) through GraphPad Software. Effect size between conditions were estimated using Cohen's d ($d = M_1 – M_2 / s$; $M_1 - M_2$ is the difference between the group means and s is the standard deviation of either group) (Sullivan and Feinn, 2012).

NMR of glutriptolides

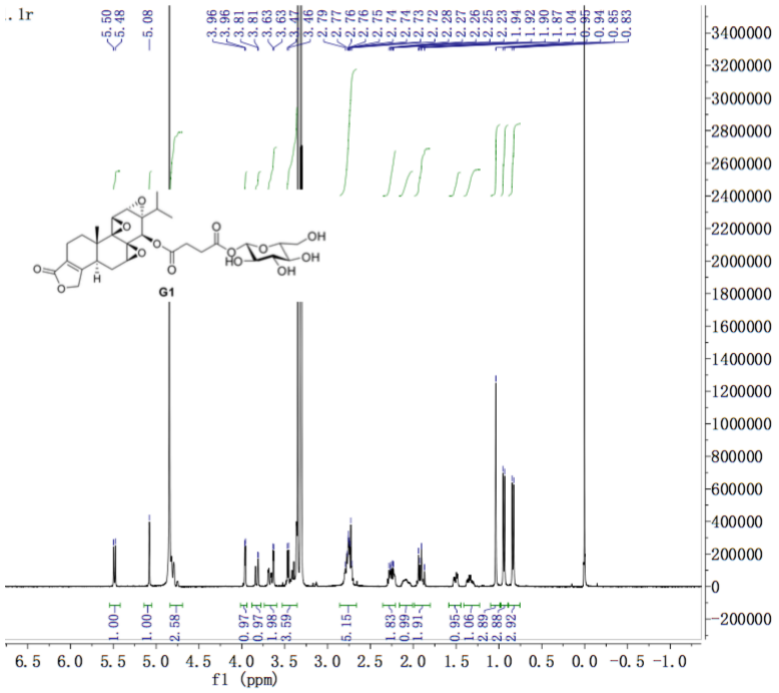

Figure S5. ^{1}H (500 MHz) – NMR of **G1** in CD_3OD, Related to Figure 1.

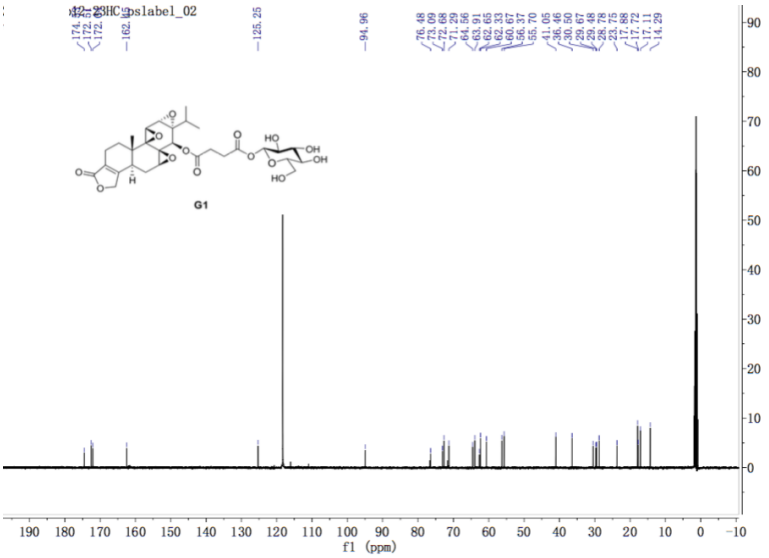

Figure S6. ^{13}C (125 MHz) – NMR of **G1** in CD_3CN, Related to Figure 1.

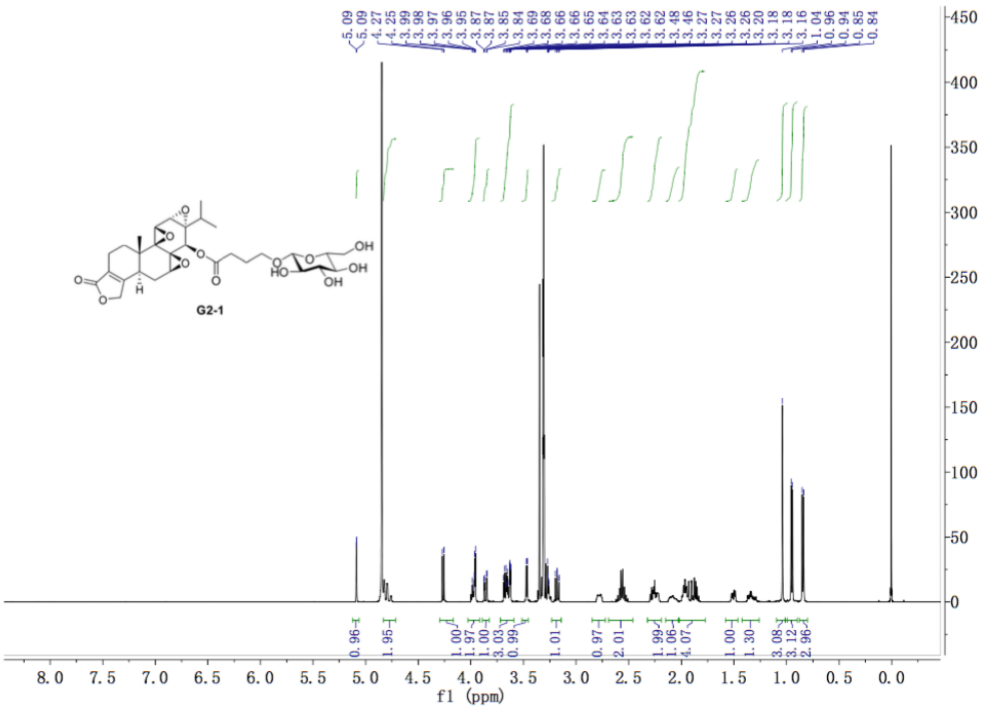

Figure S7. ^{1}H (500 MHz) – NMR of **G2-1** in CD_3OD, Related to Figure 1.

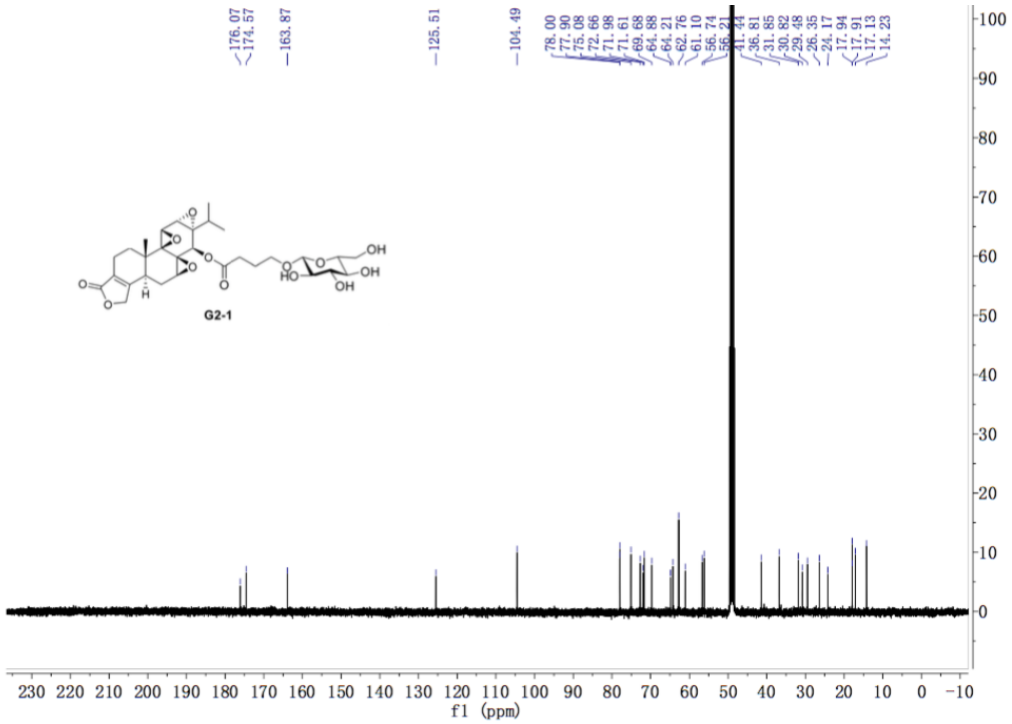

Figure S8. ^{13}C (100 MHz) – NMR of **G2-1** in CD_3OD, Related to Figure 1.

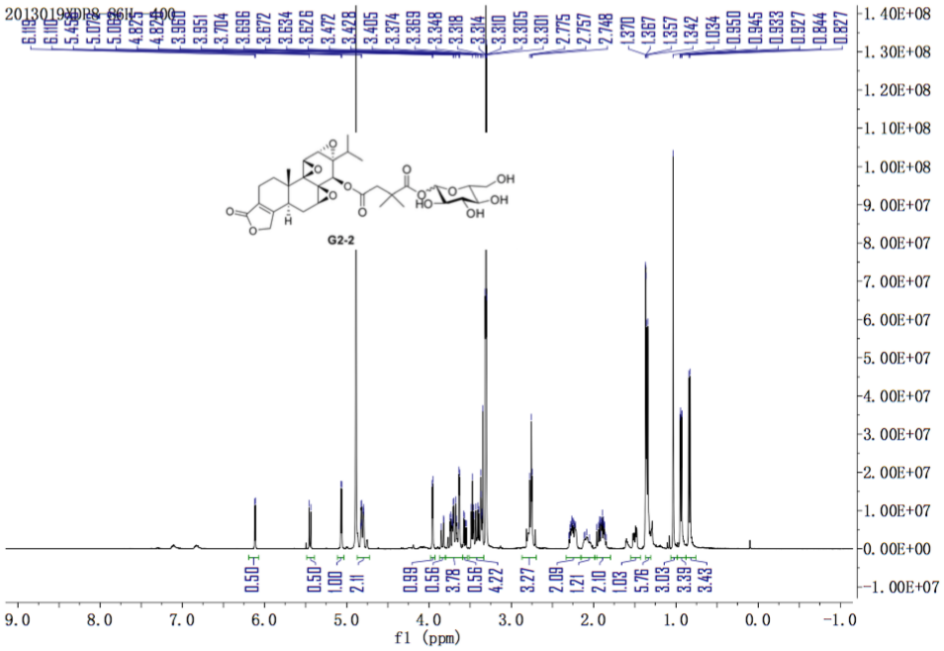

Figure S9.[1]H (400 MHz) – NMR of **G2-2** in CD_3OD, Related to Figure 1.

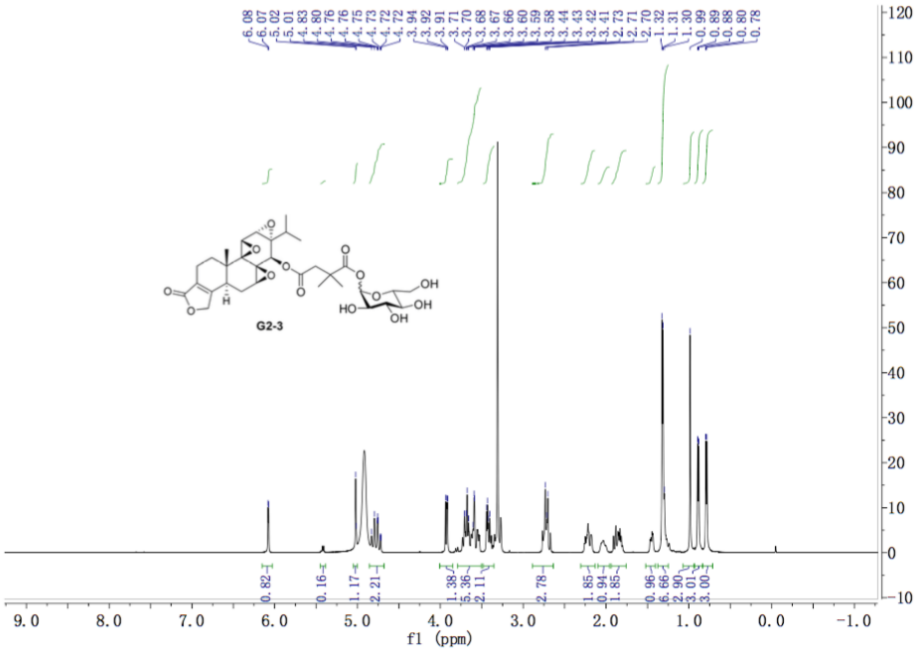

Figure S10. ^{1}H (500 MHz) – NMR of **G2-3** in CD_3OD, Related to Figure 1.

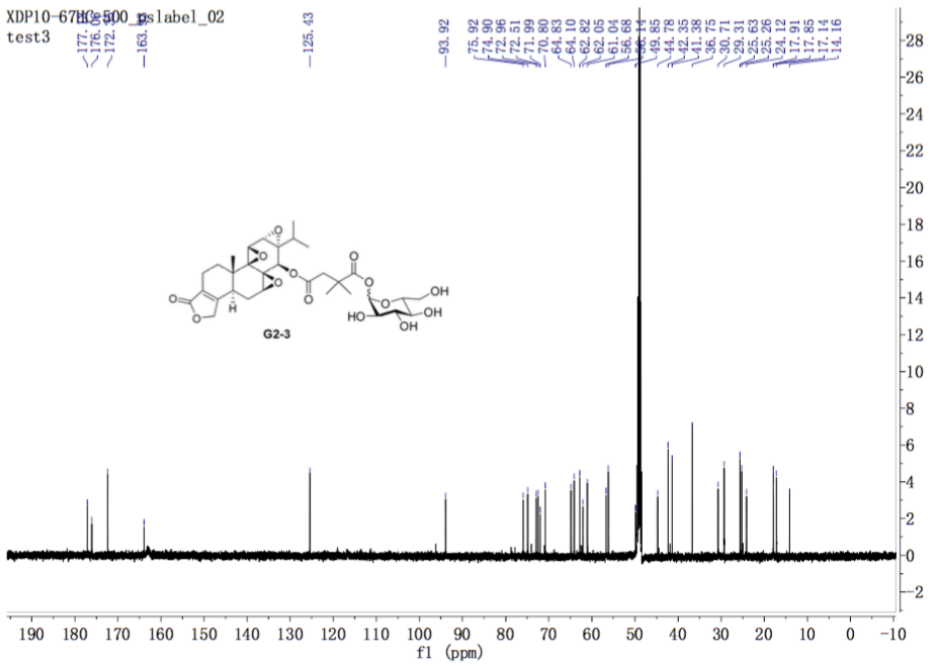

Figure S11.^{13}C (126 MHz) – NMR of **G3-3** in CD_3OD, Related to Figure 1.

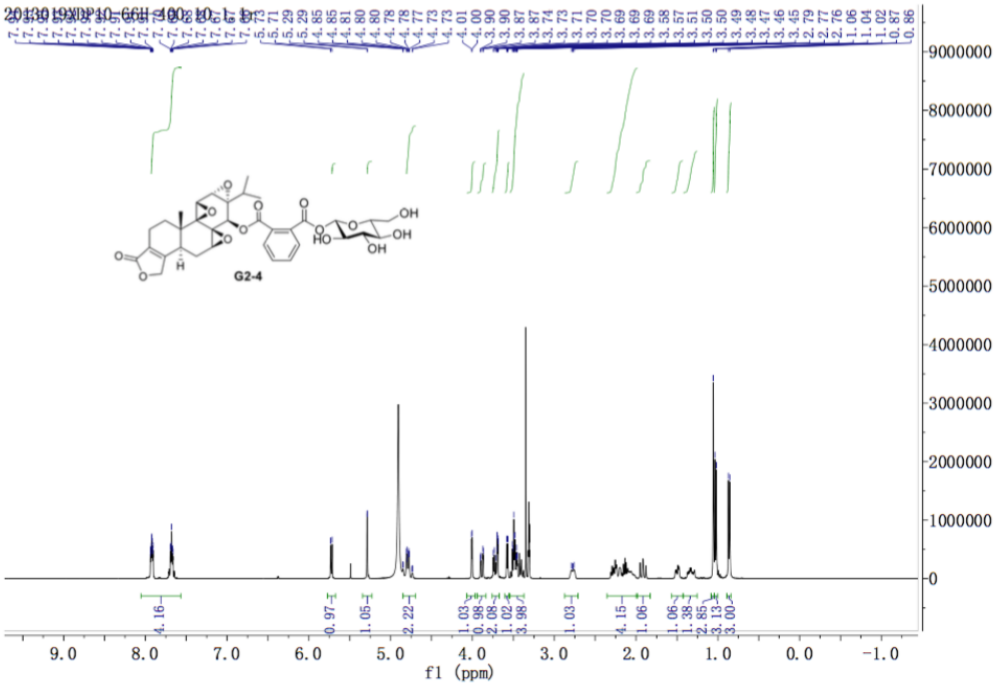

Figure S12. ^{1}H (400 MHz) – NMR of **G2-4** in CD_3OD, Related to Figure 1.

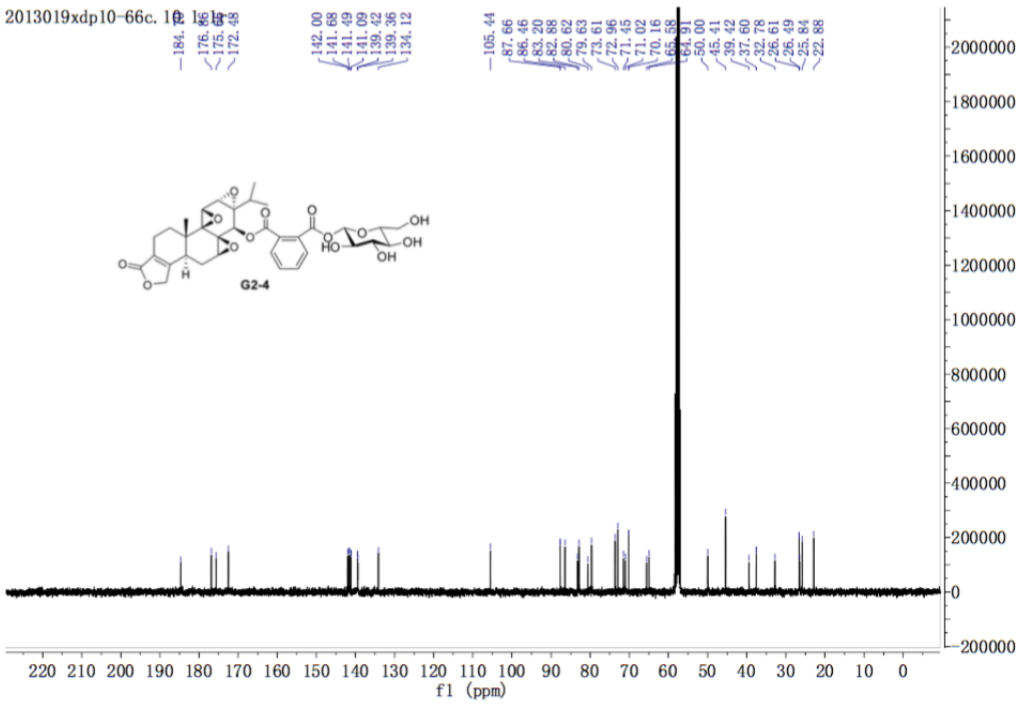

Figure S13. ^{13}C (100 MHz) – NMR of **G2-4** in CD_3OD, Related to Figure 1.

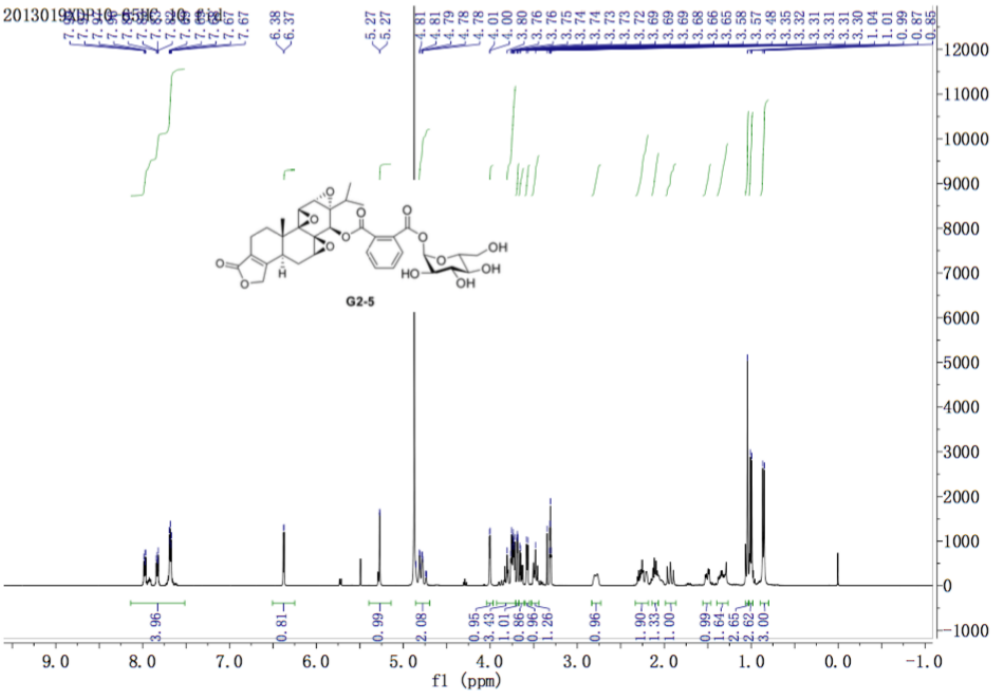

Figure S14. ^{1}H (400 MHz) – NMR of **G2-5** in CD_3OD, Related to Figure 1.

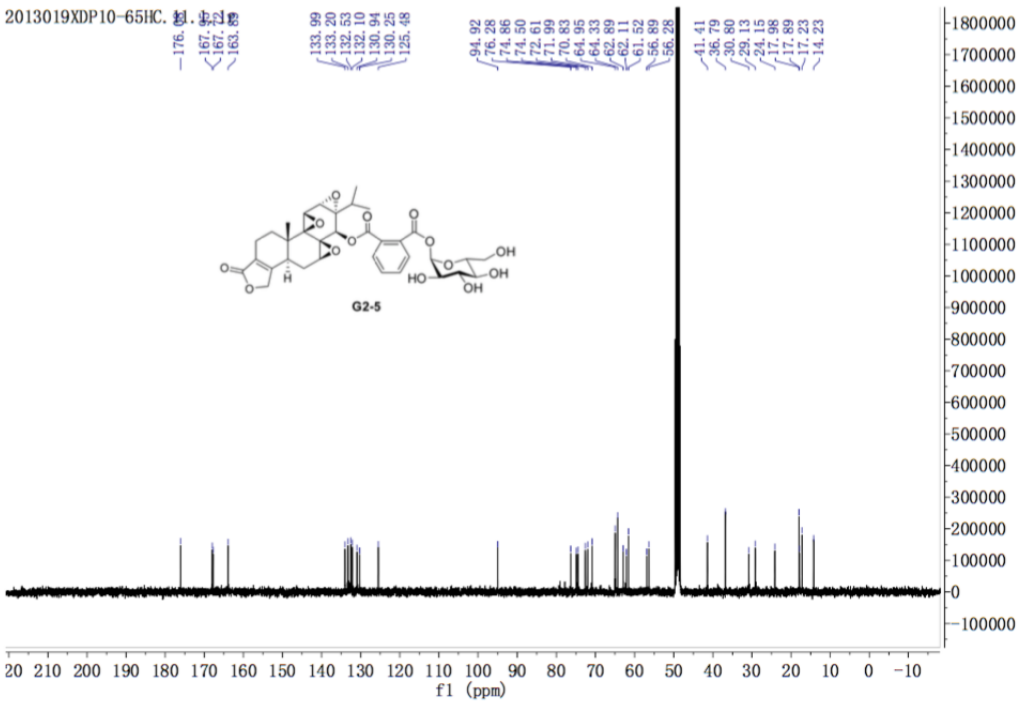

Figure S15. ^{13}C (100 MHz) – NMR of **G2-5** in CD_3OD, Related to Figure 1.

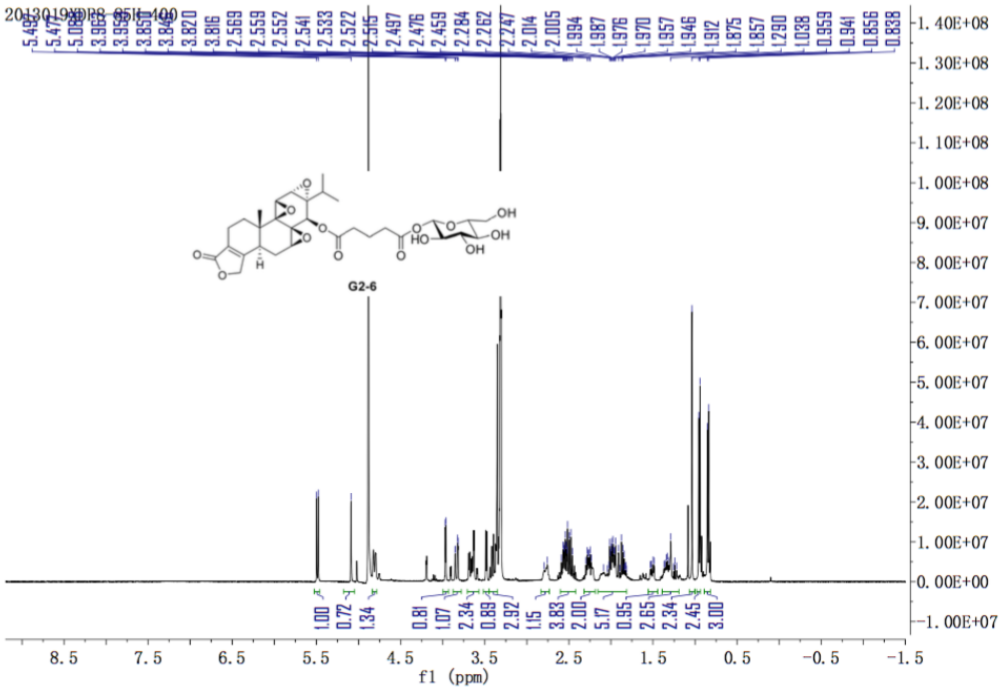

Figure S16. ^{1}H (400 MHz) – NMR of **G2-6** in CD_3OD, Related to Figure 1.

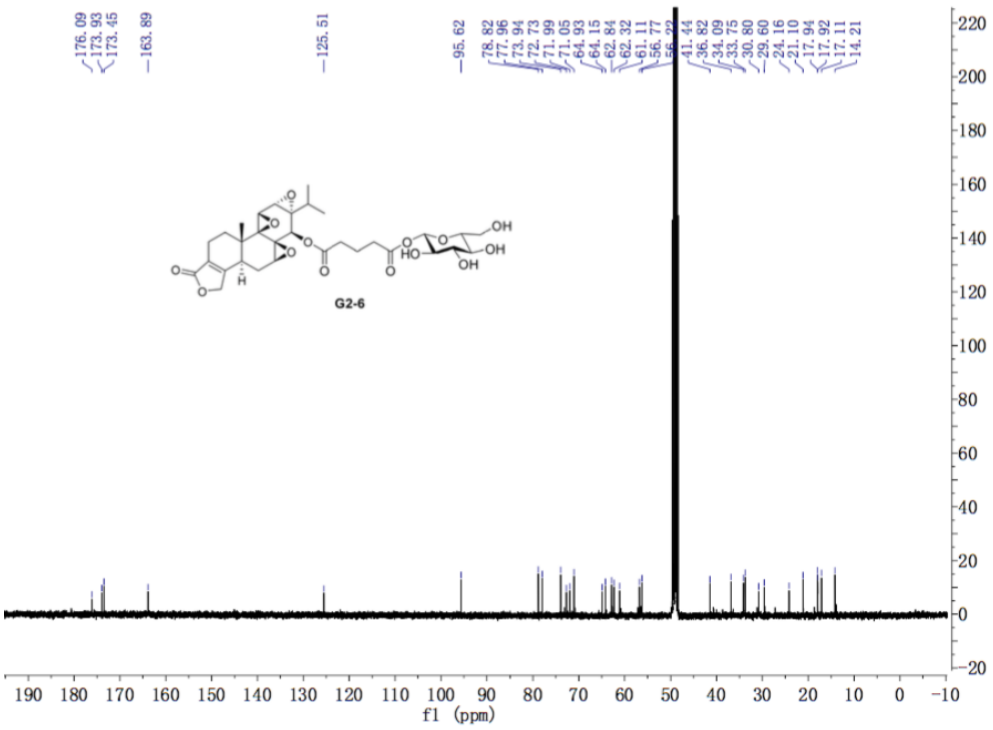

Figure S17. ^{13}C (100 MHz) – NMR of **G2-6** in CD_3OD, Related to Figure 1.

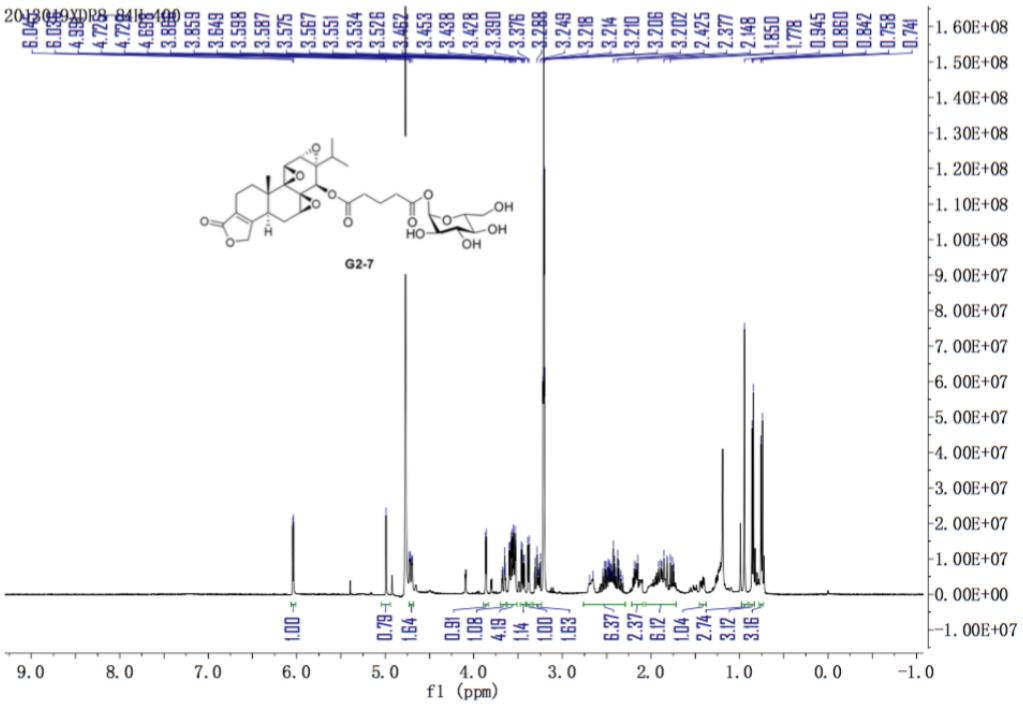

Figure S18. ^{1}H (400 MHz) – NMR of **G2-7** in CD_3OD, Related to Figure 1.

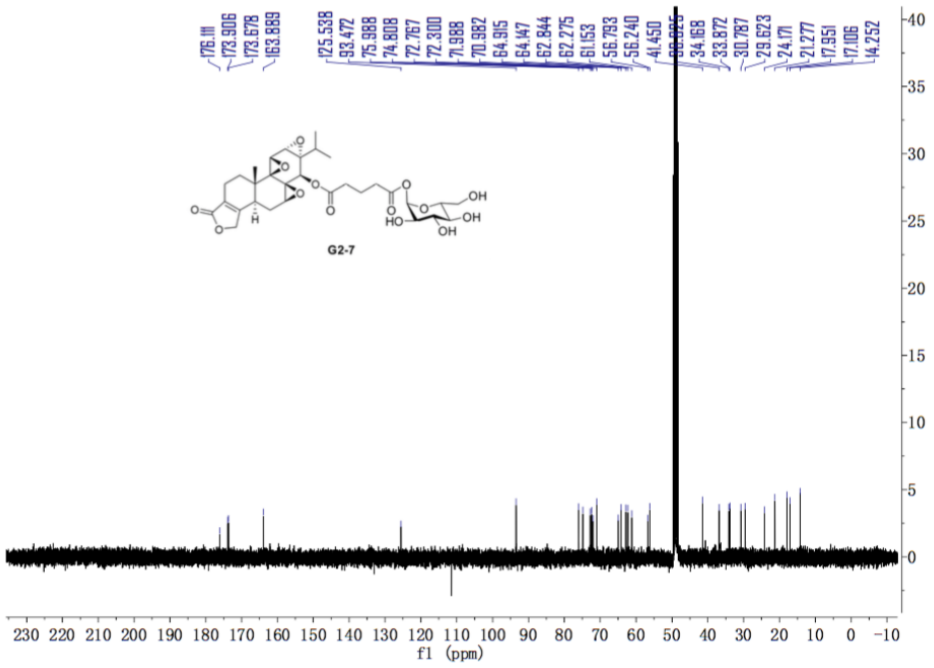

Figure S19. ^{13}C (100 MHz) – NMR of **G2-7** in CD_3OD, Related to Figure 1.

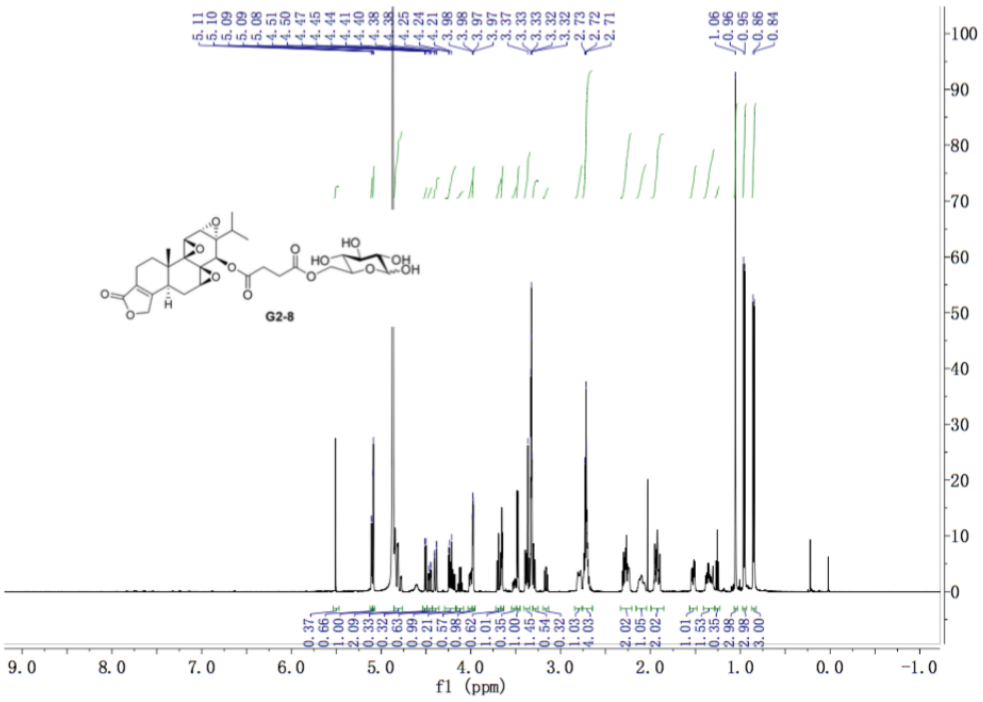

Figure S20. ^{1}H (500 MHz) – NMR of **G2-8** in CD_3OD, Related to Figure 1.

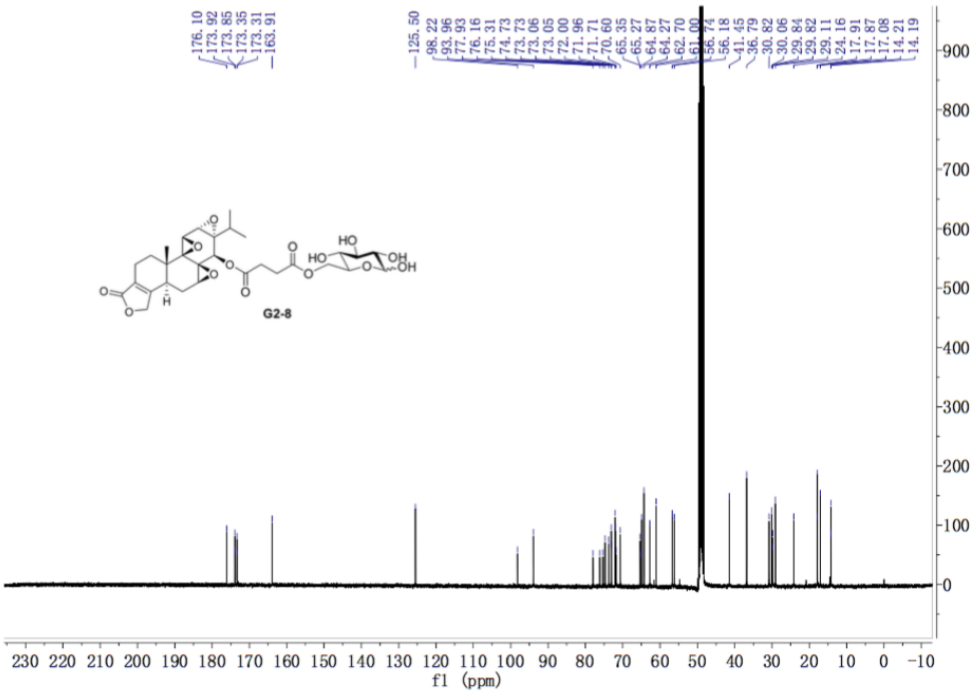

Figure S21. ^{13}C (100 MHz) – NMR of **G2-8** in CD_3OD, Related to Figure 1.

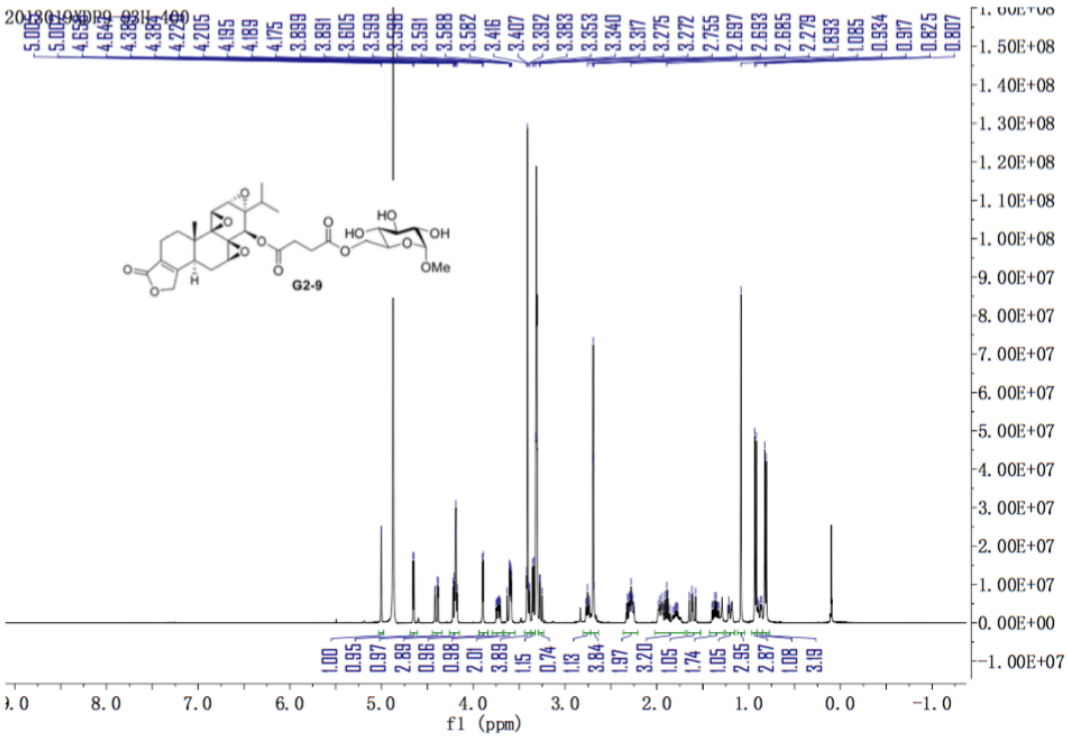

Figure S22. ^{1}H (400 MHz) – NMR of **G2-9** in CD_3OD, Related to Figure 1.

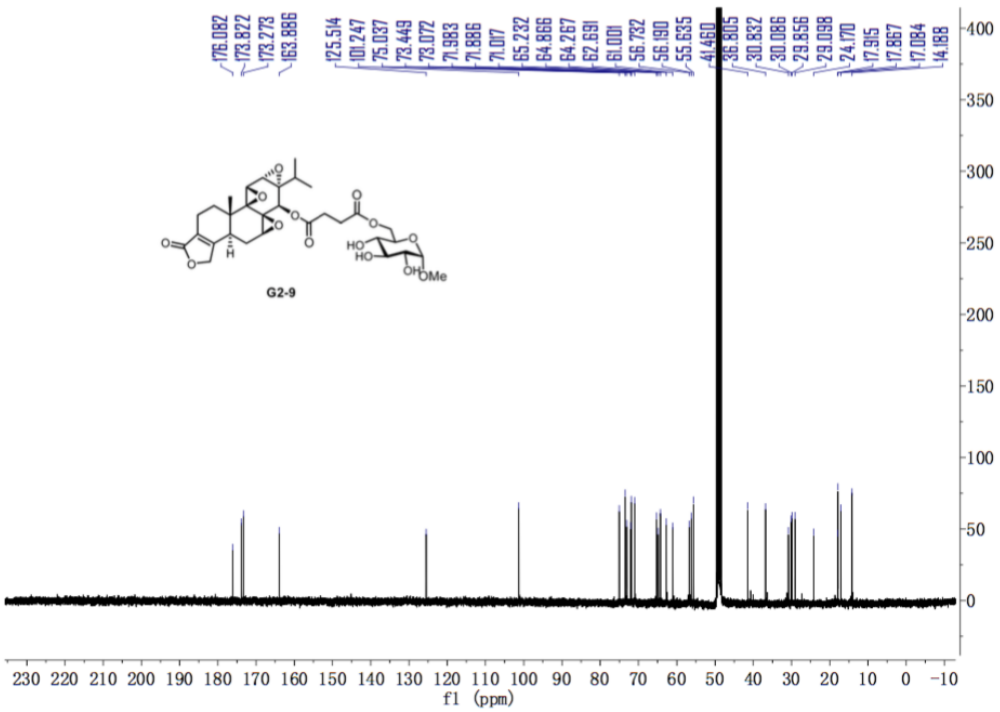

Figure S23. ^{13}C (100 MHz) – NMR of **G2-9** in CD_3OD, Related to Figure 1.

HPLC of Glutriptolides

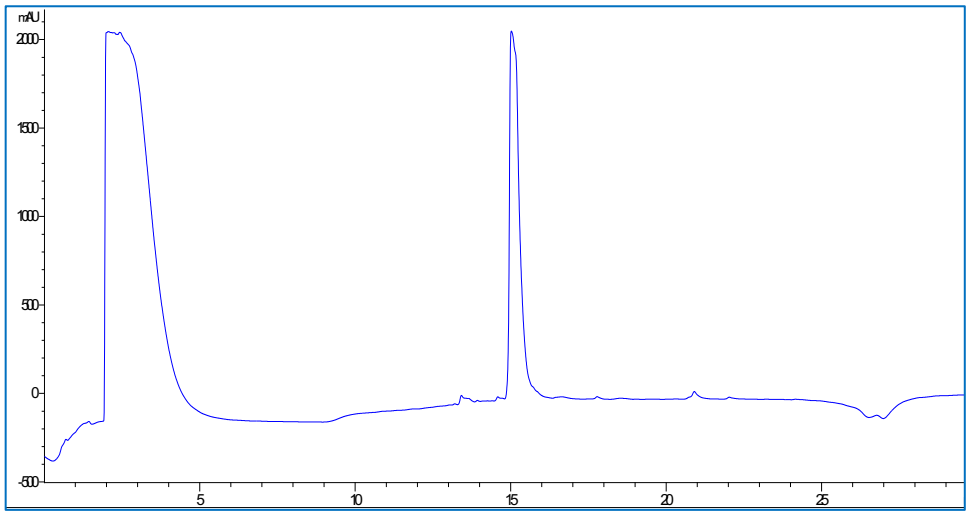

Figure S24. HPLC spectrum of **G2-3**, Related to Figure 1.

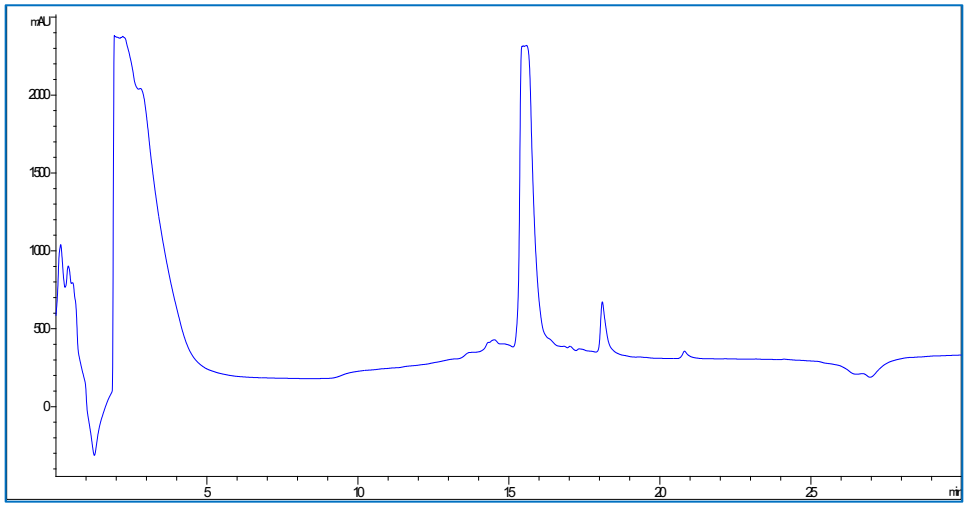

Figure S25. HPLC spectrum of **G2-4**, Related to Figure 1.

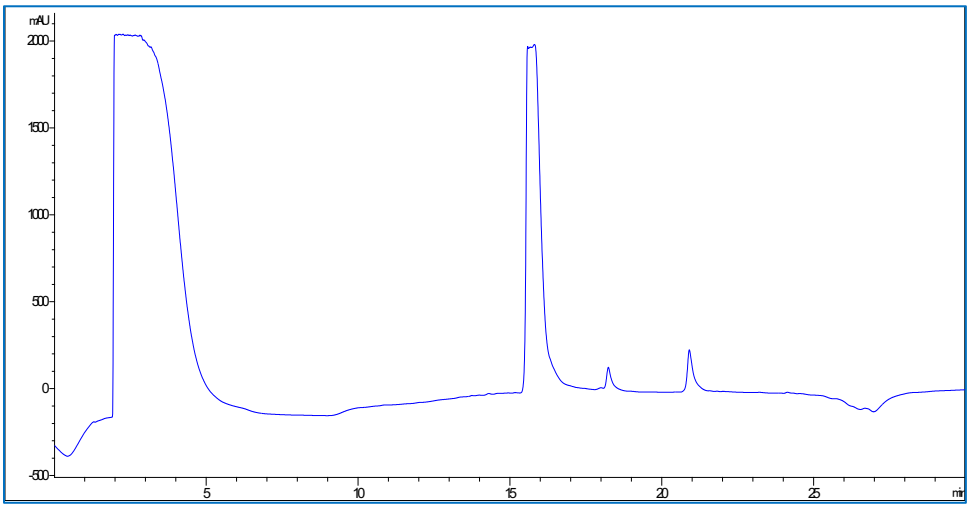

Figure S26. HPLC spectrum of **G2-5**, Related to Figure 1.

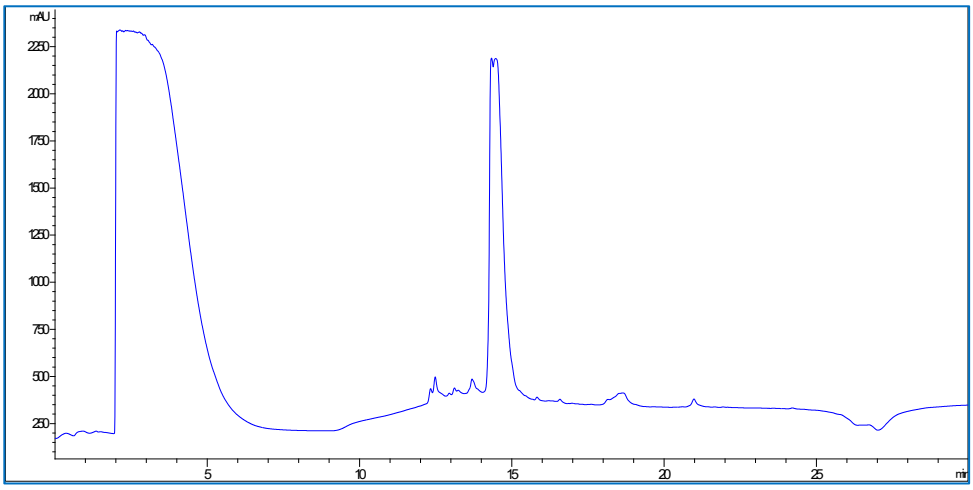

Figure S27. HPLC spectrum of **G2-8**, Related to Figure 1.

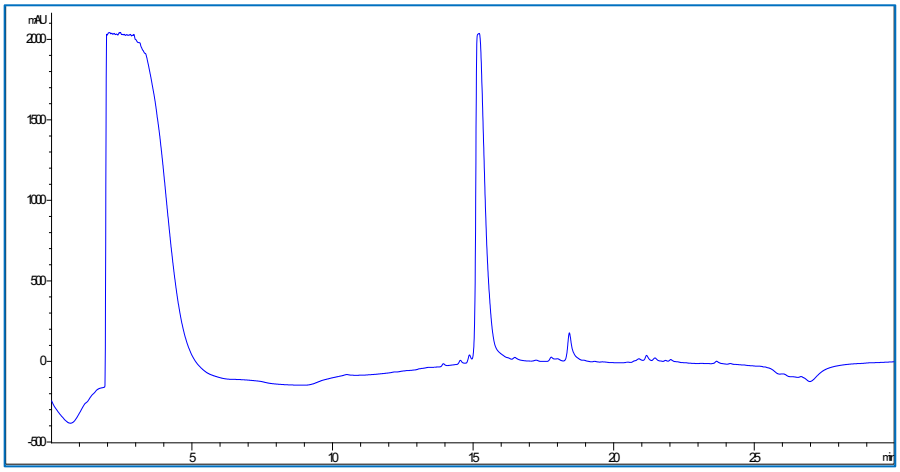

Figure S28. HPLC spectrum of **G2-9**, Related to Figure 1.

Supplemental References

Das, S.K., and Roy, N. (1996). An improved method for the preparation of some ethyl 1-thioglycosides. Carbohydr. Res. 296, 275–277.

Barry, C.; Cocinero, E. J.; Carcabal, P.; Gamblin, D. P.; Stanca-Kaposta, E. C.; Rmmert, S. M.; Fernández-Alonso, M. C.; Rudić, S.; Simons, J. P.; Davis, B. G. (2013). 'Naked' and Hydrated Conformers of the Conserved Core Pentasaccharide of N-linked Glycoproteins and Its Building Blocks. J. Am. Chem. Soc. 135, 16895–16903.

Sullivan, L.M. (2017). Essentials of Biostatistics for Public Health, 3rd Edition (Jones and Bartlett Publishers).

Sullivan, G. M., & Feinn, R. (2012). Using Effect Size-or Why the P Value Is Not Enough. Journal of Graduate Medical Education, 4, 279–282.